An investigation of non-linear transverse susceptibility as a basis for improving the measurement of anisotropy in magnetic powdered samples.

Conor Thomas Moorfield

A thesis submitted in partial fulfilment for the requirements for the degree of Master of Science (By Research)

Jeremiah Horrocks Institute

University of Central Lancashire

Preston, United Kingdom

20^{th} May 2020

Declaration

Type of Award Masters by Research

School Physical sciences and computing.

I declare that while registered as a candidate for the research degree, I have not been a registered candidate or enrolled student for another award of the University or other academic or professional institution.

I declare that no material contained in the thesis has been used in any other submission for an academic award and is solely my own work.

No proof-reading service was used in the compilation of this thesis.

Conor Thomas Moorfield

Abstract

Non-linear transverse susceptibility, χ_{nl}, has been studied as a method for measuring the magnetic anisotropy of random powder samples. Random powder samples of $\gamma - Fe_2O_3$, CrO_2 and Fe_3O_4 and a tape sample of $Co - \gamma - Fe_2O_3$ were tested. Measurement of linear transverse susceptibility, χ_t, does not produce anisotropy field measurements for some random powders. The key sample of interest in this research was the $\gamma - Fe_2O_3$ random powder as it produced no distinguishable anisotropy, when measured with the χ_t technique. The anisotropy of the $\gamma - Fe_2O_3$ random powder was measured to be $105 \pm 10\, kA/m$ when using the χ_{nl} method. The measured values were rigorously compared to both the linear method and the respective samples hysteretic behaviour, as well as previous work where it was found to agree within error.

The linear and non-linear transverse susceptibility were measured using a susceptometer which went through reliability upgrades. This included replacing the lock-in amplifier which generated an AC signal outputted to a solenoid. The new lock-in amplifier saw an improvement in signal to noise ratio of $20dB$. Anisotropy measurements were also successfully made for the CrO_2 random powder and $Co - \gamma - Fe_2O_3$. These values did not agree with the value measured using the χ_t method. This was likely due to the sample alignment as the easy axes would be aligned in one axis for the textured sample. So if that sample alignment was not in line with the measurement direction only a weaker signal was measured. This requires further testing with these samples. The Fe_3O_4 sample had no measured anisotropy. It had repeatable features at low field values so further testing is required to identify the origin of these peaks.This should be done through measurements at higher resolutions.

Contents

Acknowledgements

I would like to thank Dr Steven McCann for his continuous assistance and support throughout this project. As well as giving me the opportunity to learn so many skills that never seemed possible less than a year ago. Also thanks to Dr Tim Mercer and Prof. Phil Bissell who both acted as a great sounding board for my ideas whilst ensuring that everything kept moving forward towards the finishing of this thesis. I would also like to thank them for their endless patience in answering my many questions and queries at all hours of the day.

I would like to thank the fellow basement dwellers, Dr Zoe Henderson, Dr Simon Smalley and Jack Hanson. Without their humour, eccentric behaviour and ability to cope with my overly stressed demeanour in a reassuring way. I would like to thank Zoe for always listening even when she should be working. Simon for engaging conversations and opening my eyes to the art of biscuit concealment. Finally, Jack for that cover of "A thousand miles" every other hour.

I would finally like to thank my family for putting up with me long enough to make it to university and supporting in anyway they could even when times got tough. To my friends who listened endlessly to my many gripes and provided a welcome reprieve from the world of physics.

List of Figures

List of Tables

S.I. units have been used exclusively throughout this thesis.

Chapter 1

Introduction and Theory

The purpose of this thesis is to explore methods for measuring magnetic anisotropy based upon the transverse susceptibility of the material. The transverse susceptibility is an intrinsic property of magnetic materials, it was first theorised by Gans in 1909 [1]. It was not analysed further until the development of the Stoner-Wohlfarth model [2] in 1947. The Stoner-Wohlfarth model can be used to determine how a uniaxial, single-domain particle will behave hysteretically when the particle's saturation magnetisation and anisotropy field are known. The saturation magnetisation, the point where an increase in applied magnetic field will not increase the material's magnetisation, can be determined for bulk magnetic materials. However, the hysteretic characteristic is different for each particle with its measurement being dependent on knowing the orientation of the particle with respect to an applied field. In 1957 Aharoni et al [3] published a work which suggested a transverse susceptibility measurement of a system of Stoner-Wohlfarth type particles would yield a distribution of anisotropy fields. This was experimentally confirmed by Pareti and Turilli [4] in 1987. The work of Pareti and Turilli has since been expanded with the experimental method improved to develop a faster method for measuring the magnetic anisotropy using the transverse susceptibility of particle systems.

Anisotropy can also be measured using other methods such as the torque magnetometer. This measures the hysteretic loss of a magnetic material, which is

dependent on the particle orientation distribution and anisotropy fields [5]. The loss is caused by small changes in the angle of the applied field. The magnetic field exerts a torque on the particles which can be measured using the rotation of the sample connected to a torsion fibre. The rotation can be measured by sensors. These measurements can then produce a map of orientation distribution and anisotropy fields. The limitations of this method are first the need for a moving component. Either moving the magnetic field or the sample will be relatively difficult. As well as this, to obtain stable readings the torsion fibre must be very stiff which limits the maximum change in angle reducing the precision of the measurement [6]. A second method for measuring anisotropy is the torsion pendulum. This uses similar principles to the torque magnetometer. However, the sample is disc shaped and rotated away from the magnetic field and then released oscillating about the field direction. Anisotropy can then be extracted from a measure of the frequency of the oscillation. The method is very quick but limited because only the slope of the torque curve at the equilibrium angle is used.

Both of these methods are difficult to use when measuring the anisotropy of powder samples because of their random distribution whereas the transverse susceptibility method still produces a value for the coercivity, H_c.

By being able to measure the anisotropy, the preferred axis of magnetisation will be known, which in turn highlights the spin direction of the system. This knowledge can be used in several applications of the anisotropic magnetic particles. One such use is to align the particles along one direction by aligning their easy axes, which is known from their anisotropy. This alignment will give a stronger bulk magnetic response. This is commonly used in magnetic tapes designed for data storage, which rely on the alignment of the particles' easy axes.

Magnetic nanoparticles have many potential applications. As mentioned they have been used extensively in data storage and magnetic recording. Magnetic nanoparticles (MNPs) particularly have been explored as a way to increase the maximum data storage of recording devices such as hard drives by reducing particle size. The amount of data which can be stored in a certain volume of nanoparticles is so far limited by the superparamagnetic limit. This is due to the thermal energy of the device causing spontaneous switching in particles with a sufficiently small

volume. Current magnetic tapes can use anisotropic $\gamma - Fe_2O_3$ particles [7]. Other research has used one dimensional nanostructures made from anisotropic MNPs which have a larger density of particles capable of storing data [8–11].

Another application of magnetic nanoparticles is within magneto-mechanics and microfluids. Research has been done on the mechanical coupling of magnetic nanoparticles into nanorods, these rods have the potential to be used as actuators and valves in micromagnetic mechanisms [12–14]. Magnetic nanoparticles also have uses in Magneto-photonics, which is the magnetic control of optical properties in assemblies of magnetic nanoparticles. These properties can be used in diffraction gratings, smart windows which can control the permitted light and thermal energy passing through. There is also research into tune-able colour displays and magnetic printing where the pigment of the ink can be tuned and set by an applied magnetic field based upon the rotation of the magnetic particle moments [15–24].

Other areas of use include nanoscale electronics composed of magnetic nanoparticles. These have seen increased interest due their high conductivity in magnetic fields which can be increased further by tuning the particles based on their anisotropy [25]. Magnetic nanoparticles have also been used in catalytic converters by using magnetic particle structures to contain the catalyst. This has shown increased efficiency in the reaction with the catalyst then being able to be recycled through magnetic separation [26–28].

One of the most potentially useful areas of magnetic nanoparticle research is in the medical field. There have been proposed uses for magnetic nanotubes for fine medical use. Anisotropic magnetic nanoparticles also have use as a binding agent for chemicals in sensors, such as a sensor for the diagnosis of Alzheimer's disease [29]. Another use is in drug delivery where the drug is fixed to an anisotropic magnetic nanoparticle or held inside of a hollow magnetic nanoparticle structure which can be released by a trigger such as temperature or pH [30–34]. An extension of this process is targeted drug delivery where nanoscale motors could direct the drug to the target area [35].

This research project had two main aims. The first is to improve the stability and sensitivity of a linear transverse susceptometer at UCLan. Linear transverse susceptibility is a technique used to measure the magnetic anisotropy of a material. This susceptometer was developed for previous research at the university but was not producing stable results. There were two key pieces of equipment causing this instability. A lock-in amplifier with an internal oscillator used to generate an alternating magnetic field. This oscillator had deteriorated with age and no-longer produced a consistent waveform. To eliminate this instability a new lock-in amplifier was installed which produced a highly stable waveform and had a higher level of precision. The second piece of equipment was an audio amplifier which amplified the signal from the lock-in amplifier's internal oscillator. A new audio amplifier was installed as the previous amplifier, with age, was now inducing excessive noise into the signal. This amplified AC signal is used to generate an AC magnetic field. For the purposes of this measurement this has to be a constant single amplitude and frequency. The next step was to verify the linear transverse susceptometer's output was comparable to previous experimental measurements of various magnetic samples.

The magnetic samples being tested during this research consists of an easy axis aligned layered tape sample made of maghemite, held together with adhesive. There are also three separate powder samples: A randomly orientated maghemite powder sample; a randomly orientated magnetite powder sample and a randomly orientated sample of Chromium dioxide coated by an adhesive.

The second aim of this project was to modify the transverse susceptometer to use a different technique known as non-linear transverse susceptibility. Previous measurements have shown that for randomly orientated magnetic powder samples, the linear transverse susceptibility method smears out any anisotropy information. These types of samples are typical in recent studies of nanoparticles as they are almost always random powders. The theory for the non-linear method was developed by Chantrell et al [36], producing a technique that is less sensitive to the distribution of particles easy axes. In practice the non-linear technique can be used by modifying an existing susceptometer. It was suggested that this modification should produce a

large anisotropy signal even in materials that produce smeared features in the linear method. This non-linear method involves measuring the susceptibility orthogonal to that measured in the linear method. The alteration to the susceptometer from the linear technique is simply that the pick up coils have to be rotated by 90^o and the measured susceptibility signal has to be at twice the frequency of the AC field. As with the linear technique, several different samples were tested in this new configuration. The features produced by this method were then compared with expected theory and known measurements of the sample's characteristics.

1.1 Overview of thesis

This thesis is split into 5 chapters.

Chapter 1: **Introduction** This chapter gives a basic explanation of the contents of the thesis. A breakdown of the theory used throughout the subsequent chapters and separate sections on the following topics.

- A brief explanation of magnetic hysteresis.
- The theory of Demagnetising fields.
- The theory of Magnetic anisotropy
- A detailed look at the Stoner-Wohlfarth model for single domain uniaxial particles as well as energy models for the switching of the magnetic moments.
- An explanation of magnetic susceptibility and various methods of measurement.

Chapter 2: **Instrumentation** This chapter explains the equipment used to perform the measurements of transverse susceptibility. As well as this there is a full break down of the measurement techniques, the susceptometer configuration and an explanation of the Labview routine used through Pseudocode.

Chapter 3: **Samples** This chapter lists the samples used in this research, their lattice parameters, expected magnetic properties and measured coercivity, saturation magnetisation and remanance through hysteresis measurements.

Chapter 4: **Linear transverse susceptibility.** This chapter contains first an explanation behind the origins and function of the linear transverse susceptibility method. A mathematical derivation of the relationship it derives its name from. Measurements of both randomly orientated powder samples and magnetic tape samples presented as graphs of transverse susceptibility against the applied DC field.

Chapter 5: **Non-linear transverse susceptibility.** This chapter contains an explanation of the non-linear transverse susceptibility method and a derivation of the relevant equations for its relationship with the AC field. There are several plots showing the results using this technique to measure the anisotropy of magnetic powders and conclusions drawn from those results about its effectiveness as a method.

Chapter 6: **Conclusions and further work.** Finally the effectiveness of both the linear and non-linear transverse susceptibility methods are compared and their effectiveness as techniques for measuring the magnetic anisotropy are concluded. The future work that can be undertaken to further advance this research is also explored here.

Section 1.2 begins on the next page.

1.2 Magnetic Hysteresis

Hysteresis [37], which means to lag behind, is a phenomenon where the value of a materials property do not change at the same rate as the parameter that is causing that change. In magnetism, hysteresis occurs between a material's magnetisation, M, and the applied magnetic field, H. This hysteresis is commonly displayed in plots of M against H. A number of characteristics can be derived from a magnetic material's hysteresis loop and from there it can be deduced how suitable it would be for various applications. A labelled example of a hysteresis loop can be seen in figure 1.1.

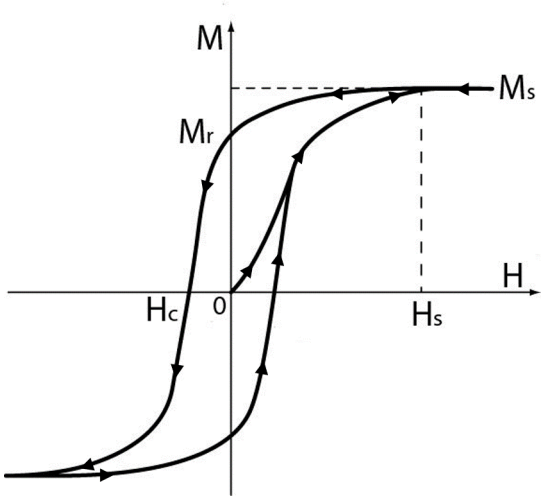

Figure 1.1: Magnetisation, M as a function of applied magnetic field, H. The hyteresis loop can be clearly seen with the key parameters labelled (Coercivity, H_c; saturation field, H_s; Remanance magnetisation, M_r and Saturation magnetisation, M_s) and defined below [38].

The first property can be derived from a hysteresis loop is a material's saturation magnetisation, M_s. For an unmagnetised material at zero applied field there is no magnetisation present. As the magnetic field is applied to the material the magnetisation will increase non-linearly. If the applied field is continuously increased eventually the material cannot be magnetised any further and will reach saturation. This is the parameter known as saturation magnetisation, denoted M_s. At this point all of the individual magnetic moments of the sample will be aligned along the applied field. The ideal saturation magnetisation is then dependent only on the magnitude of the magnetic moments and the total number of moments per unit volume. This means that the saturation magnetisation is dependent only on the material in the sample, and not structure, so a powder sample would have a

comparable saturation point to a crystal of the same material [37].

As the field is then decreased, the next property is the remanence magnetisation, M_r, where a material has magnetisation still present after the applied field has been removed. For a randomly orientated powder sample the remnant magnetisation will be equal to about half the saturation magnetisation [2]. A useful value that can be derived from this quantity is called the remanence ratio, $\frac{M_r}{M_s}$. This can be used experimentally as a measure of the distribution of the magnetic moments. This is because when the magnetic field is removed the magnetic moments will move back to the easy axis in the $+H$ direction. For a randomly orientated sample of magnetic moments the easy axes will be distributed through half of a sphere (All angles in the positive field direction). For a magnetic moment in that sphere, M_s makes an angle θ with the $+H$ direction. Therefore, it will have a magnetisation of $M_s\, cos\theta$. The remanence magnetisation can then be given as the average of $M_s\, cos\theta$ in all directions. This can be found to be,

$$M_r = \int_0^{\pi/2} M_s\, cos\theta\, sin\theta\, d\theta = \frac{M_s}{2} \tag{1.1}$$

Therefore, $M_r/M_s = 0.5$. It follows, that for any randomly orientated magnetic sample the remanence ratio should be 0.5 [6].

The coercivity is the reverse magnetic field that reduces the magnetisation from M_r to zero. On the hysteresis loop this is the point where the loop crosses the x axis, labelled H_c. The coercivity is dependent on how the sample was constructed and any external effects it was exposed to such as heat. The theory underpinning linear transverse susceptibility [3] indicates several features in the output of the susceptometer, including one at the coercive field, H_c. Therefore, by measuring this parameter using a vibrating sample magnetometer (VSM), a standard experimental technique, this can then be compared to the output of a susceptometer as a means of verification of the susceptometer.

An important note is that hysteresis loops of magnetic materials only produce distinguishable loops for ferromagnetic and ferrimagnetic materials. Ferromagnetic particles are highly susceptible to magnetisation and can form permanent magnets. This occurs when a magnetic field is applied to the particles

causing their magnetic moments to be orientated in the direction of the field. When the field is removed their magnetic moments retain some magnetic alignment. They can also exhibit spontaneous magnetisation at room temperature, this means they can behave as permanent magnets by holding some magnetisation in normal conditions. However, they will no longer spontaneously magnetise when the temperature exceeds the Curie temperature, T_c. At this point the ferromagnet becomes paramagnetic.

Ferrimagnetic materials magnetise with an applied field however it is a much weaker effect. This is because there are some magnetic moments which align parallel but opposite to the bulk moments. Ferrimagnets can also spontaneously magnetise at room temperature making them useful when looking for applications. They will however become paramagnetic, like ferromagnets, above the Curie point. Ferrimagnets are made of ionic compounds, with the ion in the compound having magnetic properties which are derived from the spins in partially filled electron shells. In the case of the samples being tested the magnetic properties in the particles come from the iron molecules. maghemite contains Fe^{3+} ions which provide magnetic properties whereas magnetite has a mixture of Fe^{3+} and Fe^{2+} ions.

The magnetic moment in each ion is given by Hund's first rule, which states that the spins in a partly filled shell are arranged so as to produce the maximum spin imbalance consistent with the Pauli exclusion principle [6]. Hund's other rules are first the total orbital angular momentum, $\underline{\boldsymbol{L}}$, has a ground state consistent with the first rule. The third rule gives the total angular momentum, $\underline{\boldsymbol{J}}$, relative to the total orbital momentum and the total spin momentum depending on how full the outer shell of the atom is.

Ferrimagnets have ions that can be split into two distinct groups based on their position within the crystal lattice. These groups called A sites and B sites were suggested to have opposing directional positions with a negative force acting between these sites, which is the case for antiferromagnets. Therefore, in ferromagnets there is a lattice of A ions magnetised in one direction and a lattice of B ions magnetised to oppose it. However, there is still a net magnetisation as the magnitudes of the A and B ions magnetisation are not equal. This implies that ferrimagnetism is an imperfect form of antiferromagnetism [6].

1.3 Demagnetising Fields

When a magnetic material is within a magnetic field, H, the magnetic induction, B, is affected by the permeability, μ, of the material. When this material has finite length, it generates a magnetic pole at each end. These poles give rise to an opposing magnetic field which acts against the applied field, H, this is called the demagnetizing field, H_d. The magnitude of the demagnetizing field is dependent on the magnetisation and shape of the material. The flux lines caused by the magnetic field, H, on a bar magnet can be seen in figure 1.2. The induction lines for that same material can be seen in figure 1.3. Both field lines are the same outside of the magnet this is due to the magnetic induction being directly proportional to the applied field in free space, $B = \mu_0(H + M)$. Inside the magnet B and H oppose each other due to the magnetisation M. The magnetisation is a product of the alignment of magnetic dipoles within the magnet. Whenever the dipoles are aligned in a material, a magnetisation will be induced and it will oppose the applied field H. It can therefore be assumed that there is a magnetic field present in the material which can be defined as the demagnetising field, H_d. The relationship between the demagnetising field and the magnetic induction differs from free space, it becomes $B = -\mu_0 H_d + \mu_0 M$. The demagnetizing field is dependent on two variables, the magnetisation of the material and a constant called the demagnetisation factor, N_d. The demagnetising field can then be detected through hysteresis measurements of magnetic materials. This is due to the hysteresis measurements directly measuring a materials magnetisation. The demagnetising field is directly proportional to the magnetisation that induces it. The proportionality constant N_d is the demagnetising factor along that axis[6]. The demagnetising factor is based purely on the shape and size of the material.

$$H_d = N_d M \tag{1.2}$$

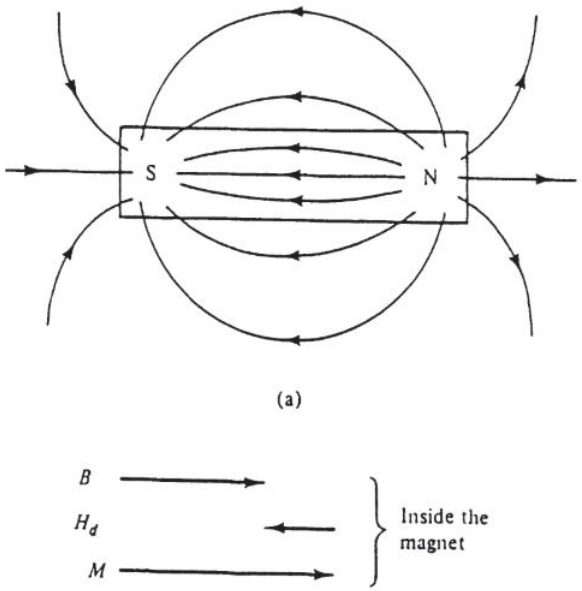

Figure 1.2: Magnetic field, H, inside and outside of a bar magnet. [6]

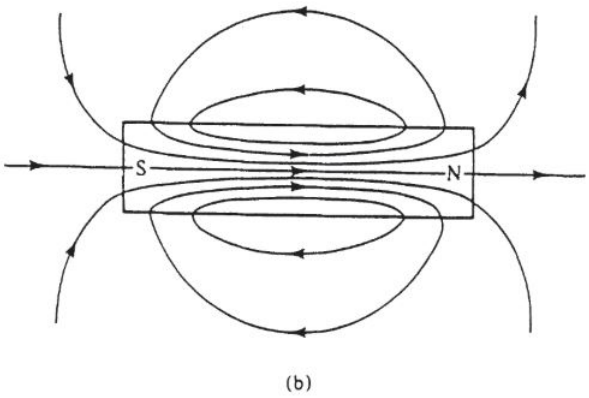

Figure 1.3: Magnetic induction, B inside and outside of a bar magnet.

Along the three axes there is a different demagnetising factor for each axis and the magnitude of each factor depends on the shape of the material being magnetised. The relationship between the three demagnetising factors have to be equal to a constant.

$$N_a + N_b + N_c = 1 \tag{1.3}$$

For a sphere the demagnetising factor has to be uniform therefore $N_d = \frac{1}{3}$.

For this research one of the samples has spherical nanoscale particles. Because of this the particles do not possess a shape anisotropy and can be considered isotropic. However, the samples being measured are not a single 10 nm spherical

particle. Instead the sample is a made up of packed spherical nanoparticles inside of a glass cuboid. Due to the packing of the spheres and in the case that they are un-coated some anisotropy can be induced by the interactions of the particles with their neighbours [39]. As well as this because the particles are packed within a cuboid the demagnetising factor for the bulk material will not be the $\frac{1}{3}$ of the constituent spheres. Instead the shape of the container will have to be taken into account [40, 41].

The demagnetising factor of a cuboid is a much more complex quantity than for a sphere or ellipsoid. Previous work has looked into the demagnetising factor of a magnetic material when it is cuboidal in shape [42]. However, this was always done with the idea that the bulk material shape was a cuboid not that particles were packed into a cuboid. To try and create a model for this quantity the first step would be modifying work by Aharoni et al [3] who produced the model for a solid cuboid. The demagnetising factor would also be affected by the sample orientations and their interactions which can induce an anisotropy. There will also be thermal energy affecting the behaviour of the particles due to their size. Being 10 nm in diameter they would be greatly affected by an environment at room temperature which can skew any models so would need to be factored in [43].

Demagnetising fields are the source of Shape anisotropy. This is because it is easier to magnetise something along a long axis than over a short axis. Therefore, magnetic particles display shape anisotropy when the shape of the particle have axes of unequal lengths and so there are one or more long axes or easy axes. This is the axis with the smallest demagnetising field.

1.4 Magnetic Anisotropy

Magnetic anisotropy [6] is defined as the phenomenon of a magnetic material having a preferred axis or axes of magnetisation for its magnetic moments. This means that some materials can be magnetised more easily in one direction than others. The direction in which a material can be easily magnetised is called the easy axis. Further to this a magnetic anisotropy field, H_k, is measured as the field value at which a magnetic particle saturates with the field applied in the direction normal to the easy axis [44](this is the hard axis). To get a moment to align along the hard axis energy must be applied to the moment to induce the directional change.

There are three major types of anisotropy. The first is crystalline anisotropy which has preferred directions of easy magnetisation with respect to the axes of the crystal lattice. This is caused by quantum coupling effects between electron spins and orbits. What is meant by coupling is an interaction between two neighbouring forces or effects. There is spin-spin coupling which is strong and keeps neighbouring spins parallel or anti-parallel and so is difficult to overcome. The energy in spin-spin coupling is dependent only on the angle formed between adjacent spins and so is isotropic and does not contribute to crystal anisotropy. There can also be orbit-lattice coupling where the orientations of the orbit are fixed to points on the lattice and they cannot be changed by large applied fields. The final interaction is formed from the spin and orbital movement of each electron in the crystal lattice. When a field is applied to the lattice it attempts to re-orientate the spin of the electron which in turn re-orientates the orbit. However, the orbit experiences strong coupling with the crystal lattice and so resists the rotation of the spin axis. The energy to overcome this coupling and move the spin away from the easy axis which aligns with the orbital coupling is the "anisotropy energy".

The second is shape anisotropy which has an easy axis direction defined by the overall shape of the particle. In this case the long axes are easier to magnetise than shorter ones due to the relative demagnetizing fields of the particle. The third is stress anisotropy which occurs when the material experiences a deformation along an axis induces a non-uniformity in its shape. For the materials in this project, they

are assumed to have a combination of shape and crystalline anisotropy, where the combination of the two produces a single easy axis for the particle.

Magnetising a material from its preferred axis to a hard axis requires energy. This energy can be thought of as stored relative to the axis with the easy axis having more stored energy than the hard axis. This can be seen in figure 1.4, where the easy axis has a higher energy density than the hard axis.

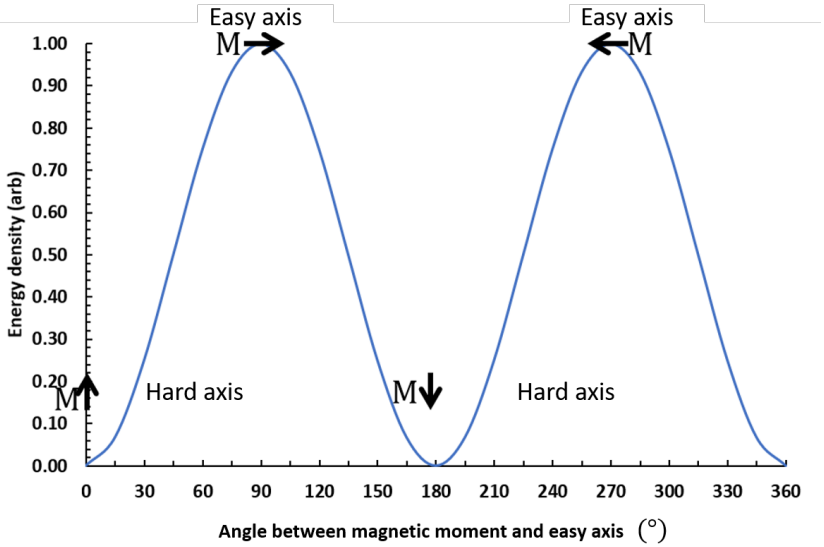

Figure 1.4: Uniaxial anisotropy energy density against the angle between the magnetic moment and the easy axis [37]. The labels M denote the magnetisation and depict the easy axis and hard axis.

For a cubic crystal lattice and magnetised to saturation such that its magnetisation vector, M_s, makes angles a, b, c with the crystal axes, the crystalline anisotropy energy is then given by,

$$E = K_0 + K_1(\alpha_1{}^2\alpha_2{}^2 + \alpha_2{}^2\alpha_3{}^2 + \alpha_3{}^2\alpha_1{}^2) + K_2(\alpha_1{}^2\alpha_2{}^2\alpha_3{}^2) + ... \qquad (1.4)$$

where $\alpha_1, \alpha_2, \alpha_3$ are cosines of angles a, b, c respectively. K_0 is independent of angle so can be ignored as only the change in the energy, E, is of interest K_2 and above can also be neglected. Neglecting these terms we can consider a crystal with uniaxial anisotropy. Therefore, equation 1.4 becomes,

$$E = K_1 sin^2\theta + K_2 sin^4\theta \qquad (1.5)$$

Shape anisotropy can also be expressed as the systems stored energy when the magnetisation vector is moved from the easy axis direction. A prolate spheroid is uniaxially anisotropic due to its shape and it has anisotropy energy given by,

$$E = K_s sin^2\theta \tag{1.6}$$

where θ is the angle between the particle moment and the easy axis. K_s is the shape anisotropy. This equation is comparable to the first term of equation 1.5 for uniaxial crystalline anisotropy. Shape and crystal anisotropy can be combined by forming a prolate spheroid from an anisotropic crystal. The resulting particle also possesses uniaxial anisotropy which is a resultant vector from the shape anisotropy easy axis and the crystal anisotropy easy axis. This combined anisotropy is given by,

$$E = K_u sin^2\theta \tag{1.7}$$

This is the uniaxial anisotropy used in the Stoner-Wohlfarth model of uniaxial particle rotation and switching is based [45].

In the case of fine particles, the anisotropy energy is as stated in equation 1.7. If the particle has a volume V, with an energy barrier ΔE, that must be exceeded to cause a switch in direction of the magnetisation, then the energy required is KV. This energy will decrease with particle size, so as $V \to 0$ the energy required to cause switching decreases. Because of this, spontaneous switching can occur in such particles due to thermal fluctuations in the environment which overcome the energy barrier. When a field is applied to such particles the moments of the particles will align. However, when the particles are at higher temperatures they have higher thermal energy, this causes the moments to dis-align. This behaviour is analogous to paramagnets and the theory of paramagnetism for single atoms proposed by Langevin in 1905 [46]. The theory of Superparamagnetism was proposed by Bean and Livingston in 1959 [47] to explain this phenomena. For a single domain isotropic particle of magnetic moment, μ, directed at an angle θ by an applied field, H, its energy can be given by $-\mu H cos\theta$. For particles of this nature held at a temperature, T, reaching thermal equilibrium gives a Boltzmann distribution of angles over the particle system. When $cos\theta$ is averaged over the Boltzmann distribution of angles, the amount of the assemblies magnetisation aligned with the field is then given

by the Langevin function $L(a) = coth(a) - \frac{1}{a}$, where $a = \mu H/kT$. However, in practice ferromagnetic particles do not exhibit isotropic behaviour. They are instead anisotropic and so possess an anisotropy energy given by, $E_k = KVsin^2\theta$. Where K is the anisotropy energy per unit volume and V is the particle volume. For a particle in applied field, H, its energy will be $KVsin^2\theta - \mu Hcos\theta$. In this system, the magnetisation curve will change in shape depending on the ratio between the anisotropy energy and the thermal energy given by KV/kT. The shape can be modelled upon the Langevin function, as given above. However, for low fields the value of a is instead, $\mu H/3kT$.

Figure 1.5 shows the difference in M-H behaviour for superparamagnetic particles compared to ferromagnetic particles. There is no hysteresis for the superparamagnetic particle and the magnetisation is reversible.

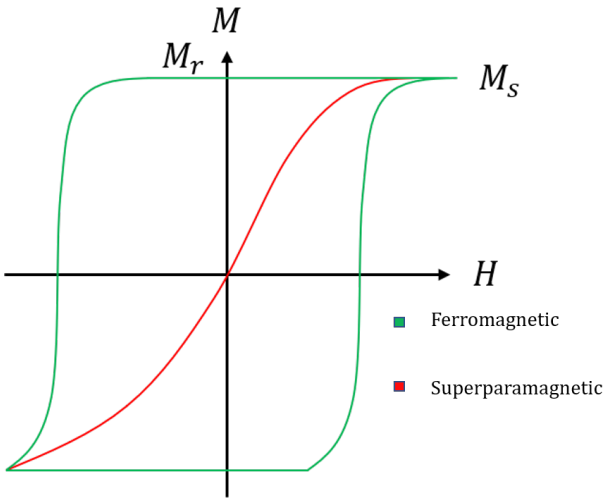

Figure 1.5: M-H Curve for a Ferromagnetic and superparamagnetic magnetic particle. M_r is the remanant magnetisation, M_s is the saturation magnetisation.

Because of the affect thermal energy can have on the switching of magnetic particles a principle called the superparamagnetic limit was needed. This limit sets the minimum size for magnetic particles used in data storage such as hard drives. This is to stop spontaneous switching within the drive causing data loss.

Magnetic particulate materials exhibit a phenomenon called magnetic texture caused by a distribution in easy axes. For the powder samples that are used in this project, there should be a random distribution of easy axes. However, for the more classical tape samples, an ideal case would have all easy axes in alignment. Partial alignment is defined as the texture of the material.

1.5 Stoner-Wohlfarth Model

The Stoner-Wohlfarth model is a theorised explanation for the hysteresis observed in certain magnetic materials [2]. For this model it is assumed that all particles are single domain and uniaxial. All magnetic moments in a particle remain coherent during rotation where the moments of the constituent atoms rotate as one. Therefore, the particle will have a constant magnitude of magnetisation. By knowing the magnetisation will only fluctuate with direction it is possible to find the total energy minima which can be used to predict the magnetisation rotation behaviour of the particle being acted upon by an external field [45]. Using single domain uni-axial magnetic particles a relationship can be found between the particles anisotropy energy, its magnetisation and an applied field as shown in equation 1.1. A coordinate system for such a particle can be seen in figure 1.6.

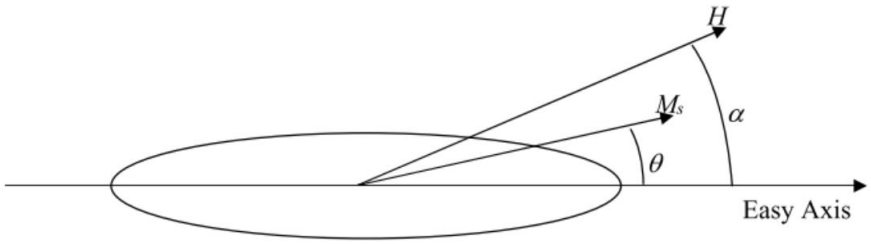

Figure 1.6: Coordinates for a single domain uni-axial Stoner-Wohlfarth particle with reference to the easy axis of magnetisation, the applied field. H and the saturation magnetisation, M_s [6].

In the case of a single domain uniaxial particle as shown in figure 1.6, the anisotropy energy can be given by,

$$E_a = K_u sin^2\theta \tag{1.8}$$

Where E_a is the anisotropy energy, K_u is the anisotropy constant which characterises the shape, stress and crystalline anisotropy of the particle. The angle θ is the angle made between the saturation magnetisation M_s and the easy axis.

The potential energy, E_p due to an applied external magnetic field, H across the particle at an angle α with respect to the easy axis is given by,

$$E_p = -HM_s cos(\alpha - \theta) \tag{1.9}$$

Therefore the total energy can be calculated where,

$$E = E_a + E_p \tag{1.10}$$

Then substituting 1.1 and 1.2 into 1.3 gives,

$$\longrightarrow E = K_u sin^2\theta - HM_s cos(\alpha - \theta) \tag{1.11}$$

The anisotropy field, H_k is defined as the field value at which the particle saturates with the field applied in the direction normal to the easy axis. It can be shown the this anisotropy field is equal to

$$H_k = \frac{2K_u}{M_s} \tag{1.12}$$

It is then possible to use this anisotropy field value to obtain a reduced field, h where $h = H/H_k$ so equation 1.5 becomes,

$$E = H_k M_s(\frac{1}{2} sin^2\theta - hcos[\alpha - \theta]) \tag{1.13}$$

Equation 1.13 can then be used to create a model for the energy of the particle depending on assigned values of α, h and a range of values for the angle θ.

1.5.1 Effect of the applied field direction, α

a)Particles where $\alpha = 180°$

Figure 1.7 shows the energy of particles with $\alpha = 180°$ as a function of θ. In this scenario the applied magnetic field is anti-parallel to the direction of magnetisation of the particle. When the reduced field, h, is equal to zero there are two minima which occur at $\theta = 0°$ and $\theta = 180°$. However, as the applied magnetic field

is increased the minima at $\theta = 0°$ is significantly reduced whilst the minima at $\theta = 180°$ becoming a much deeper energy well.

The minima at $\theta = 0°$ is at a stable equilibrium when $h = 0$ however as the applied field is increased the minima destabilises and begins to flatten out at $h = 1$ becoming unstable at points after this. Therefore, when a field greater than $h = 1$ is applied any particle moments at an angle of $\theta = 0°$ would instantly switch to $\theta = 180°$ position. This switching point is known as the switching field or coercivity field and is denoted as H_c In the case of figure 1.7 $H_c = h$ where $h = 1$.

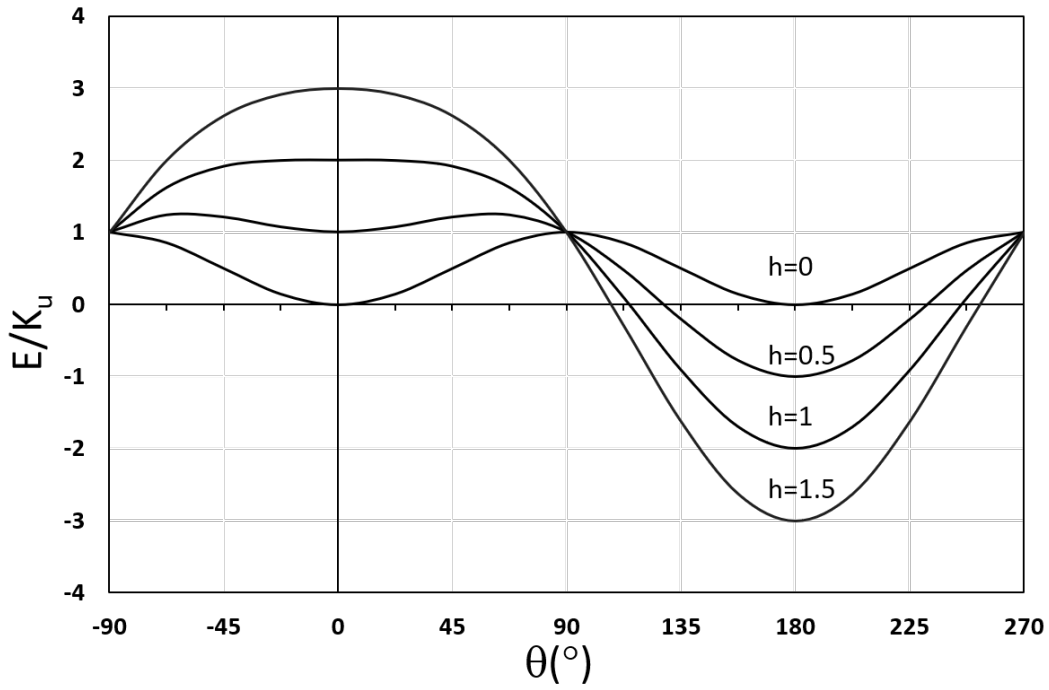

Figure 1.7: Energy as a function of reduced field, h and the angle between the saturation magnetisation and the easy axis, θ for a particle with $\alpha = 180°$ [modelled using equation 1.13]. E/K_u is the anisotropy energy density

b)Particles where $\alpha = 90°$

Figure 1.8 shows the energy function of particles with the magnetic field is applied perpendicular to the easy axis direction, meaning $\alpha = 90°$. As the applied field is increased the minima angular positions begin to move inwards. At $h = 1$ it can be seen that the minima at $\theta = 0°$ and $\theta = 180°$ begin to merge together to form one large minima at $\theta = 90°$.

As the minima move position with increasing field the magnetisation vector will continuously rotate between the easy and hard axis without any switching points.

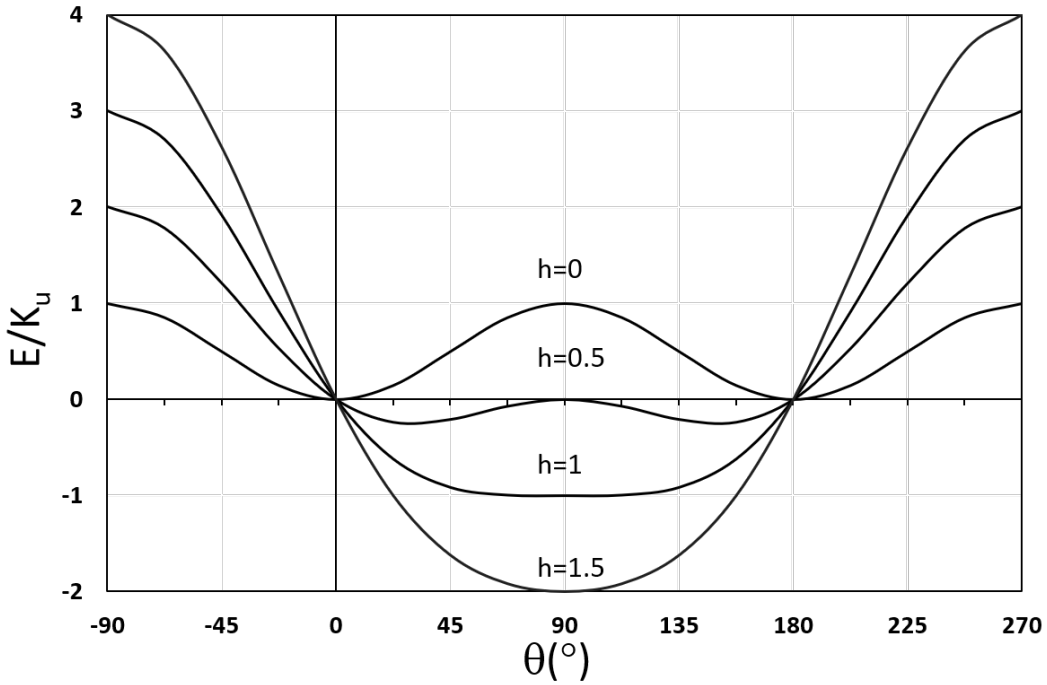

Figure 1.8: Energy as a function of reduced field, h and the angle between the saturation magnetisation and the easy axis, θ for a particle with $\alpha = 90°$

c)Particles where $90° < \alpha < 270°$

For particles with $90° < \alpha < 270°$ both switching and rotation occur depending on the angle of rotation, where $\alpha = 180°$ is an exception such that there are only strong switching events. For particles in this range an example has been produced for $\alpha = 135°$ shown in figure 1.9. As the magnetic field is applied from $\theta = 0°$ the particles begin to rotate until the energy curve becomes a point of inflection at $h = 0.5$. This inflection then causes switching in the magnetisation of the particles. As the magnetic field is increased further the magnetisation direction will rotate however it will never equal α unless $h = \infty$.

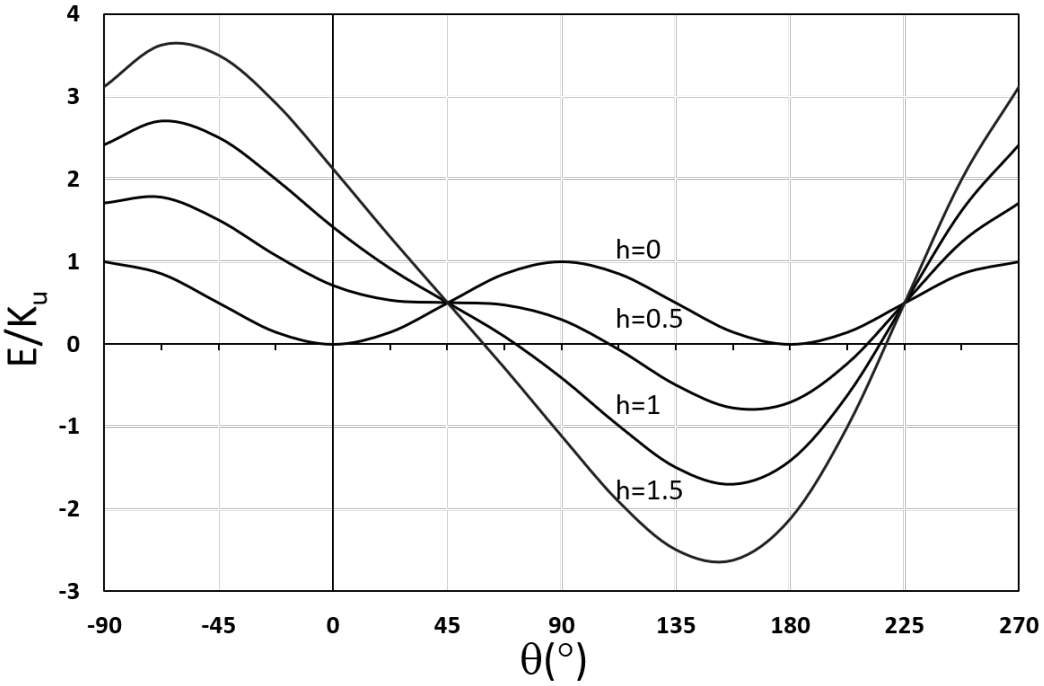

Figure 1.9: Energy as a function of reduced field, h and the angle between the saturation magnetisation and the easy axis, θ for a particle with $\alpha = 135°$

d) General case

In the general case, the magnetisation will rotate with the applied field reaching saturation in the direction of the applied field. When the magnetic moment direction is greater than 90° a switching event will occur. This switching occurs when the energy minimum, that moment sits in, becomes a flat point of inflection. Therefore, for a point of inflection the first and second derivatives of the energy equation 1.13 are equal to zero. So, $dE/d\theta = 0$ and $d^2E/d\theta^2 = 0$. The solution then to equation 1.13 gives two equations as solutions.

$$tan^3\theta_c = -tan\alpha \tag{1.14}$$

$$h_c^2 = 1 - \frac{3}{4}sin^2 2\theta_c \tag{1.15}$$

It is then possible to determine the switching field, h_c as a function of the switching angle, θ_c. This relationship has then been plotted below. What can be seen is that the maximum switching field is equal to the anisotropy field H_k and occurs when the switching angle is parallel or orthogonal to the easy axis. This can be seen in figure 1.10.

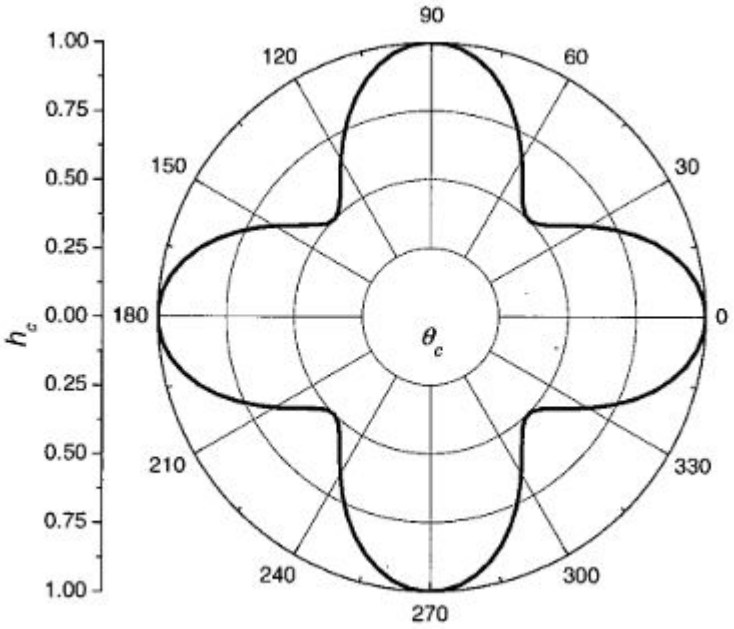

Figure 1.10: Reduced switching field, h_c as a function of switching angle θ_c [45]

The result of the solution to this equation is that by knowing the values of the saturation magnetisation, M_s and the anisotropy field value, H_k, the behaviour of a Stoner-Wholfarth particle can be completely described. This information can then be used to map hysteresis loops as the switching behaviour can be predicted for each angle of rotation. Therefore as a Stoner-Wohlfarth particle is magnetised from a low field strength to saturation it's switching angles can be calculated. These values can then be plotted to show the switching points at both h_c and H_k. The historically predicted loops from the original Stoner-Wohlfarth research [2] can be seen in figure 1.11.

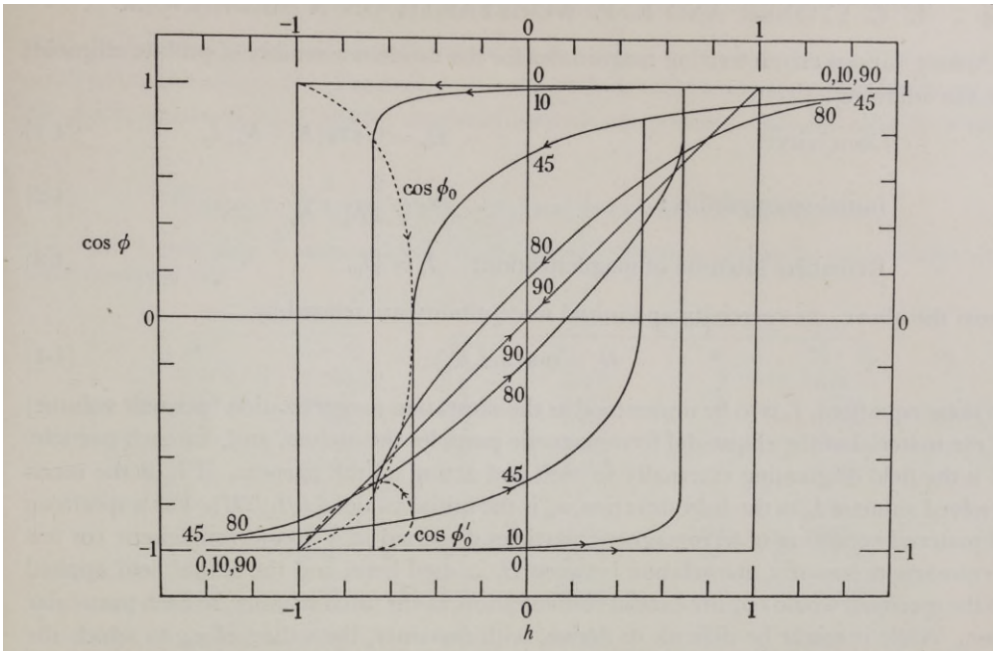

Figure 1.11: Theoretical hysteresis loops for prolate spheroids at different angles of applied magnetic field with reference to the easy axis from E.C. Stoner and E.P. Wohlfarth's 1948 publication "A Mechanism of Magnetic Hysteresis in Heterogeneous alloys" [2].

Figure 1.11 shows the individual Stoner-Wohlfarth hysteresis loops for various angles between the easy axis and the applied field. This figure shows that as the angle of the applied field is changed with respect to the easy axis the shape of the hysteresis loop changes. Regardless of the orientation of easy axis to applied field, M_s remains the same. The largest coercive field occurs when the applied field is parallel with the sample's easy axis. The magnetisation is saturated in the positive direction and then instantaneously switches to be saturated in the negative direction. This is due to the particles switching instantaneously to a position of lower energy into an energy well as shown in figure 1.7. This

instantaneous switching occurs at the point $h = 1$. At the point $h = 1$ the applied field is equal to the anisotropy field, the key parameter we are trying to measure. It is also important to note that this switching event also intercepts the x axis at $h = 1$ therefore at this orientation of applied field the coercive field and anisotropy field are equal. It is this switching mechanism that leads to the formation of the hysteresis loop. When the field is applied transverse to the easy axis there is no switching event only rotation as shown in figure 1.8 where the two energy minima merge into one. Since there is no switching, there is no hysteresis. Any α between 0^o and 90^o will have some switching and some rotation as seen in Figure 1.9.

Section 1.6 begins on the next page.

1.6 Magnetic Susceptibility

Magnetic susceptibility is defined as the amount a material will magnetise in an applied magnetic field. This is given by the following equation,

$$\chi = \frac{\mathbf{M}}{\mathbf{H}} \tag{1.16}$$

There are several ways of defining magnetic susceptibility along with different methods for measuring it. The most common are volume susceptibility; χ_ν, mass susceptibility; χ_{mass} and molar susceptibility, χ_{mol}. The units of this susceptibility are often given as m^3kg^{-1}.

Volume susceptibility, χ_ν is measured by applying a magnetic field across a magnetic sample and then measuring the change in force of the sample using a balance. The change in weight of the sample is proportional to the magnetic field applied across the sample. This type of system can also be used in conjunction with a temperature control system to find the magnetic volume susceptibility at different temperatures.

Mass and Molar susceptibility are both related to the volume susceptibility so are measured in the same way with a conversion applied using the following equations.

$$\chi_{mass} = \frac{\chi_\nu}{\nu} \tag{1.17}$$

$$\chi_{mol} = M\chi_{mass} \tag{1.18}$$

If an AC field is applied to a sample then the resultant change in moment defines its AC susceptibility given by,

$$\chi_{AC} = \frac{dM}{dH_{AC}} \tag{1.19}$$

χ_{AC} is measured in this study transverse to an applied field. It is therefore denoted as transverse susceptibility, χ_t.

There is a more specific case of AC susceptibility that occurs when the AC magnetic field is applied perpendicular to the direction of the signal detection called transverse susceptibility, χ_t. The transverse susceptibility measurements have a foundation in the Stoner-Wohlfarth model and were developed by Aharoni in 1957 [3]. Within his work he developed equations which could be used to model transverse susceptibility and published several figures containing single sweep models of the transverse susceptibility.

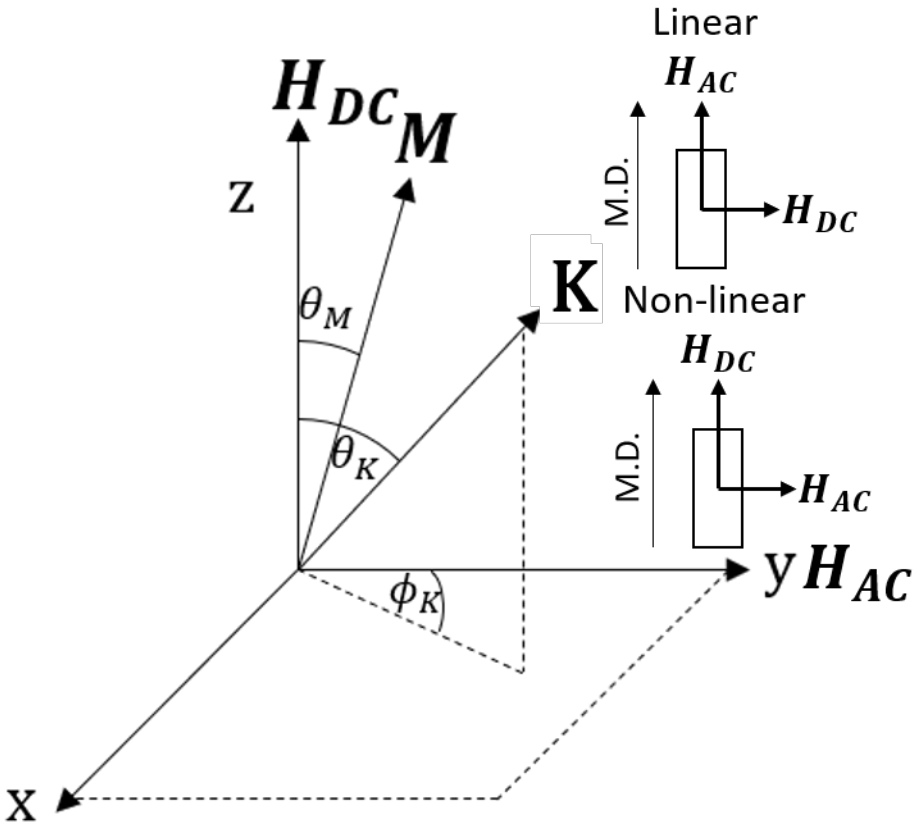

Figure 1.12: Polar coordinate system for anisotropy constant, K, and the magnetisation, M in respect to the DC field, H_{DC} and the AC field, H_{AC}. The angles θ_K, θ_M and ϕ_K are the angles made between the applied field, the resultant magnetisation, M, and the materials anisotropy, K. Also shown is the field directions for the two transverse susceptibility techniques with their respective measurement directions, labelled " M.D.".

Figure 1.12 is the coordinate system for a Stoner-Wohlfarth particle within a susceptometer, with respect to an applied DC and AC field. θ_M is defined as the angle between the Magnetisation and the direction of the applied DC field. θ_k is defined as the angle formed between the applied DC field and the easy axis, k.

Finally, ϕ_k is the angle formed between the applied AC field and the easy axis k. In the linear, case it can be seen that anisotropy and magnetisation are measured in the direction of the AC field orthogonal to the DC field, this is more clearly shown in figure 1.13. Whereas in the non-linear case it is measured with respect to the DC field orthogonal to the AC field. M.D. is the measurement direction of the two arrangements.

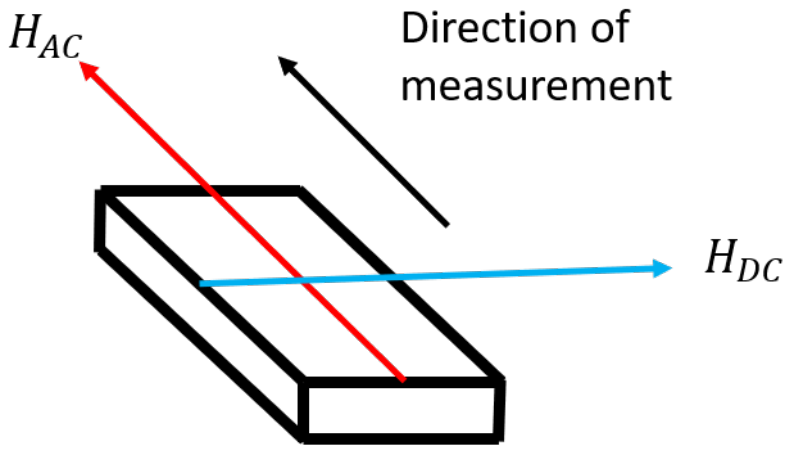

Figure 1.13: Orientation of the magnetic field for a cuboid magnetic sample when using the linear transverse susceptibility method.

Single Particle.

The equation below derived by Aharoni et al [3] gives the linear transverse susceptibility response of a single Stoner-Wohlfarth particle,

$$\chi_0 = \frac{{M_s}^2}{3K}$$

$$\frac{\chi_t}{\chi_0} = \frac{3}{2}[cos^2\phi_k \frac{cos^2\theta_M}{hcos\theta_M + cos2(\theta_M - \theta_k)} + sin^2\phi_k \frac{sin(\theta_k - \theta_M)}{hsin\theta_k}] \tag{1.20}$$

This particle has both a magnetisation, M, and an anisotropy constant, k. Where the term χ_0 is a constant proportional to the particle's saturation magnetisation. The anisotropy axis can be described by two spherical polar coordinates seen in figure 1.12. These are θ_k and ϕ_k. Similarly, the magnetisation vector can also be described by θ_M. The values for θ_M for these equations are taken from the Stoner-Wohlfarth model. The reference axis for these angles is the axis of the applied DC field, H_{DC}.

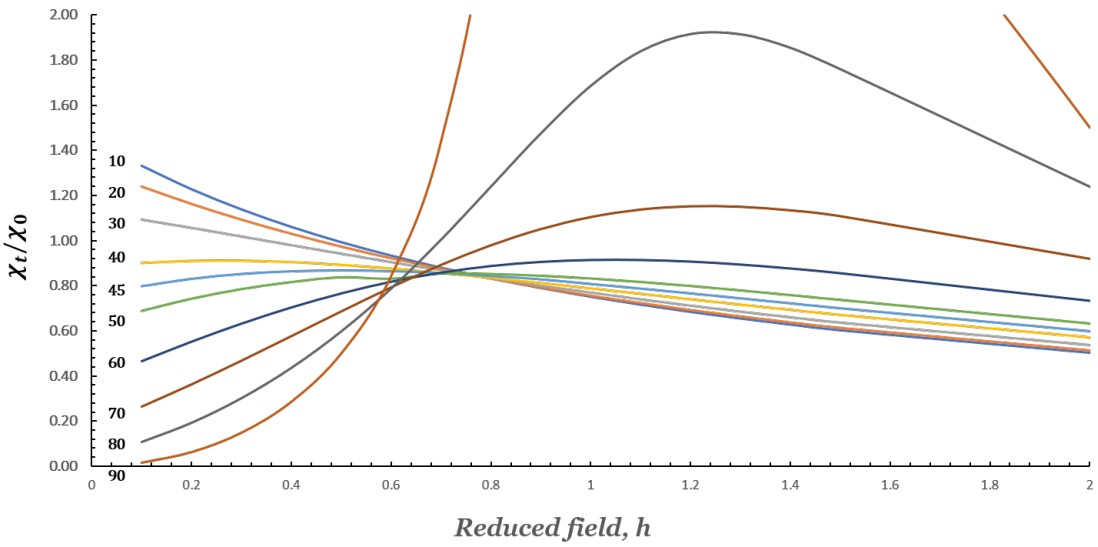

Figure 1.14: Change in transverse susceptibility for individual particles with a changing reduced field. Modelled from equation 1.20 with $\phi_k = 90^o$ substituted in. Where each line has a different θ_k value.

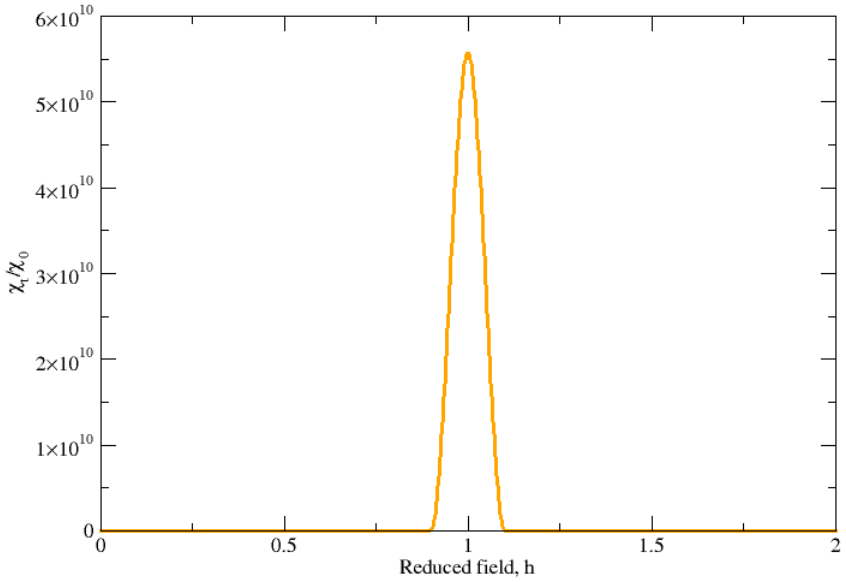

Figure 1.15: Expanded view of Figure 1.14 to show the full scale of the curve at $\theta_k = 90°$.

As can be seen in figure 1.14 there is a strong response in susceptibility at the anisotropy field position where $h = 1$ the strongest response occurs when the easy axis is orthogonal to the applied DC field and in-line with the perturbing AC field. The reason for this response can be seen in figure 1.8. As the angle θ moves from 0 the minima shifts towards to 90^o. At this point the minima has become a large

energy well so the moment cannot escape so no further switching occurs. This causes the large response for the line at $\theta_k = 90$ in figure 1.14. The full extent of this response can be seen in figure 1.15 where the largest response occurs at the anisotropy field point $h = 1$. The transverse susceptibility calculated at h=1 for $\theta_k = 90$ is an order of 10^{10} higher than the other modelled values. The reason for this can be seen in figure 1.7 as H_{DC} goes to H_k where there is a large flat bottom. Any perturbing field applied on the moment will cause a relatively large movement in the moment which will induce a large output signal. As the DC field is further increased the area the moment can move in the energy well will decrease which will in-turn decrease the output signal.

Assembly of Particles.

However, the samples that we tested using this transverse susceptibility theory are not single particles. The majority are a randomly orientated collection of particles. To account for the random assembly (which most of the proposed tested samples were) equation 1.20 is averaged over θ_k.

Equation 1.20 then becomes,

$$\frac{\bar{\chi_t}}{\chi_0} = \frac{3}{4}\int_0^{\pi/2} [\frac{cos^2\,\theta_M}{hcos\theta_M + cos2(\theta_k - \theta_M)} + \frac{sin(\theta_k - \theta_M)}{h\,sin\theta_k}] sin\theta_k\, d\theta_k \qquad (1.21)$$

As previously stated the values of θ_M are taken from the Stoner-Wohlfarth model. The results of these calculations can be seen plotted in figure 1.16.

Equation 1.21 was then used to create a model for an assembly of particles through a positive to negative magnetic field sweep. This as stated previously is an equation to calculate the transverse susceptibility response from a randomly oriented particle sample. The results from this model can be seen in figure 1.16. This is particularly important for this research as the curve labelled χ_t is the shape that is expected from the transverse susceptibility measurements that will be measured in the section entitled Linear transverse susceptibility. There are three distinguishable peaks the first at $h = 1$ this is the point where $H = H_k$ therefore this peak represents the

anisotropy field. This is also the peak that was shown in figure 1.14 that produced a singularity that reduced through the averaging process. It is also reflected in the negative x direction. There is also a third peak in the negative x direction which corresponds to the coercivity field of the sample, H_c.

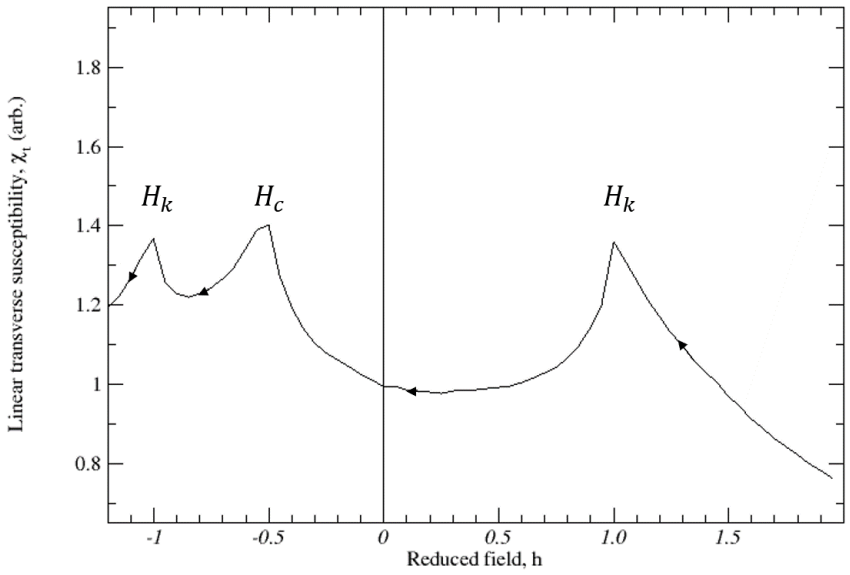

Figure 1.16: The reversible transverse susceptibility, χ_t of an assembly of randomly orientated particles having positive uniaxial anisotropy, plotted as a function of reduced field, h [3].

Magnetic texture is a measure of the alignment of a particle's easy axis where this is no applied magnetic field. Therefore a sample is said to be highly textured if all of the easy axes in the sample are aligned towards the same direction. A sample is said to be untextured when the easy axes of the particles are randomly orientated. Previous experimental work has examined randomly orientated powder samples [48–50] that the linear transverse susceptibility does not always show the Anisotropy peaks nor coercivity peak shown in figure 1.9. Their conclusion for the suppression of features having a high sensitivity to texture effects, with highly textured samples always showing the features whereas samples with a large distribution of easy axes the features become smeared and finally suppressed. When the field is applied to these samples the easy axis is fixed but the magnetic moments are free to rotate with the applied magnetic field. The effects of texture on transverse susceptibility

measurements have been explored in several different papers. These results can be seen in the published work of Hoare et al [50] and Sollis et al [51].

The majority of samples being tested are untextured. As stated, previous research yielded smeared and suppressed peaks for some untextured samples. Therefore, a new method is required to measure the anisotropy field. This new method is a variation on magnetic susceptibility based on the above linear transverse susceptibility. It is called "non-linear" transverse susceptibility named for the relationship between the AC magnetic field and the magnetic susceptibility. This theory was proposed by Chantrell et al [36].

This theory aims to provide a single point detection technique for determining a materials magnetic anisotropy. The first major difference is that the detection coils are rotated by 90^o from their location in the linear technique. Therefore the pick-up coil is orthogonal to the AC field and parallel with the DC field, shown in figure 1.17.

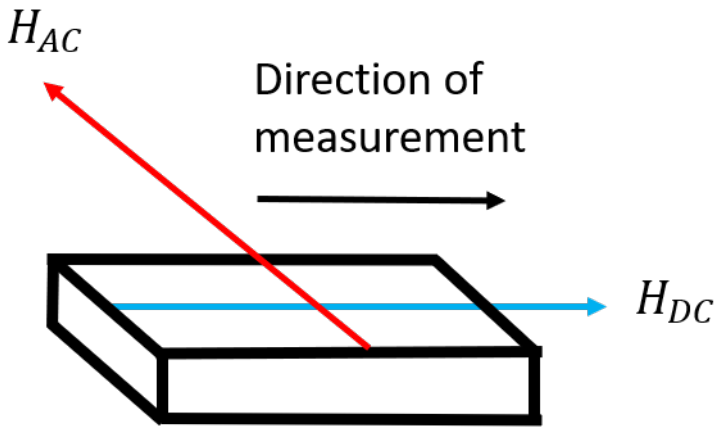

Figure 1.17: Orientation of the magnetic fields for non-linear transverse susceptibility measurements on a cuboid sample of a magnetic material.

Figure 1.18 shows that for each sweep of the AC field causing movement in the magnetic moment vector, μ, the change in magnetic moment, $\Delta\mu$ goes through one complete oscillation before returning to it's initial position. The oscillation that magnetic moment experiences is equal to only half of the a cycle for the AC field. Therefore, for a full cycle of the AC field, $\Delta\mu$ will experience two sweeps. This means that the change in magnetic moment $\Delta\mu$ is related to twice the frequency of

the AC field, f_{AC}.

$$\Delta\mu \propto 2f_{AC}$$

The theory predicts that a plot of non-linear transverse susceptibility as a function of DC field should be strongly divergent as the anisotropy field, H_k is approached and will produce an undefined region at H_k.

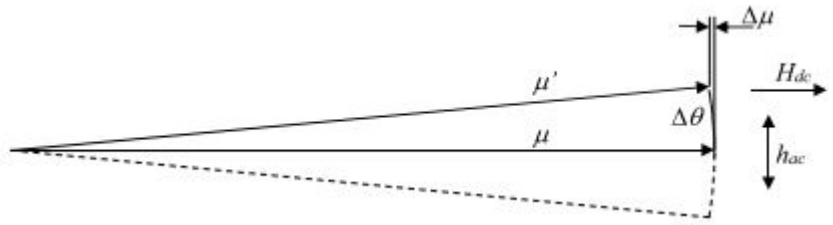

Figure 1.18: Change in magnetic moment, $\Delta\mu$ in the direction of the DC field due to the applied AC field. μ is the magnetic moment, μ' is the magnetic moment under the affect of the AC field and $\Delta\theta$ is the angle between those moments.

This method uses a separate equation to Aharoni's theory. This is to adapt the transverse susceptibility response to the arrangement of easy axes in the sample being tested. There is also a texture function for having a randomly orientated particulate sample. The output from this equation for different values of reduced field h can be seen in figure 1.19. The original notation in this publication had the non-linear transverse susceptibility as χ_q. As can be seen from this plot at the point where the reduced field, h is equal to one there is strongly divergent behaviour. This is the anisotropy field value. In practice such behaviour may not be observed because it was assumed all particles had the same anisotropy value. Thermal effects and particle interactions were also not accounted for. The other drawback to this theory is that only the positive sweep was modelled so it is unknown from this model if there is a coercivity feature.

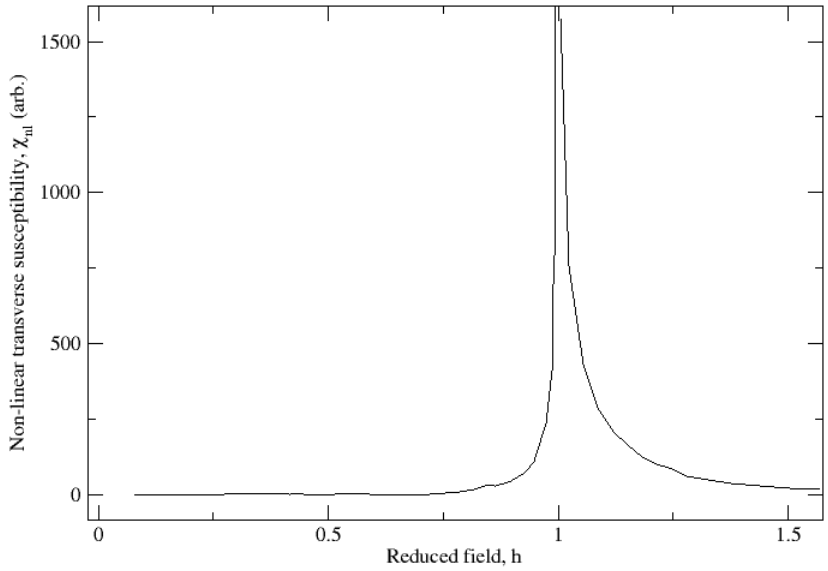

Figure 1.19: The non-linear transverse susceptibility, χ_{nl} for a particulate sample. Data extracted and re-plotted from Chantrell et al [36].

Chapter 2 begins on the next page.

Chapter 2

Instrumentation

In the previous chapter the theory of linear transverse susceptibility, χ_t, was discussed. It requires a large variable DC magnetic field applied across a sample. The susceptibility is then measured transverse as a function of the DC field. The device constructed for performing this measurement is called a susceptometer which will be able to fulfil the conditions laid out by the theory. In this section the working of the susceptometer will be discussed including a breakdown of it's constituent instruments and how they combine together to measure the transverse susceptibility. As well as this, the improvements and modifications made to the susceptometer will be discussed. These changes were made to make the suceptometer more stable and sensitive. The other technique mentioned in the theory, the non-linear transverse susceptibility, χ_{nl}, will also be discussed. This will include the modifications to the susceptometer needed for the technique.

2.1 Composition of the Linear transverse susceptometer

The linear transverse susceptometer is designed to measure the susceptibility of a material transverse to an applied DC field. The susceptibility measurements require an AC magnetic field, of constant magnitude, applied along the sample and a large variable DC magnetic field applied transverse to the AC field. The orientation of the applied fields and the direction of measurement can be seen in figure 1.13.

A block diagram has been produced to show the arrangement of the instruments making up the susceptometer shown in figure 2.1. The operation of the susceptometer is controlled by a LabVIEW subroutine. This routine reads measurements from the instruments as well as sending out commands to control the production of the AC and DC magnetic fields. The measured values are also plotted on a graph in real time. The plot is of the transverse susceptibility, χ_t, against the applied DC field, H_{DC}. This is useful as it allows comparison to the theoretical expectations and historical measurements of the susceptibility whilst the measurement is ongoing. The LabVIEW program will be discussed later in the chapter with the front panel being visible in figure 2.14.

The DC magnetic field is generated by a 2 Tesla (1600 kA/m) electromagnet. The electromagnet consists of 2 coils connected to the pole caps of the electromagnet. There is a EAPS-9080 power supply which provides the current to the electromagnet. It has a maximum power output of 3.2 kW with a maximum current of 80A. This power supply is controlled by the LabVIEW routine. The output current of the electromagnet is directly proportional to the magnetic field up to a maximum of $80\,A$. From the theory of linear transverse susceptibility proposed by Aharoni et al [3] it is seen in figure 1.16 that there are three features present in a positive field to a negative sweep. For the two polarities to be produced a device is needed to change the polarity. This is done with a switching mechanism which when switched on changes the polarity of the DC field, it is operated automatically by the LabVIEW routine when the applied field becomes zero. The DC field is measured using a Hall probe connected to a FW Bell Guassmeter. The measurements from Hall probe are sent to the LabVIEW

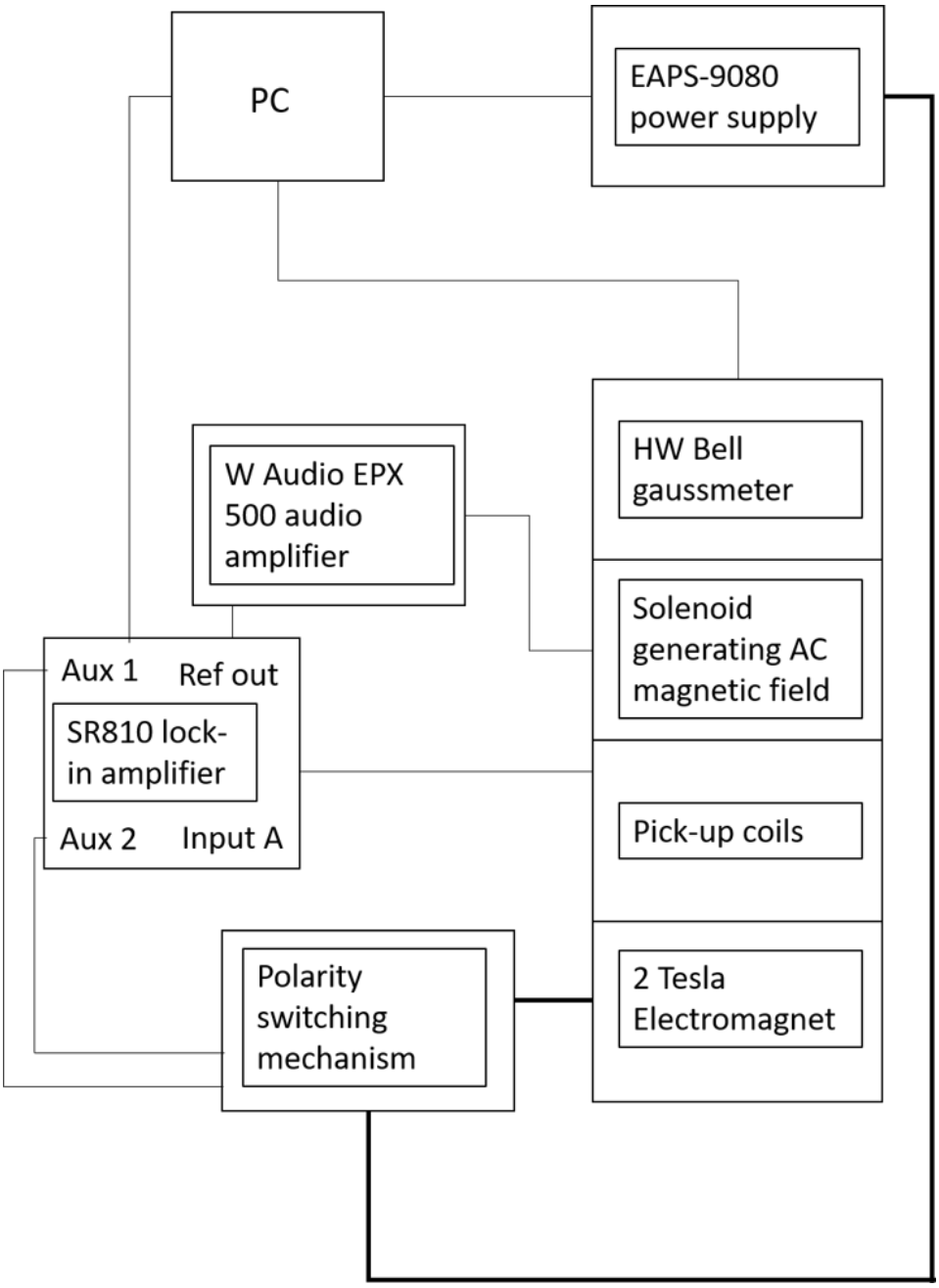

Figure 2.1: Block diagram of the susceptometer, depicting wire connections and component locations.

routine.

The AC magnetic field in theory needs to be constant amplitude and infinitely small. In practice that is not possible to achieve.In reality a small perturbing field can be generated through controlling the amplitude of alternating current. An alternating current is produced using the internal oscillator of a SR810 Lock-in amplifier. This current has a fixed output with a frequency set to 20 kHz using the lock-in amplifier.

The current output from the lock-in is then fed through a W audio EPX 500 audio amplifier. This is used to amplify the alternating current and enables the user a level of control over the strength of the AC field. Finally, the amplified current is passed into a double counter-wound solenoid assembly to produce the AC field which can be seen in figure 2.2. The solenoid assembly consists of an air cored solenoid with a second solenoid wound around it in the opposite direction. The reason for this is to limit the leakage of the AC field into the pole caps of the electromagnet. This is because the permeability of the pole caps changes with the DC field, which in turn alters the path of AC field fringing through it. This in turn affects the AC field strength in the centre of the solenoid. This was modelled previously [45].

The transverse susceptibility signal is measured by two sensing coils which are counter wound and placed parallel to each other as shown in figure 2.2. They are identical in their size and number of turns however one is used as the sample coil and the other is used as a compensation coil. The two coils are connected in series and then wired across a compensation circuit which allows the output circuit to be 'balanced', where there is zero output voltage when no sample is present. The compensation circuit is composed of four multiturn pots which can be seen in figure 2.3. The output of the compensation circuit is then connected to the lock-in amplifier.

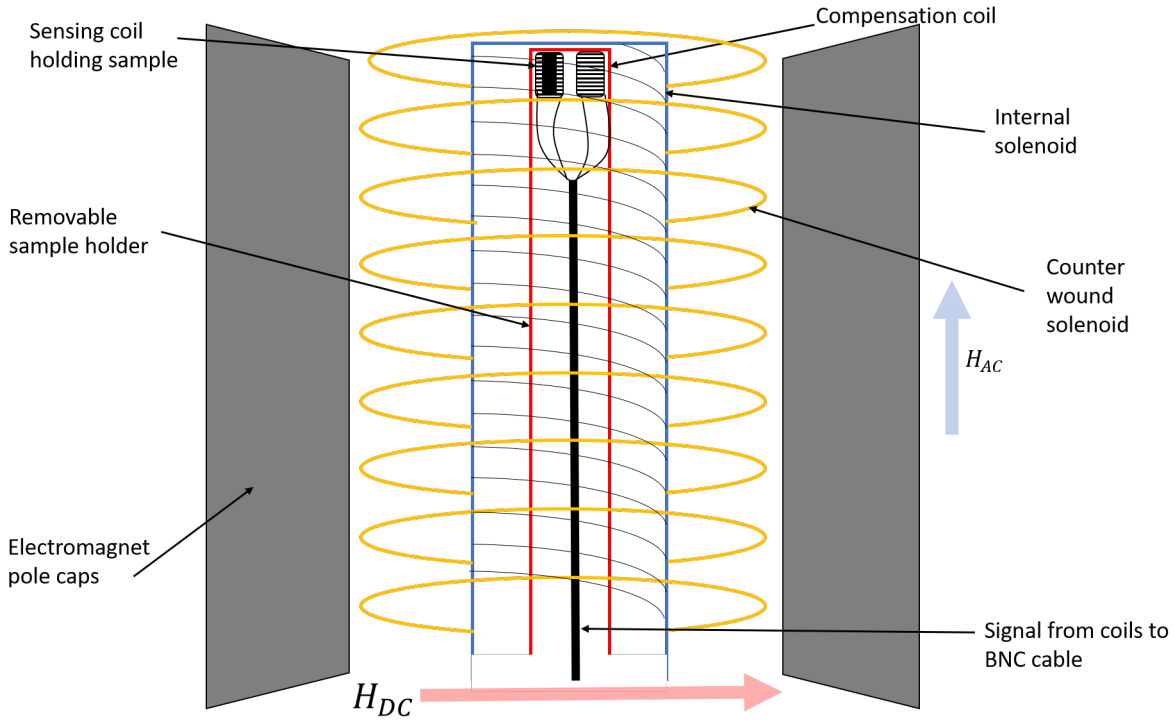

Figure 2.2: Planview layout of the susceptometer for the linear transverse susceptibility measurements. Not shown is the Hall probe measuring the DC field held between the pole caps above the solenoid.

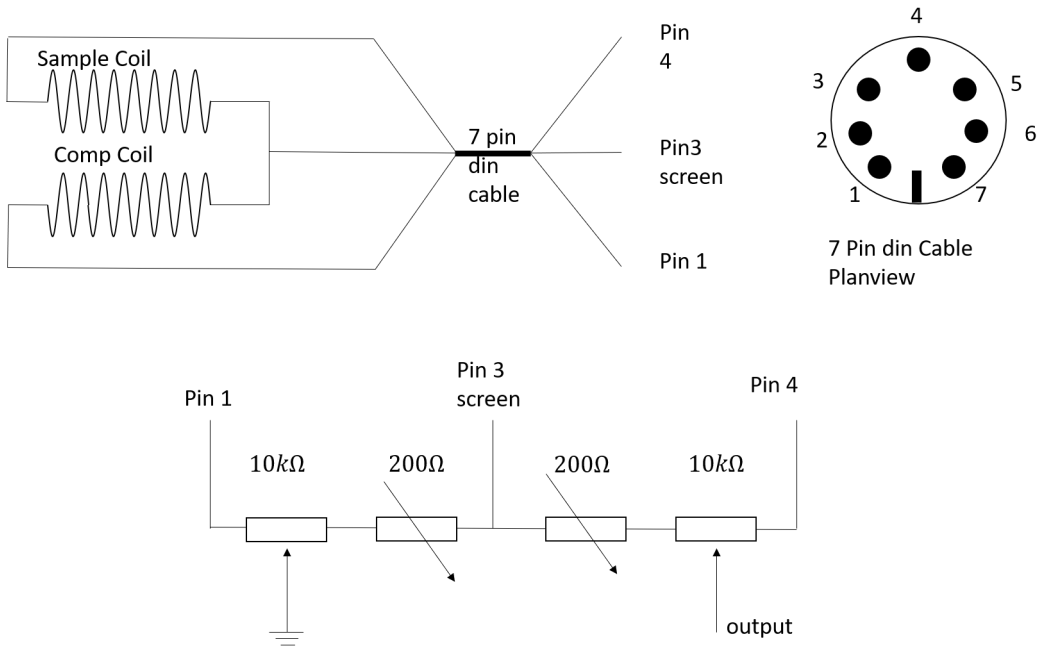

Figure 2.3: Circuit diagram of the linear transverse susceptibility sensing coils and their compensation circuit

The reason for using two coils instead of just one can be seen by deriving an equation for each coils instantaneous emf generated when placed in a changing magnetic field. This is Faraday's law given by,

$$\varepsilon = -\frac{d\Phi}{dt} \tag{2.1}$$

Where ε is the induced emf, and Φ is the magnetic flux through the coil.

Flux linking the coil is given by,

$$\Phi = NBA \tag{2.2}$$

where A is the cross sectional area of the coil and N is the number of turns. Therefore,

$$\varepsilon = -NA\frac{dB}{dt} \tag{2.3}$$

For an air cored inductor, $B = \mu_0 H$, so for any air cored conductor in a changing magnetic field, the induced emf becomes,

$$\varepsilon = -NA\mu_0\frac{dH}{dt} \tag{2.4}$$

For the susceptibility measurements part of the air core will be replaced with a magnetic sample with relative permeability μ_r and cross sectional area, A_s, the emf then becomes,

$$\varepsilon = -NA_s\mu_0\mu_r\frac{dH}{dt} \tag{2.5}$$

Now by adding the emf from equation 2.4 to 2.5 whilst compensating for the air in the sample coil, the emf becomes,

$$\begin{aligned}
\varepsilon &= -NA\mu_0\frac{dH}{dt} - NA_s\mu_0\mu_r\frac{dH}{dt} + NA_s\mu_0\frac{dH}{dt} \\
&= -N\mu_0\frac{dH}{dt}(A + A_s\mu_r - A_s) \\
&= -N\mu_0\frac{dH}{dt}(A + A_s[\mu_r - 1]) \\
&= -N\mu_0\frac{dH}{dt}(A + A_s\chi_m)
\end{aligned} \tag{2.6}$$

The magnetic susceptibility of a sample χ_m, is equal to $(\mu_r - 1)$. By using two coils one air cored (compensating coil) and one containing the sample, the induced emf for the sum of both coils can be obtained by subtracting, 2.4 from 2.6 which gives,

$$\begin{aligned}\varepsilon &= -N\mu_0\frac{dH}{dt}(A + A_s\chi_m) + NA\mu_0\frac{dH}{dt} \\ &= -N\mu_0\frac{dH}{dt}(A + A_s\chi_m - A) \\ &= -N\mu_0\frac{dH}{dt}A_s\chi_m \end{aligned} \tag{2.7}$$

This equation shows that the emf induced on the counter-wound coils is directly proportional to the sample's transverse susceptibility. The other factor of using two coils is that both coils need to be balanced. This requires the use of the resistor circuit shown in figure 2.3. The two coils are balanced to have a net emf of zero before the sample is inserted into the sample coil.

Section 2.2 begins on the next page.

2.2 Calibration of the AC field

Several tests were completed to quantify the susceptometer's properties. The first measurement was of the AC magnetic field generated by the solenoid. For a standard solenoid a raised plateau is expected. However, as this is a double counter-wound solenoid, the AC field will cancel out in some places which leaves this two peaked shape. This was measured along several points along the length of the double counter-wound solenoid. The results were plotted in figure 2.4. It can be seen that there is a saddle like feature between 43 cm and 55 cm. The peaks in figure 2.4 occur when the AC field is at its maximum. For this reason the sensing coils are placed at approximately 50 cm so the maximum AC field will coincide with the sample. The uncertainties for this experiment come from the ruler used to measure the position of the signal coils and the uncertainty in the measurement of the Hall probe. The uncertainty in the ruler is $\pm 0.5 cm$ and the uncertainty in the Hall probe is $0.25\% + 3\, counts$ where a count is the lowest unit on the display so in this case is 0.001.

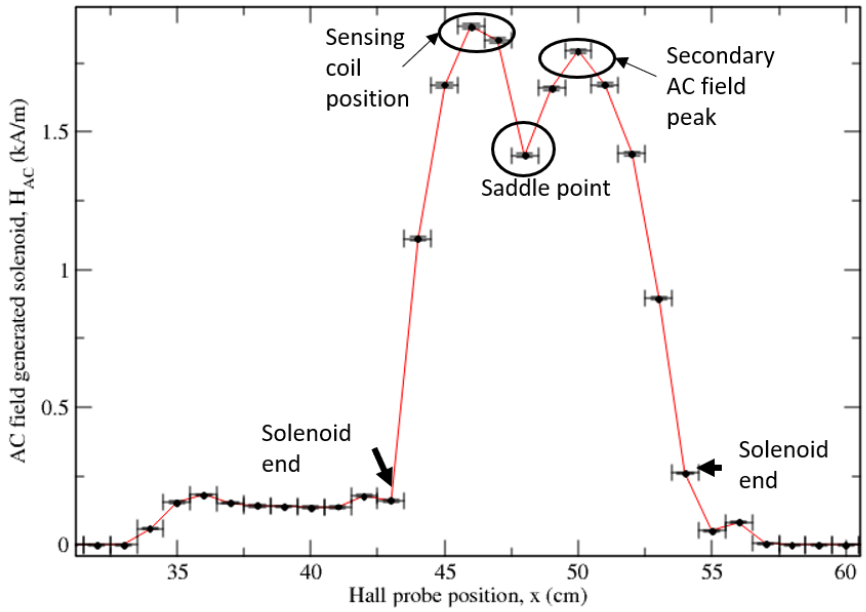

Figure 2.4: A plot of the AC magnetic field generated by the double wrapped solenoid against the position of the axial Hall probe. The saddle point is caused by the AC fields interacting.

2.3 Changes to the linear susceptometer.

It was stated that a stable consistent AC field is needed for the linear transverse susceptibility to produce reliable results. This was difficult to achieve as the instruments present on the susceptometer struggled to produce a stable ac field. This field was being generated by sending an alternating current in the form a sinusoidal wave using the internal oscillator of a Stanford Instruments SR510 lock-in amplifier. The issue was that the internal oscillator had degraded with age and so the signal produced excessive noise.

A typical waveform generated by this oscillator can be seen in figure 2.5. This resulted in less stable measurements and fluctuations in the AC field which greatly affected the measured susceptibility. The signal to noise ratio for this alternating signal was found to be $35.4dB$. This was calculated from the signal voltages measured using an oscilloscope and the equation, $SNR = 20log_{10}(\frac{V_s}{V_n})$. Where, SNR is signal to noise ratio, V_s is the signal voltage and V_n is the voltage of the noise. The issue with the unstable ac field was rectified by replacing the lock-in amplifier with a new Stanford Instruments SR810 Lock-in amplifier with a much cleaner oscillator output and an auto phase function for finding the maximum susceptibility signal from the sample (is not available on the SR510). A typical waveform for the new internal oscillator in the SR810 can be seen in figure 2.6. The Signal to noise ratio was calculated for the new waveform and was found to be $55.1dB$. Therefore, the signal to noise ratio has been improved by $20dB$.

Figures 2.5 and 2.6 can be seen on the next page.

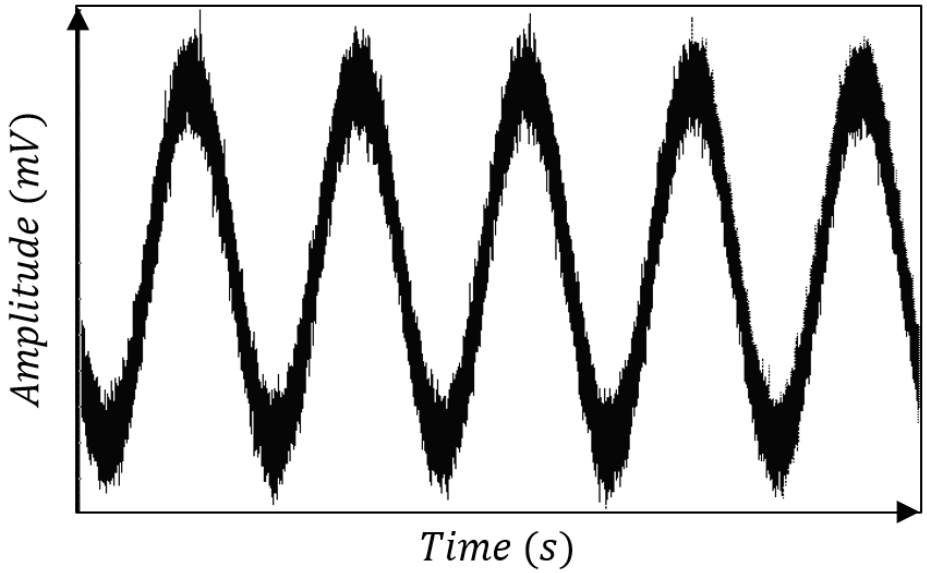

Figure 2.5: The Voltage-time graph at 20kHz from an oscilloscope for an SR510 lock-in amplifier. The amplitude is the AC field current. The SNR for this waveform is $35.4dB$.

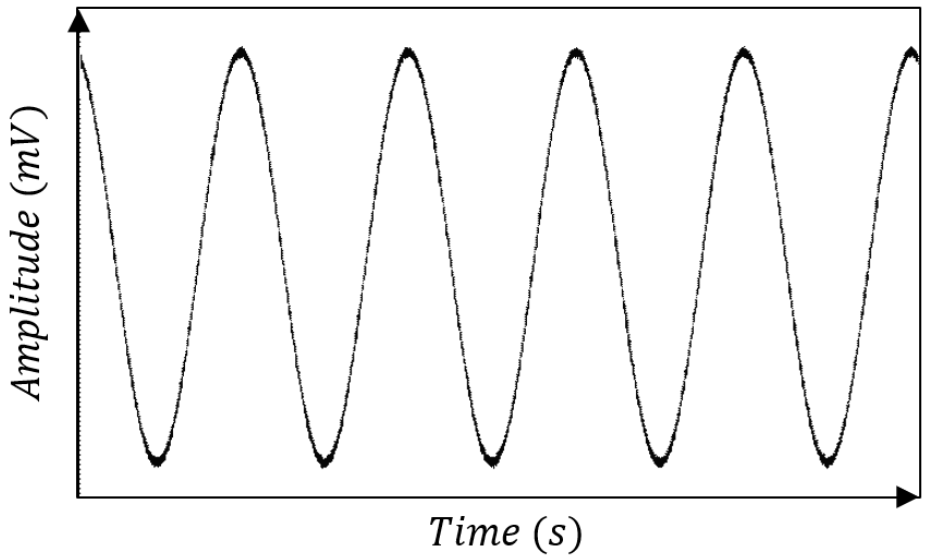

Figure 2.6: The Voltage-time graph at 20kHz from an oscilloscope for an SR810 lock-in amplifier. The amplitude is the AC field current. The SNR for this waveform is $55.1dB$.

2.4 Linear response to the variation of AC field.

The linear transverse susceptibility response is most strongly present in the particles whose easy axes are parallel to the AC magnetic field with a DC bias field at the anisotropy position, H_k applied along them [3, 50]. This bias field causes a rotation of the magnetic moment from the easy axis towards the hard axis. The relationship between the particle axis and the AC and DC field can be seen in fig 2.7. For a small

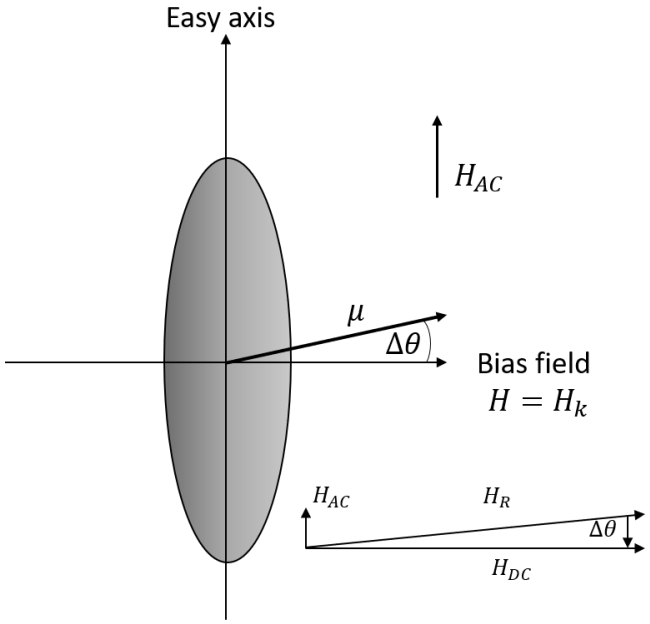

Figure 2.7: Response of a particles magnetic moment, μ when acted upon by an applied DC field, H_{DC} and an instance of the applied peak AC field, H_{AC}. The resultant field is H_R, which is parallel to the orientation of the particle's magnetic moment and will change with the oscillation of the AC field.

AC magnetic field the displacement angle of the particle, $\Delta\theta$, will be proportional to H_{AC} as shown in 2.7. Therefore,

$$\Delta\theta \cong \frac{H_{ac}}{H_{dc}} \tag{2.8}$$

The change in the magnetic moment, $\Delta\mu$, measured along the easy axis is given by,

$$\Delta\mu = \mu sin\Delta\theta \tag{2.9}$$

Using the small angle approximation $sin\theta \approx \theta$ as $\theta \to 0$ equation 3.2 becomes,

$$\Delta\mu = \mu \cdot \Delta\theta \tag{2.10}$$

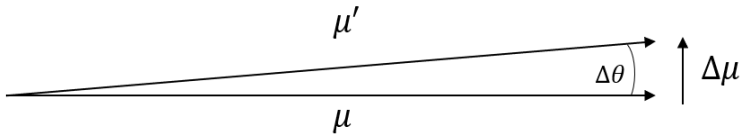

Figure 2.8: Change in magnetic moment, $\Delta\mu$ in the direction of the DC field due to the applied instantaneous AC field which is oscillating. μ is the magnetic moment, μ' is the magnetic moment under the affect of the AC field and $\Delta\theta$ is the angle between those moments.

A substitution can then be made for $\Delta\theta$ from equation 3.1,

$$\Delta\mu = k_1\mu \cdot H_{ac} \tag{2.11}$$

where k_1 is a constant of proportionality [45]. As can be seen from the resultant equation the relationship between the AC field and the magnetic moment, which is proportional to the transverse susceptibility, is linear. This relationship was then tested experimentally using the susceptometer. The AC field was changed incrementally and the induced susceptibility was recorded. A plot of those results can be seen in figure 2.9 which is a highly correlated linear relationship with a correlation coefficient of r=0.9998. Therefore this susceptometer behaves exactly as theory suggests. The vertical error bars were not included on this figure as their magnitude was significantly smaller than the horizontal error bars.

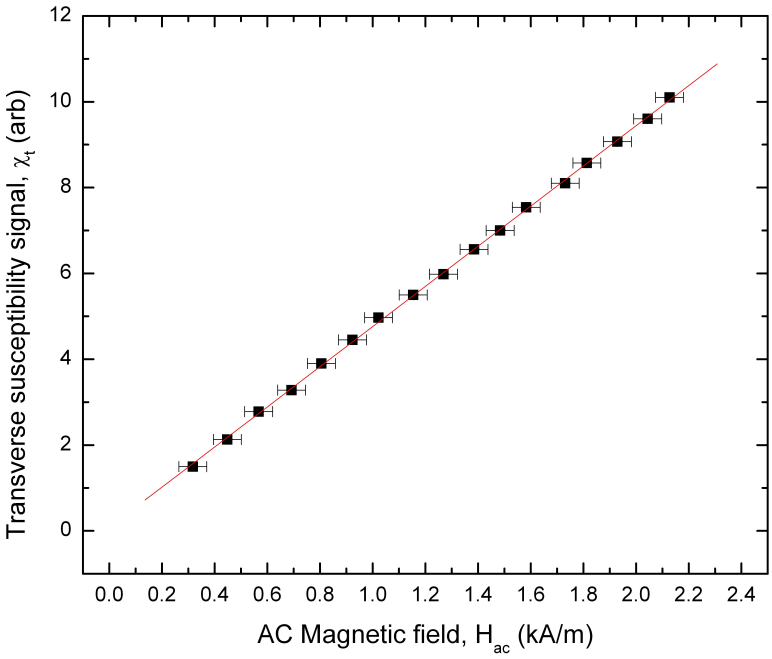

Figure 2.9: Plot of the transverse susceptibility signal against the AC magnetic field generated by the solenoid.

2.5 Non-linear transverse susceptometer

The non-linear transverse susceptometer is designed to measure the susceptibility of a magnetic material, which parallel with the DC magnetic field and transverse to a constant amplitude AC magnetic field. The requirements for the AC field are the same in this method as the linear transverse susceptometer. The key difference is that now the sample is in line with the DC field and orthogonal to the AC field. The direction of measurement is in plane with the DC field. The orientation of these fields can be seen in figure 2.10.

The susceptometer is still connected together as shown in figure 2.1. The only difference in hardware is the sensing coils. Due to the sample being re-orientated in plane with the DC field a different set of coils was needed to facilitate this. This change can be seen in figure 2.10. Here it is shown that there are two coils present as with the linear method. However, only one coil is in use. The reason for this is explained below.

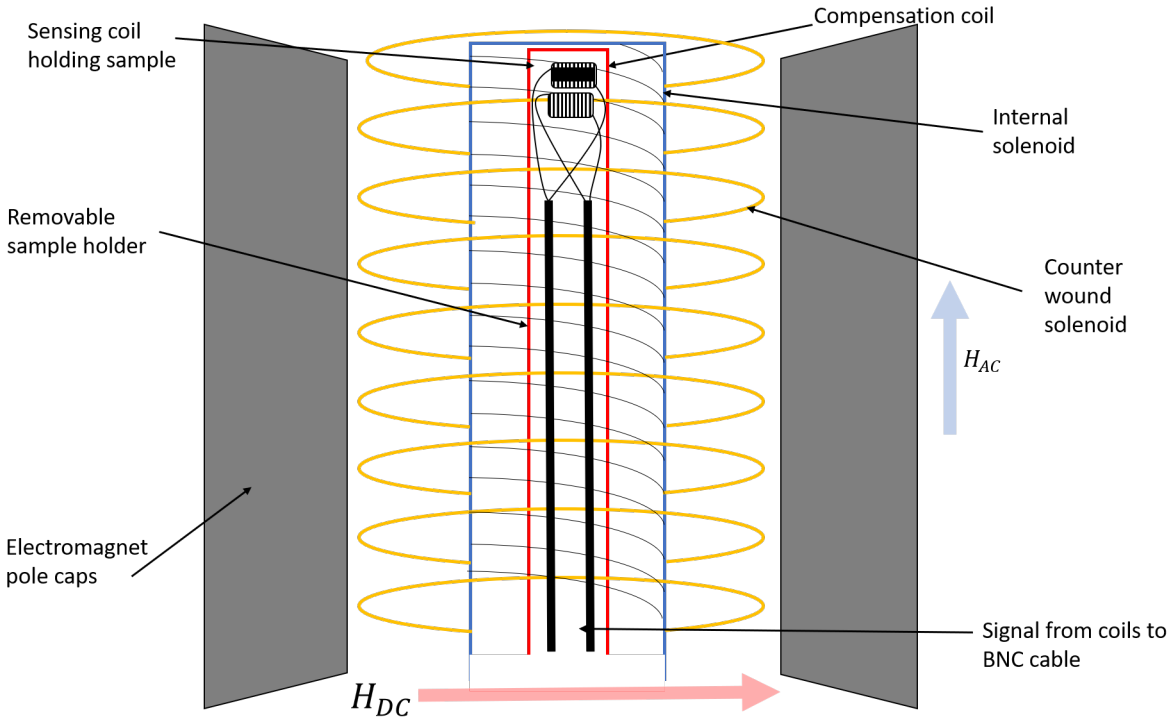

Figure 2.10: Layout of the susceptometer for non-linear transverse susceptibility measurements

The main software change involves the lock-in amplifier. As was previously mentioned the lock-in amplifier uses the frequency of the emitted AC signal to measure the susceptibility signal. However, in the non-linear case from Chantrell et al [36] the susceptibility is proportional to the second harmonic of the frequency, not the first. The reason for measuring at the second harmonic can be explained using

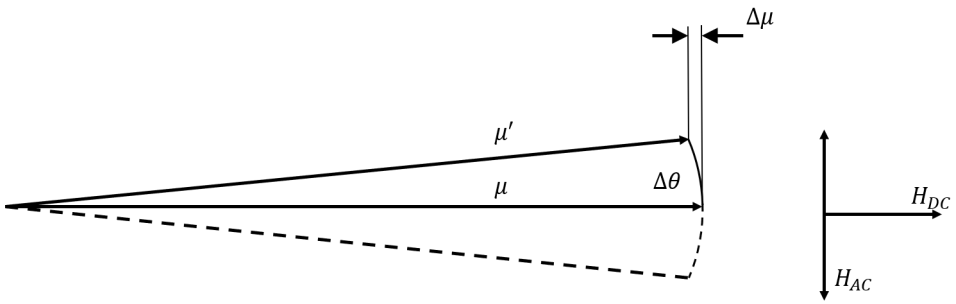

Figure 2.11: Change in magnetic moment, $\Delta\mu$ in the presence of the DC field due to the instantaneous transverse AC magnetic field. μ is the magnetic moment, μ' is the magnetic moment under the affect of the AC field and $\Delta\theta$ is the angle between those moments.

figure 2.11. In the non-linear case the change in magnetic moment is measured in the direction of the DC field. For each oscillation of the AC field it can be seen that the magnetic moment, μ, will oscillate from the rest position in line with the DC field to the position at μ'. On the return oscillation in the opposite direction the moment will move to a mirrored position and then return to its origin. This means that for each oscillation of the AC field the change in magnetic moment $\Delta\mu$ will go through two cycles. The frequency is double that of the AC field, $2f_{ac}$. This change to $2f_{ac}$ is done experimentally using the lock-in amplifier. It has a setting which allows the user to issue a command to change the reference frequency in relation to the output of the AC field. This is therefore set to read at the second harmonic. This also allows the use of only one sensing coil due to it not picking up other signals at $2f_{ac}$.

Section 2.6 continues on the next page.

2.6 Non-linear susceptibility response to variation of the AC field.

The non-linear transverse susceptibility is also proportional to the AC field and thus a relationship can be determined as was done in section 3.2. For a small AC field ($H_{ac} \to 0$) with a constant DC field along the sample, the displacement angle, $\Delta\theta$, will be proportional to the AC field,

$$\Delta\theta = k_1 \Delta H_{ac} \tag{2.12}$$

where k_1 is a proportionality constant. The change in magnetic moment, $\Delta\mu$, is measured in the direction of the constant DC magnetic field is given by,

$$\Delta\mu = \mu - \mu cos\Delta\theta$$

$$\Delta\mu = \mu(1 - cos\Delta\theta) \tag{2.13}$$

A series expansion for $cos\Delta\theta$ can be used to simplify equation 4.2.

$$cos\Delta\theta = 1 - \frac{(\Delta\theta)^2}{2!} + \frac{(\Delta\theta)^4}{4!} - \frac{(\Delta\theta)^6}{6!} + ... \tag{2.14}$$

So for small angles $cos\theta$ can be approximated as $1 - \frac{(\Delta\theta)}{2!}$. Therefore equation 4.2 can be given as,

$$\Delta\mu = \mu(1 - [1 - \frac{(\Delta\theta)}{2!}])$$

$$\Delta\mu = \frac{\mu}{2}(\Delta\theta)^2 \tag{2.15}$$

Making a substitution for $\Delta\theta$ in equation 4.1 the change in magnetic moment becomes,

$$\Delta\mu = \frac{\mu}{2}(k_1 \Delta H_{ac})^2$$

$$\Delta\mu = k_1^2 \Delta H_{ac}^2 \tag{2.16}$$

where k_1^2 is a constant of proportionality. From this derivation it can be observed that the relationship between the non-linear transverse susceptibility and the applied AC field should be square when the DC field is constant. This was tested experimentally with a constant DC field and a changing AC field. The AC field

was altered by changing the amplification of the field on the audio amplifier. The response of the sensing coil is shown in figure 2.12. The relationship is non-linear however, it does not strongly correlate. The reason this measurement was not strongly consistent with theory is likely due to the DC field the sample is experiencing. The constant DC for better results should be at an anisotropy point. In the case of this measurement it was not at an anisotropy point causing a weaker correlation. Another issue stems from how much the AC signal needs to be amplified by the audio amplifier. The non-linear susceptibility signal is very small and so to induce change with the current system it had to be amplified to a larger amount. This has also caused the relationship to shift due to the sample experiencing thermal effects through a higher current. To improve this measurement the DC field should be kept constant at the anisotropy field value and as small an AC field as possible. The AC field value should also be changed in very short increments which was not possible due to the nature of the amplifier being used.

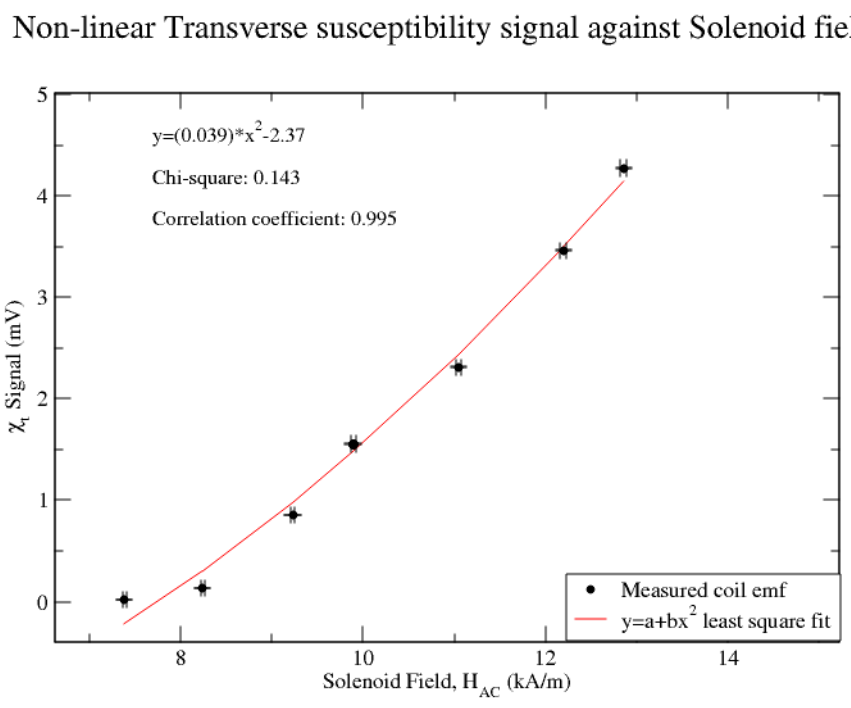

Figure 2.12: A plot of the non-linear transverse susceptibility against the AC magnetic field produced by the solenoid. Here, the variables x and y represent AC field and non-linear transverse susceptibility respectively.

2.7 LabVIEW Program

The majority of the instrumentation in the susceptometer was controlled using a LabVIEW program. This included initialising the instruments, controlling them through a series of commands unique to each device and finally storing and processing data read from each device. The instruments directly controlled by the VI are the lock-in amplifier, the polarity switching mechanism and the power supply. The routine then read data from a Hall probe measuring the DC field and the induced emf caused by the susceptibility on the lock-in amplifier. The process the LabVIEW routine uses can be seen in the form of a flow chart displaying the pseudo code in figure 2.13.

The set up of the LabVIEW routine for experimentation can be explained using the front panel seen in figure 2.14. In the initial stage of operation the maximum DC field must be set as well as the field resolution. The default values can be seen in the figure however, the magnet is capable of fields as high as 2T.

Before the measurement can begin the lock-in amplifier has to be initialised to ensure it has been configured for either linear or non-linear measurements. The VI can then be run at this stage a window will pop up asking for the user to name a file to record the measured values. The VI will then run until the DC field has been swept from the positive maximum field value to the negative maximum field value and back again. Throughout the measurement run the measured DC field and voltage from the lock-in amplifier will be plotted in real time on the axis seen in figure 2.14.

As was mentioned above the lock-in amplifier was updated to a newer model. This caused issues with the original configuration of the LabVIEW code due to the two devices using separate languages for their operating codes. The first being a simple ASCII based language on the SR510 and the second based on the IEEE-488.2 Standard commands for programmable instruments (SCPI). This meant that all code concerning the lock-in amplifier had to be checked and updated to account for the new device. This is also included the switching mechanism as that was controlled through ports on the lock-in which would switch when a command was sent to the relevant auxiliary port. There were no discernible differences in the

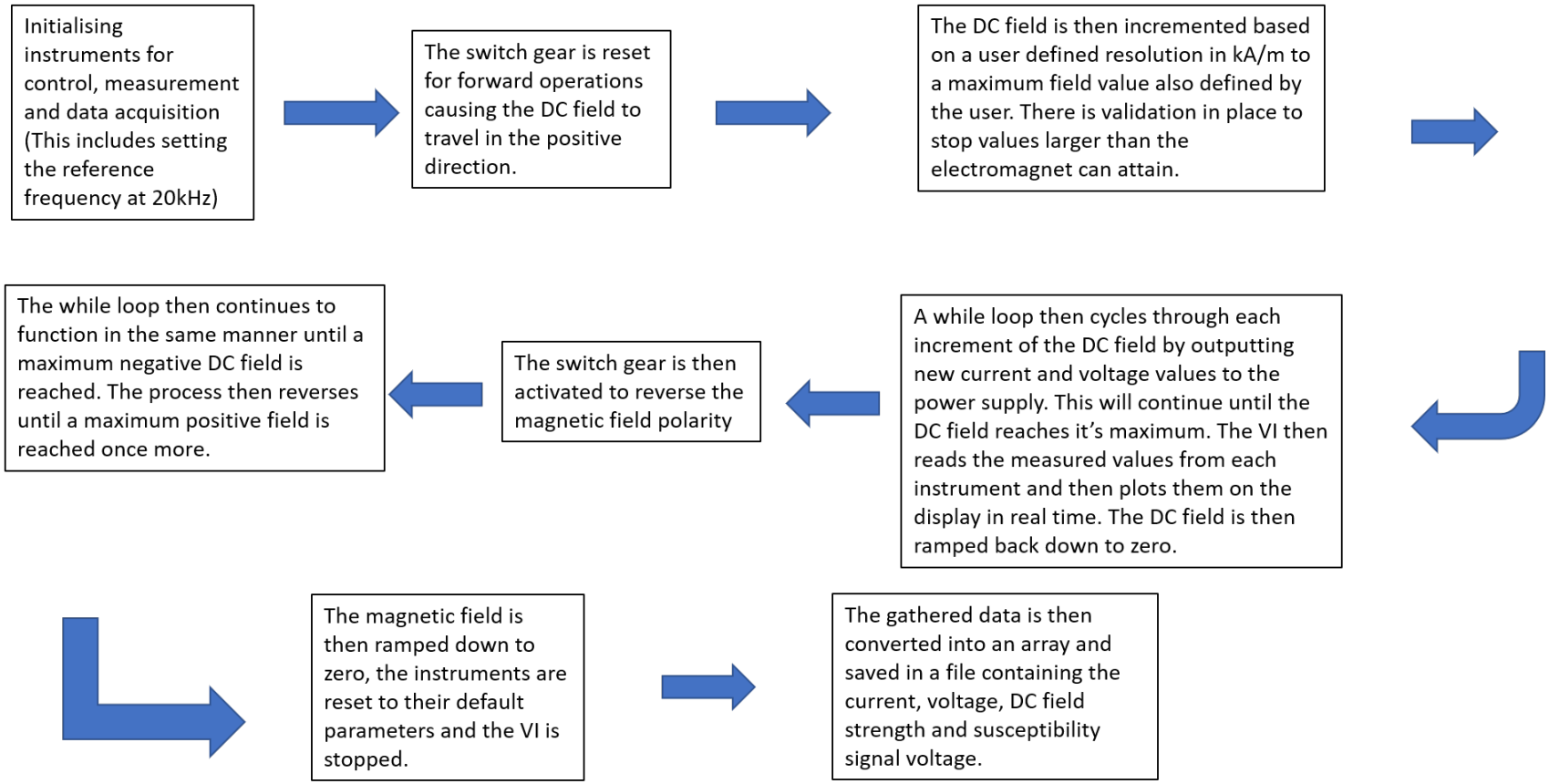

Figure 2.13: A flow chart indicating the pseudocode of the LabVIEW program. This indicates the process the program goes through in a typical experiment.

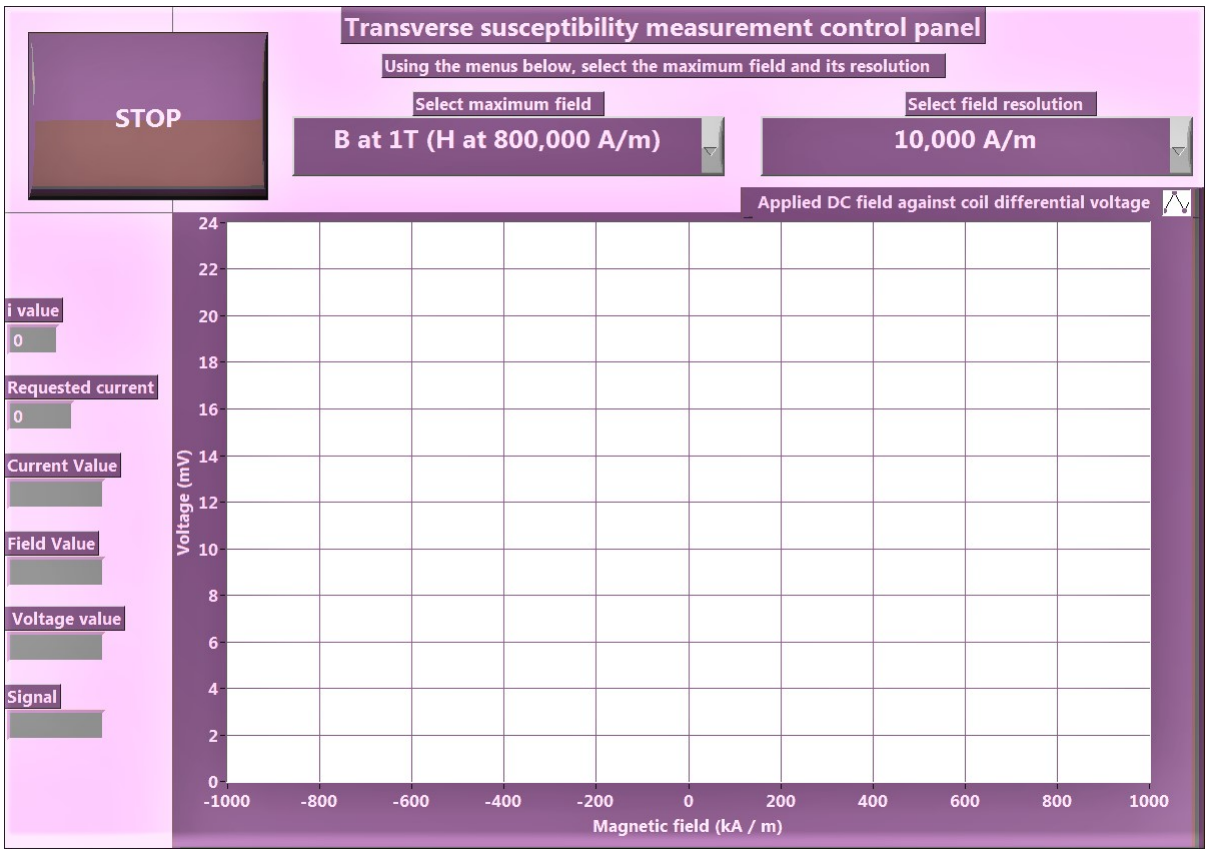

Figure 2.14: Front panel of the LabVIEW VI used to control the susceptometer

operation of the routine after the lock-in was replaced. However, the measurements achieved were consistently better with a much cleaner signal.

There are some improvements that could be made to the VI to improve the measurements of the transverse susceptibility. The information of interest in these measurements is in the anisotropy distributions and switching points. Due to the nature of the samples being tested, the switching points all occur at very low field values. The code could therefore be improved by dynamically changing the DC field resolution so as it approaches a low field more measurements are taken at incrementally smaller steps. This would allow for greater clarity in the switching behaviour. The reason high resolutions weren't used by default, was due to the total measurement time greatly increasing with an increase in resolution. Therefore a dynamic resolution would only have a high resolution at the points of interest and the rest of the sweep could occur at a low resolution bringing the overall measurement time down.

Chapter 3

Samples

There were three different magnetic materials used during the course of this project. The first was maghemite, $\gamma - Fe_2O_3$, which was tested as both a magnetic tape and a random powder. The second was a magnetite powder, Fe_3O_4. Finally a pseudo-tape sample of Chromium Dioxide, CrO_2, was used as it is known to produce strong susceptibility signals when using the linear transverse susceptibility signal regardless of texture.

The properties of each sample was also examined using a vibrating sample magnetometer. The materials saturation magnetisation, coercivity and remnant magnetisation will all be measured. The coercive field measured here should be consistent with the output of the linear susceptometer as stated by theory [3].

3.1 Maghemite ($\gamma - Fe_2O_3$).

Maghemite is a ferrimagnetic member of the iron oxide family, that is most commonly used in magnetic recording media. Maghemite, $\gamma - Fe_2O_3$, is produced by oxidising Fe_3O_4 under specific conditions. Elongated particles of $\gamma - Fe_2O_3$ are mostly commonly made into magnetic tapes due to it's magnetic properties and the high Curie temperature of 600^oC, which stops unwanted behaviour due to thermal energy at normal operating temperatures. Maghemite has a cubic crystal structure with a tetragonal supercell, its' space group is $P4_132$. The maghemite

crystal can be seen in figure 3.1, it has the lattice parameters: $a = b = 8.33\text{Å}, c = 24.99\text{Å}$, $\alpha = \beta = \gamma = 90°, z = 8$, and super-cell volume, $V = 1743.02\text{Å}^3$. This material was chosen for testing as it was previously tested in transverse susceptibility research in the department by Cookson. The sample tested is a randomly orientated magnetic powder with a grain size of approximately 0.5 micrometres. A vibrating sample magnetometer (VSM) was

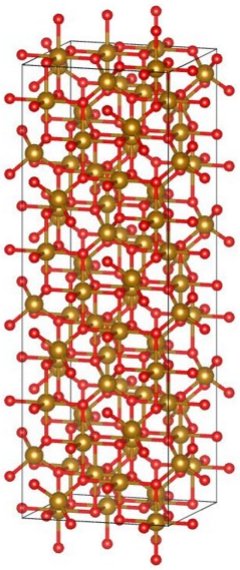

Figure 3.1: The crystal lattice of $\gamma - Fe_2O_3$. With lattice parameters obtained from Pecharroman et al[52].

used to measure the magnetic properties of the sample of randomly orientated $\gamma - Fe_2O_3$ powder. The hysteresis loop generated by the powder sample can be seen in figure 3.2. The saturation magnetisation, coercivity and remanance can be can be seen in table 3.1 with uncertainties. The coercivity, H_c was measured as $32 \pm 5\,kA/m$, typical values range from $25 - 30\,kA/m$ [37]. The measured value was within error of the expected range of values. The other parameter of interest from the hysteresis loop is the remanence ratio, which has a value here of 0.5 ± 0.1. This is of interest as the remanence ratio can be used as a measure of the orientation of the magnetic moments in the sample. A more ordered sample has a remanence closer to 1, with randomly orientated moments having a remanence of about 0.5. Therefore, the magnetic moments of this sample are randomly orientated.

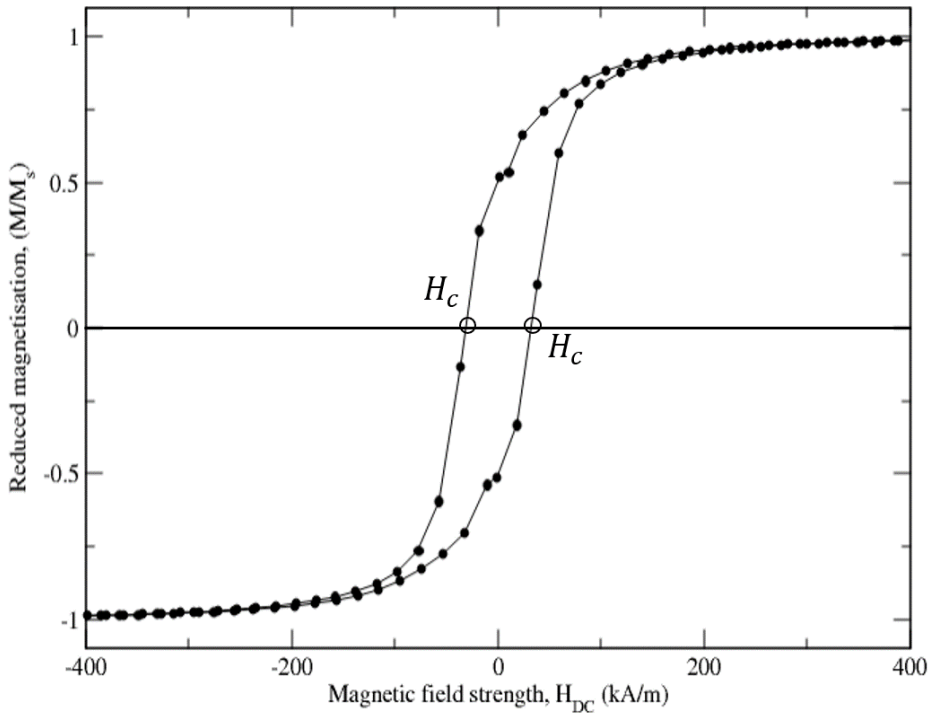

Figure 3.2: A hysteresis loop generated by a VSM for a randomly packed powder sample of $\gamma - Fe_2O_3$.

$M_s(Am^2)$	H_C(kA/m)	$\frac{M_r}{M_s}$
$(9.70 \pm 0.02) \times 10^{-4}$	32 $\pm$5	0.5 $\pm$0.1

Table 3.1: Magnetic properties of $\gamma - Fe_2O_3$ with uncertainties.

3.2 Magnetite, (Fe_3O_4).

Magnetite is another Ferrimagnetic member of the iron oxide family. It is naturally occurring material and was the first permanent magnetic material recognised. This was due to naturally magnetised chunks of magnetite, called lodestones, attracting iron, a property discovered over 2500 years ago. In the area of magnetic recording media, magnetite was the first material made into magnetic tapes. However, more recent applications focus on the use of magnetite nanoparticles in medical research. For this reason, the magnetite sample used in this research is a randomly orientated powder sample. Magnetite has a cubic crystal structure with space group: $Fd\bar{3}m$. The magnetite crystal structure can be seen in figure 3.3, it has lattice parameters: $a = b = c = 8.397\text{Å}, \alpha = \beta = \gamma = 90°, z = 8$, and volume, $V = 575.9\text{Å}^3$. This sample of magnetite consists of randomly orientated spherical particles with a grain size of approximately $10\,nm$. It was produced by a chemist at UCLan. Due to their spherical shape this sample should not possess any shape anisotropy due to the uniformity of the axes. However, the particles are dry and uncoated, this causes agglomeration. The agglomerated particles form misshapen clumps which are non-uniform and so have small amounts of induced anisotropy. Due to the size of the particles the net magnetic moment is much weaker than a ferromagnetic or ferrimagnetic material. The anisotropy energy is dependent on a particles size. Therefore, particles with a small diameter will have a limited anisotropy energy which can be smaller than the thermal energy. In this case, the thermal energy will cause the magnetic moment to randomly switch and rotate: this simulates paramagnetic behaviour but with a much larger magnetic moment. This is superparamagnetic behaviour [53]. The VSM was also used to measure the magnetic properties of this magnetite sample. The hysteresis loop generated is shown in figure 3.4. The saturation magnetisation,coercivity and remanance can be can be seen in table 3.2 with uncertainties. The coercivity was measured as $3 \pm 1\,kA/m$. As stated above, this material exhibits superparamagnetic behaviour. Because of this it is expected for the hysteresis loop to be closed. Therefore, having no coercivity as it is quickly demagnetised by the applied field. However, due to nanoparticles agglomerating into non-uniform clumps, a small amount of anisotropy is induced. This causes the bulk sample to be more resistant to

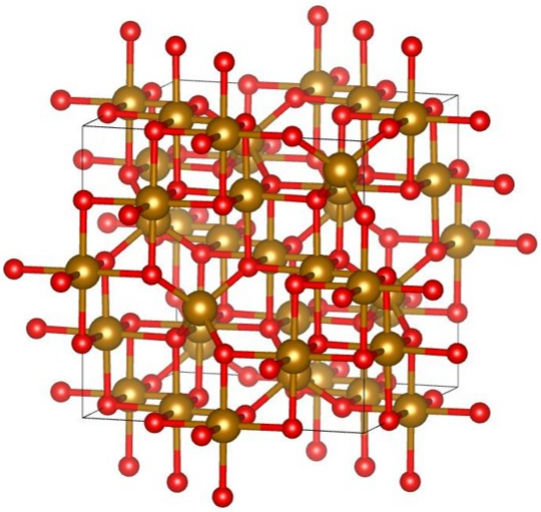

Figure 3.3: The isometric crystal lattice of magnetite, Fe_3O_4. With lattice parameters obtained from Gatta et al [54]

demagnetisation by an applied field but as can be seen here the measured coercivity is close to zero. The remanence ratio was measured to be 0.10 ± 0.04. Values below 0.5 indicate that the sample is orientated perpendicular to the measurement direction. However, in the case of magnetite it behaves as a superparamagnetic particle. Superparamagnetic particles do not experience any hysteresis effects and so do not retain any remanent magnetisation. This can be seen in figure 1.5 where the M-H curve for a superparamagnetic passes directly through the origin in both the x and y axis. In the case of this measurement, the value was zero due to the induced anisotropy in the agglomerated particles.

$M_s(Am^2)$	H_C(kA/m)	$\frac{M_r}{M_s}$
$(1.04 \pm 0.02) \times 10^{-4}$	3 $\pm$1	0.10 $\pm$0.04

Table 3.2: Magnetic properties of the magnetite sample with uncertainties.

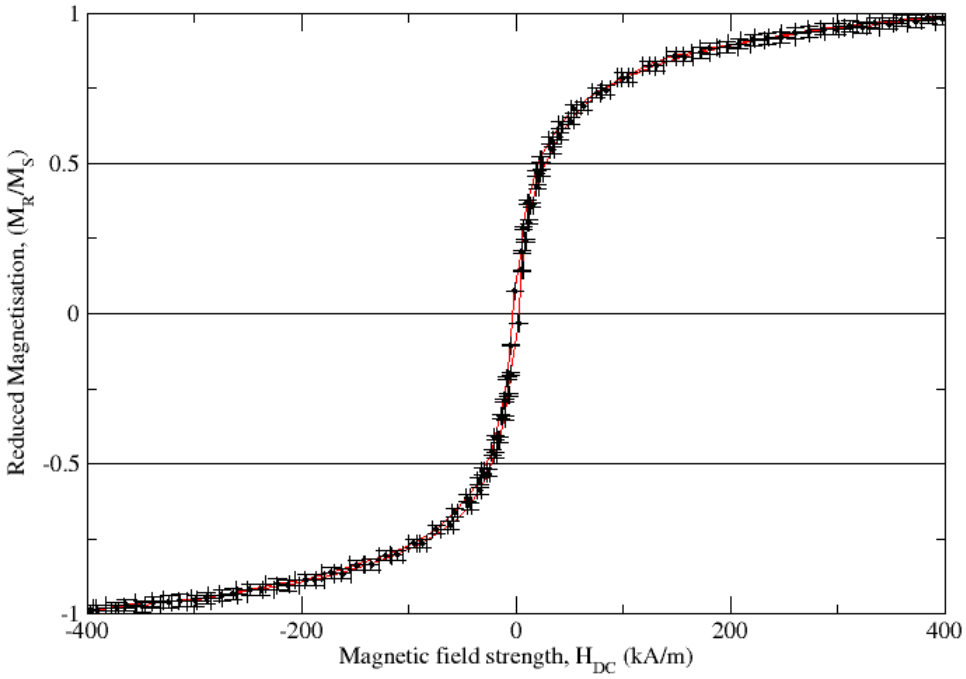

Figure 3.4: A hysteresis loop generated by a vector VSM for a randomly packed powder sample of magnetite.

Section 3.3 continues on the next page.

3.3 Chromium Dioxide (CrO_2).

Chromium dioxide a ferromagnetic oxide, of which there is only one other known compound, EuO. The latter has a curie temperature of 77K so is not useful in real world applications whereas CrO_2 is ferromagnetic at room temperature. CrO_2 is mostly used in magnetic recording media due to it having desirable magnetic properties such as a high coercivity. It was for this reason that it replaced $\gamma - Fe2O3$ as the highest quality material for magnetic recording tapes. This is due to it having a much smaller grain size of about $0.4\,\mu m$ allowing for a higher particle density. CrO_2 has a primitive tetragonal crystal structure, its' space group is $P4_2/mnm$. It's crystal structure can be seen in figure 3.5, it has lattice parameters: $a = b = 4.41\text{Å}, c = 2.91\text{Å}\,\alpha = \beta = \gamma = 90°, z = 8$, and volume, $V = 56.59\text{Å}^3$. Unlike maghemite, CrO_2 has a relatively low curie temperature of $128°C$, this makes it more temperature dependent. This material was included in this work as it is both widely used in magnetic media and can be directly compared with prior work in this area. The sample is a randomly orientated powder set in araldite. The hysteresis

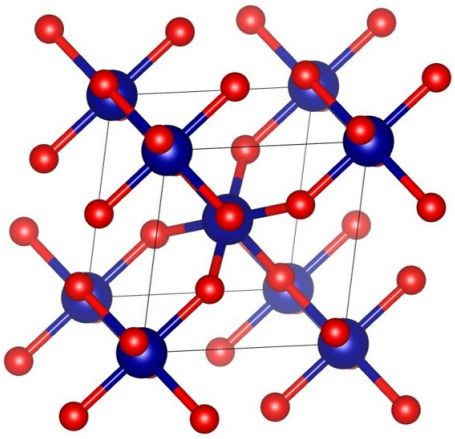

Figure 3.5: The crystal lattice of CrO_2. With lattice parameters obtained from Glemser et al [55].

was also measured using the VSM for this sample. It can be seen in figure 3.6. The saturation magnetisation, coercivity and remanence can be can be seen in table 3.3 with uncertainties. The coercivity was measured to be $54 \pm 5\,kA/m$, with typical values ranging from $30 - 80\,kA/m$ [37] depending on the shape and packing of the particles. The remanence ratio was measured as 0.46 ±0.10, this gives further confidence to the sample being randomly orientated due to it being close to 0.5.

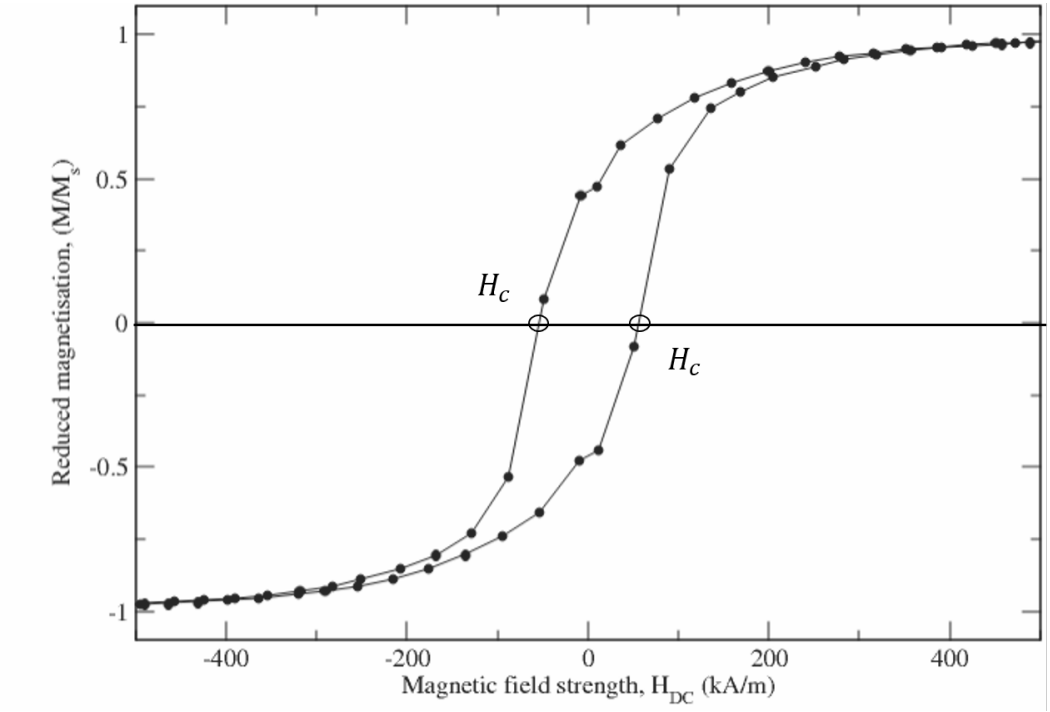

Figure 3.6: A Hysteresis loop generated by a vector VSM for a random powder sample of CrO_2 set in araldite.

$M_s(Am^2)$	H_C(kA/m)	$\frac{M_r}{M_s}$
$(2.24 \pm 0.01) \times 10^{-4}$	54 $\pm$5	0.5 $\pm$0.10

Table 3.3: Magnetic properties of the CrO_2 sample.

Section 3.4 continues on the next page.

3.4 Cobalt surface-modified gamma ferric oxide.

Cobalt doped gamma ferric oxide is a modification to $\gamma - Fe_2O_3$ tapes during the manufacturing process. The cobalt is added to the existing maghemite at the end of the sample processing directly before the tape is coated in the magnetic sample. It was developed as an alternative to $\gamma - Fe_2O_3$ and CrO_2 as a highly coercive and cheap magnetic coating was required to improve the performance of magnetic recording media. It has a higher coercivity than $\gamma - Fe_2O_3$ at about $48\,kA/m$ [37] compared to $32\,kA/m$ for the $\gamma - Fe_2O_3$. CrO_2 is quite expensive to manufacture and so, despite performing to a high level, it was deemed necessary to replace it with a cheaper alternative. The addition of the cobalt to the $\gamma - Fe_2O_3$ sample increases the anisotropy and in turn the coercivity making it perform better in magnetic recording. However, this lowers the curie temperature making it more sensitive to high temperature fluctuations.

This sample was tested in the VSM and the hysteresis loop produced can be seen in figure 3.7. The saturation magnetisation, coercivity and remanence can be can be seen in table 3.4 with uncertainties. The coercivity was measured as 57 ± 5.00. The measured value is higher than that given by Jiles [37]. However, it is within error of the value measured by Cookson [45] who found a value of 52.8 ± 3.1. The remanence ratio was measured to be 0.72±0.10. Magnetic tape needs to be highly textured, where the magnetic moments are aligned along one axis. This is can judged through the remanence ratio as when this value is larger than 0.5 it indicates that the particles are not randomly orientated.

$M_s(Am^2)$	H_C(kA/m)	$\frac{M_r}{M_s}$
$(2.180 \pm 0.005) \times 10^{-4}$	57 ±5	0.7 ±0.1

Table 3.4: Magnetic properties of the Cobalt doped $\gamma - Fe_2O_3$ sample.

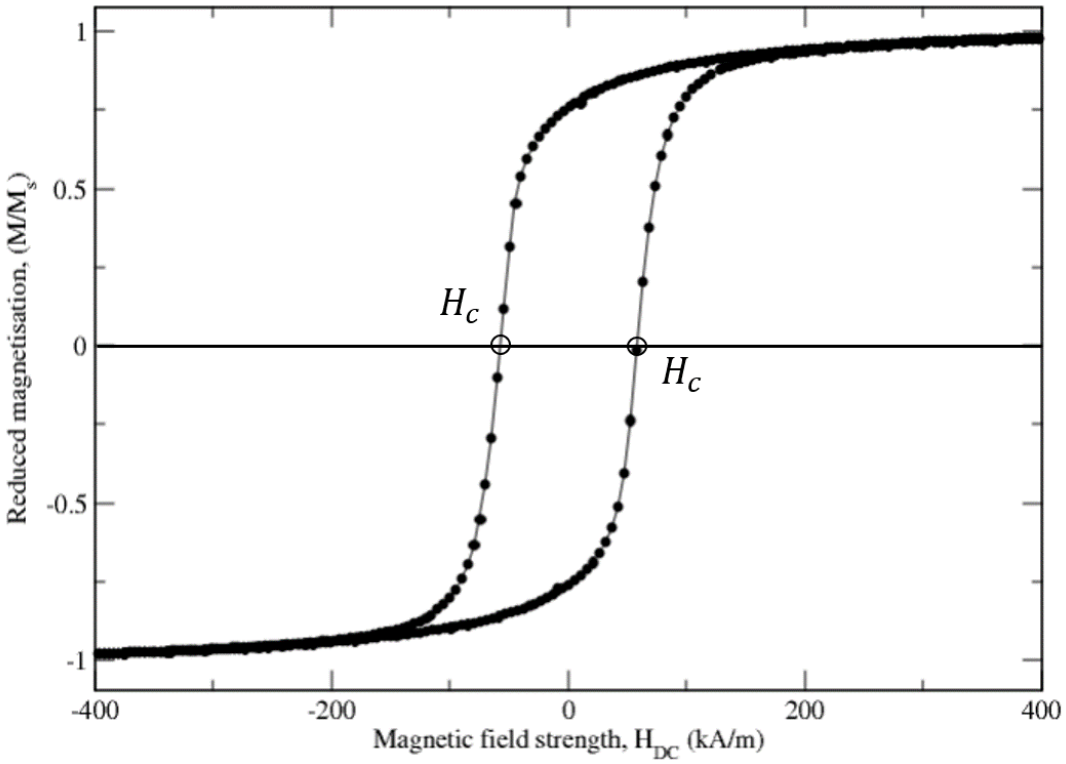

Figure 3.7: A Hysteresis loop generated by a vector VSM for a random powder sample of Cobalt doped $\gamma - Fe_2O_3$.

Chapter 4 begins on the following page.

Chapter 4

Linear Transverse Susceptibility

4.1 Previous work

The theory of linear transverse susceptibility first stemmed from work on reversible transverse susceptibility (RTS) a concept explored by Gans [1] in 1909. The RTS is the initial transverse susceptibility of magnetic material measured transverse to an applied DC bias field. This work was then expanded by Aharoni et al in 1957 [3] who derived an equation for RTS for Stoner-Wohlfarth particles. [2]. In 1987 Pareti and Turilli [4] proved that the model derived by Aharoni was only applicable to particles that did not form magnetic domains by having smaller volumes than the size required to form multi domains and so could not be bulk materials.

LeDang et al [56] looked at transverse susceptibility measurements of amorphous thin films made on glass substrates with high anisotropy. Their results showed a dependence on alignment and directions of the easy axes of the sample. This was the first set of results to be independent of the Aharoni method and displayed the first signs of texture dependence of transverse susceptibility measurements. Powdered samples were first investigated for anisotropy information using the transverse susceptibility technique by Richter in 1990 [57]. It was found that though the method was much faster for determining the magnetic anisotropy compared to other measurement techniques, such as the torque magnetometer which measures hysteresis losses [5], the signal was affected by particles interactions and a hysteresis effect that had not yet been theorised.

The effects of texture on the transverse susceptibility signal and corresponding anisotropy peaks was examined experimentally and theoretically by Sollis et al [49],[48] and Hoare et al [50] in 1992 and 1993. Within these papers it was shown the texture greatly affected the shape of the χ_t plot. In the case of particulate samples, it was an almost flattening of the anisotropy peaks due to interactions between the moments of the randomly orientated particles. It was also shown that a system perfectly aligned, with the particles having the same easy axis orientation, produced a more defined anisotropy peak.

The effects of thermal switching and interactions on transverse susceptibility was explored over a number of years by, Lu et al [58], Huang & Lu[59, 60], Lee et al [61] and Chang & Yang [62]. It was shown that the anisotropy information was unaffected by thermal switching. However, the coercivity was lessened. It was also observed that as the interactions increased the anisotropy shifted position to lower DC field values closer to the coercivity features. It will eventually combine with the coercive field.

Sollis et al [51], in 1996 and 1997, produced results which displayed texture as the important factor in the improvement of anisotropy peaks. With more textured samples producing well defined anisotropy peaks and un-textured or low-textured samples producing suppressed anisotropy peaks. Chantrell et al [63] later published a paper explaining a technique for obtaining anisotropy field distributions from the transverse susceptibility peak by performing a deconvolution on texture of the sample.

It was shown by Spinu et al [64, 65], using a high-frequency oscillator to measure the transverse susceptibility, that with temperature the anisotropy information is lost due to particles becoming superparamagnetic.

Görnert [66] carried out a study comparing the measurement techniques for finding the anisotropy field of magnetic powders. He examined both transverse susceptibility and Singular point detection techniques. When using these techniques to measure anisotropy it was found to be a lower measured value than other techniques. It was suggested these techniques, such as using the transverse susceptibility, were

less accurate because they do not take into account induced switching from particle interactions nor thermal effects. He also measured the anisotropy of samples using "stiffness" techniques such as the torsion pendulum and ferromagnetic resonance. He drew the conclusion that so called "stiffness" techniques to measure a more realistic anisotropy.

In 2002, Cookson worked on a series of measurements in regards to linear magnetic susceptibility using the experimental rig at UCLan [45].He used this rig to measure the RTS of several magnetic tape samples. Using the same method some randomly orientated powdered samples such as maghemite ($\gamma - Fe_2O_3$) were tested and produced suppressed anisotropy peaks. The previous work completed on this technique has shown a heavy dependence on texture to produce anisotropy distributions from transverse susceptibility measurements. This is an issue for measurements on particulate textured samples as shown in both Richter's work [57] and the work of Sollis et al [48]. Measuring the linear transverse susceptibiltiy of some untextured samples produces anisotropy information that is heavily suppressed leading to difficulties in extracting useful information. Because of this and the more prevalent use of powdered samples in modern technology a technique is required that can find anisotropy information less sensitive to the texture of the sample.

Further theoretical work has been published relating to the transverse susceptibility. First Cimpoesu et al [67] proved that the Aharoni model for transverse susceptibility could theoretically be used for modern nanostructured materials. However, there would be significant effects caused by particle interactions, ac field amplitude and thermal effects. In 2014 Dumitru et al [68] measured the reversible transverse susceptibility in large frequency domains up to $2\,GHz$. Much larger than used in this thesis. The anisotropy feature was shown not to change at low frequencies.

4.2 Experimental set-up and Method

For linear transverse susceptibility measurements the susceptometer has a specific set of sensing coils arranged to perform these measurements as can be seen in figure 2.2. In this configuration there are two sensing coils that are counter-wound with respect to each other. The coils are fixed onto a rod which can be inserted into the double wrapped solenoid and supported at the centre. The coils are also fixed at the saddle point of both the electromagnet seen in figure 2.2 and the solenoid. This ensures it experiences the maximum possible AC magnetic field.

The two sensing coils are wired together and feed into 7 pin DIN cable. This cable is then connected to a balance circuit which can be seen in figure 2.3. The circuit is balanced so that the lock-in amplifier it is connected to is zero. This is necessary as a single coil would also be magnetised by the resultant magnetic fields and so the measurements read from the lock-in amplifier would not be exclusively from the sample. This is counteracted by the second sensing coil being counter-wound to the first and so when they are placed in close proximity they cancel each other out leaving only the magnetisation produced by the sample.

The coils are then removed and the sample is inserted into a sensing coil. The coils are then reinserted into the solenoid and the experiment can begin. The measurement direction is aligned with the AC field.

4.3 Results

4.3.1 Tape samples

The original work on transverse susceptibility was carried out on magnetic tapes. This was done as they are a commonly used magnetic medium. At the time this work was being developed magnetic tapes were widely used in data storage and so being able to measure their magnetic anisotropy was a useful tool.

The tape sample consisted of 32 layers of cobalt surface-modified $\gamma - Fe_2O_3$ VHS tape bonded together with adhesive between each strip and then bound in pressure-sensitive tape. The sample dimensions were made to fit flush within the sensing coil of the susceptometer with a width of 5 mm and a length of 9 mm.

Figure 4.1 contains plots of the transverse susceptibility and reduced magnetisation against applied DC field. Plot 1 displays the results of the linear transverse susceptibility measurement. Plot 2 displays the hysteresis measurement of the same sample seem previously in figure 3.7. They have been plotted on the same scale to allow direct comparison of the measured coercivity.

The transverse susceptibility graph shows four distinct switching events, two due to switching, labelled H_s and two due to anisotropy, labelled H_k. The anisotropy was measured to as $123 \pm 10\,kA/m$ in both peaks. The coercivity was measured as $27 \pm 10\,kA/m$. This value can be compared to the coercivity measured through the hysteresis loop, which was measured as $57 \pm 5\,kA/m$. The difference between measured coercivities can be first attributed to the resolution of the susceptibility measurement as it can be seen around the coercivity point there are not many data points. It is possible the coercivity is closer to that measured through the hysteresis. When comparing measurements past measurements of cobalt surface modified maghemite this same trend can be seen. In the case of both Cookson's and Sollis' work there is a discrepancy between the coercivity measured on the VSM and that measured using linear transverse susceptibility. Unfortunately neither publication provided numerical values or uncertainties for these

measurements however it can be read of included plots that there is a physical difference in the measured coercivities. The susceptibility measurement can be compared to the theoretical expectations postulated by Aharoni et al [3]. It can be observed that the shape of the susceptibility curve does produce the expected features proposed by Aharoni et al [3] in figure 1.16. There it is suggested there will be 3 features in each sweep from high positive to high negative field. There were 3 features measured as expected by Aharoni. The peaks which correspond to the positive and negative anisotropy distributions are labelled H_k. The troughs that occur at the switching field are labelled, H_s, which are not peaks as Aharoni's theory predicted. The main difference between Aharoni's theory and the measured values is that instead of a single peak for the anisotropy we instead get a distribution of anisotropy fields in a more rounded peak.

This was explored experimentally by Hoare et al [50] in which similar curved peaks were measured. The distribution of anisotropy fields was then assumed to have a log-normal distribution which was used to fit the transverse susceptibility equation for an ensemble of particles to the experimental curve. The other factor in understanding the curves at the anisotropy field is the texture of a sample. A samples texture has a mathematical expression based on the distribution of easy axis orientations. There is a separate expression for each possible texture including randomly orientated powder samples. Therefore it is apparent that the shape of the curve will also differ depending on the samples texture. Further to this however, it is possible to use these expressions to perform a deconvolution [63] in which the exact anisotropy distribution can be obtained from an integration of Aharoni's χ_t equation providing a log normal distribution is used to describe the peak and the texture function is included.The deconvolution of the results is still an ongoing area of research which exceeds the scope of this thesis. Further work is being completed by Dr Steve McCann in this area.

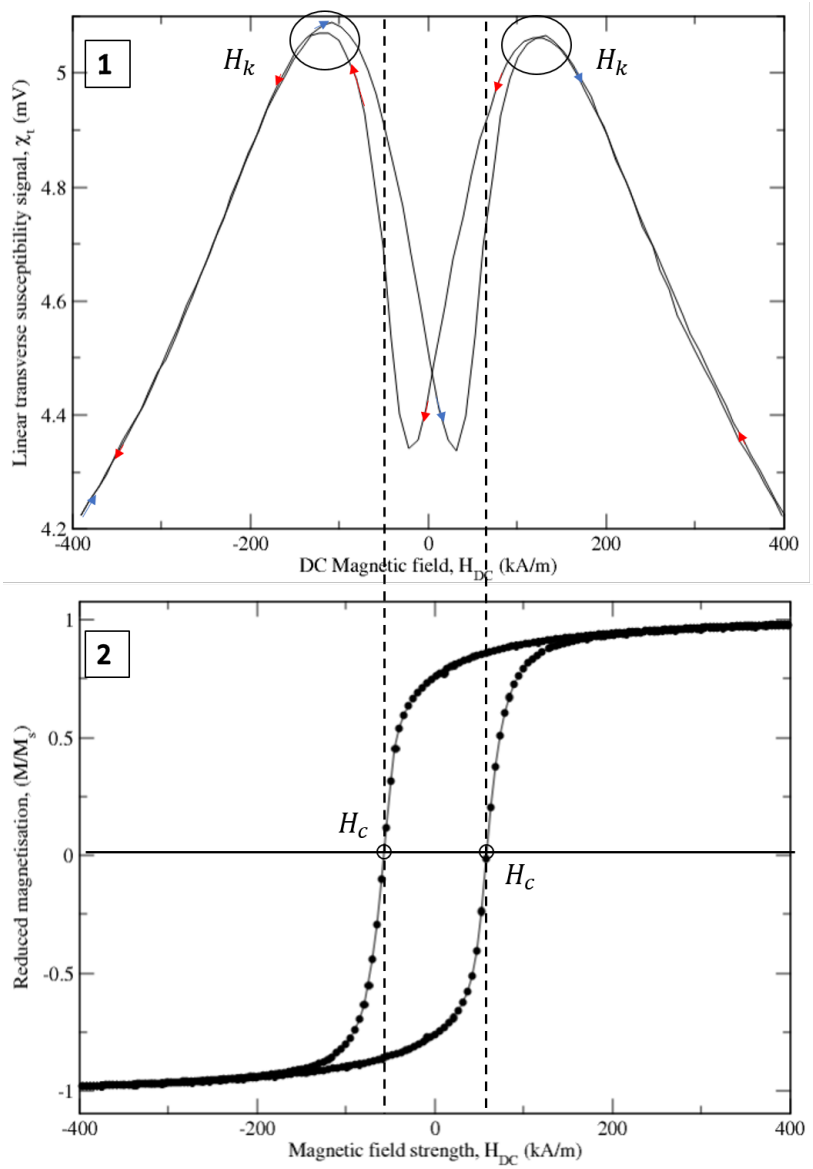

Figure 4.1: Plot of linear transverse susceptibility signal against DC Bias field for a sample of layered γFe_2O_3 VHS tape.

4.3.2 Powder samples

Maghemite - $\gamma - Fe_2O_3$ randomly orientated particulate sample.

Magnetic powders are useful due to their myriad of applications including magnetic refrigeration and medical treatment with nanoparticles [69, 70]. In the case of linear transverse susceptibility certain magnetic materials do not produce distinguishable peaks for the magnetic anisotropy. This occurs in $\gamma - Fe_2O_3$ when it is untextured as is the case for the randomly packed powders used in these measurements. The results from measurements on this material can be seen in figure 4.2. As can be seen from this plot there are almost no distinguishable features. The circled points are the switching points labelled H_s. The anisotropy has been smeared out. The reason for this is the texture dependence of the method. This powder sample is randomly orientated and so its easy axes are spread in all angles. Many of the easy axis will point in opposing direction reducing the bulk magnetic moment of the sample. This reduces the signal strength and so causes the anisotropy features to merge together.

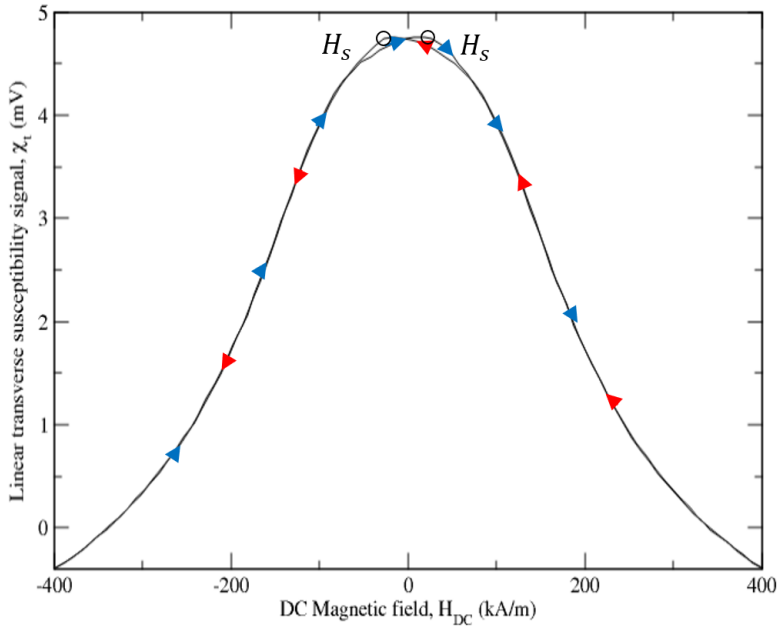

Figure 4.2: Plot of linear transverse susceptibility signal against DC Bias field for a sample of randomly packed γFe_2O_3 powder.

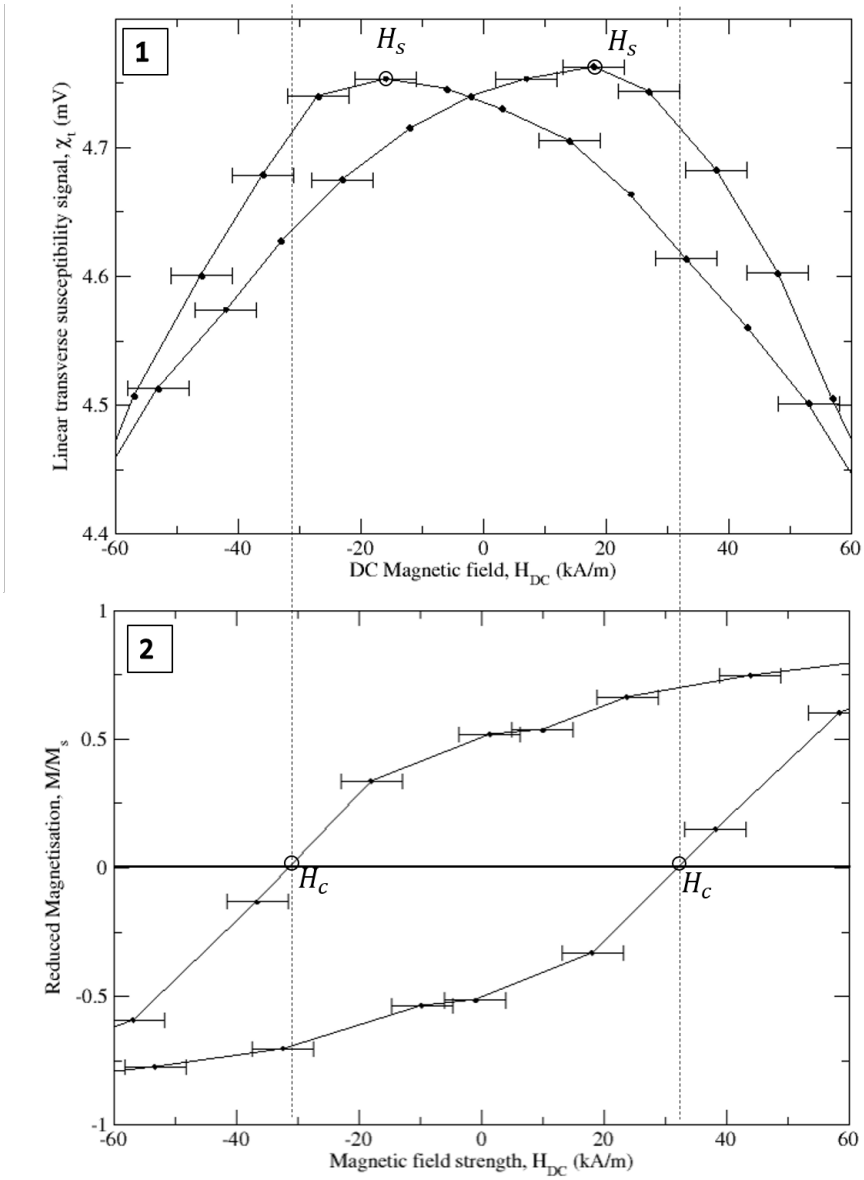

Figure 4.3: Plot 1 contains the data seen in figure 4.2 zoomed in on the coercivity points that occur. Plot 2 contains the hysteresis data measured for that same sample focused on the coercivity points.

Figure 4.3 contains two plots one the linear susceptibility of the γFe_2O_3 powder sample and the other the hysteresis of that same sample labelled 1 and 2 respectively. Comparing the two plots, it can be seen qualitatively that the two measured coercivities do not match. Numerically the measured coercivity for the linear transverse susceptibility method is, $18 \pm 5\, kA/m$. The value measured using the VSM, as seen in table 3.1, is $32 \pm 5\, kA/m$. Therefore, they don't align within error. The discrepancy in measured values is likely due to the resolution used in the susceptibility measurement. This is the reason for the large uncertainty. This result can also be compared to previous work by Cookson who measured the same randomly orientated maghemite powder sample and produced a very similar shape which can be seen in figure 4.4. The switching occurred at approximately $20 \pm 10 kA/m$ (the uncertainty is high in this case as the value was estimated from the figure). The previous work does agree with the switching measured here.

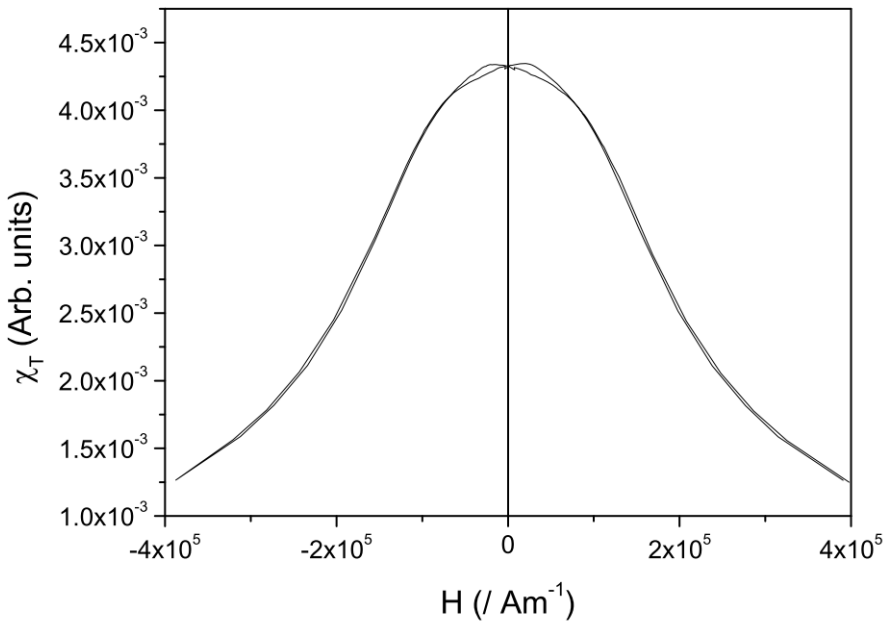

Figure 4.4: Linear transverse susceptibility against DC field for a randomly orientated sample of $\gamma - Fe_2O_3$ measured by Cookson [45].

Chromium dioxide - CrO_2

The next sample that was tested using this method is the sample of Chromium dioxide CrO_2. The measurements of this sample produce peaks for the both the coercivity and the anisotropy in accordance with Aharoni's theory. Figure 4.5 shows both the plot of linear transverse susceptibility and the hysteresis measurement plotted on the same scale. This allows for direct comparison between the two methods. The peaks are identified through the labels H_s for the switching peak and H_k for the anisotropy and H_c for the coercive field.

The anisotropy peak occurs at $183 \pm 10\,kA/m$. The coercivity measured using this method is $57 \pm 10\,kA/m$. Comparatively the value obtained from the hysteresis measurement is $55 \pm 15\,kA/m$. Therefore, both measurements are within error and compare with values quoted by Jiles [37]. The anisotropy measurement also aligns closely with that measured by Cookson who measured a value of $183\,kA/m$ with no supplied uncertainty. As well as this, the shape of the susceptibility curve is very close to measurements made by sollis et al [51] and Cookson [45]. Although neither publication provided numerical values for the coercivity, the peaks occur in comparable positions and can be seen in figures 4.6 and 4.7. This leads to the conclusion that there is a strong agreement between each measurement of this sample.

A question that remains from this measurements is that given that this sample of chromium dioxide has randomly orientated easy axes, why does it produce distinguishable anisotropy peaks when $\gamma - Fe_2O_3$ particles do not? The possible reason is that CrO_2 has a much smaller particle size and so a higher density of particles can be achieved in comparison to the maghemite. CrO_2 can also be refined and manufactured to a higher standard than maghemite. It can achieve greater elongation and thus larger shape anisotropy It can also be made considerably smoother which allows for further increase in packing density [6].

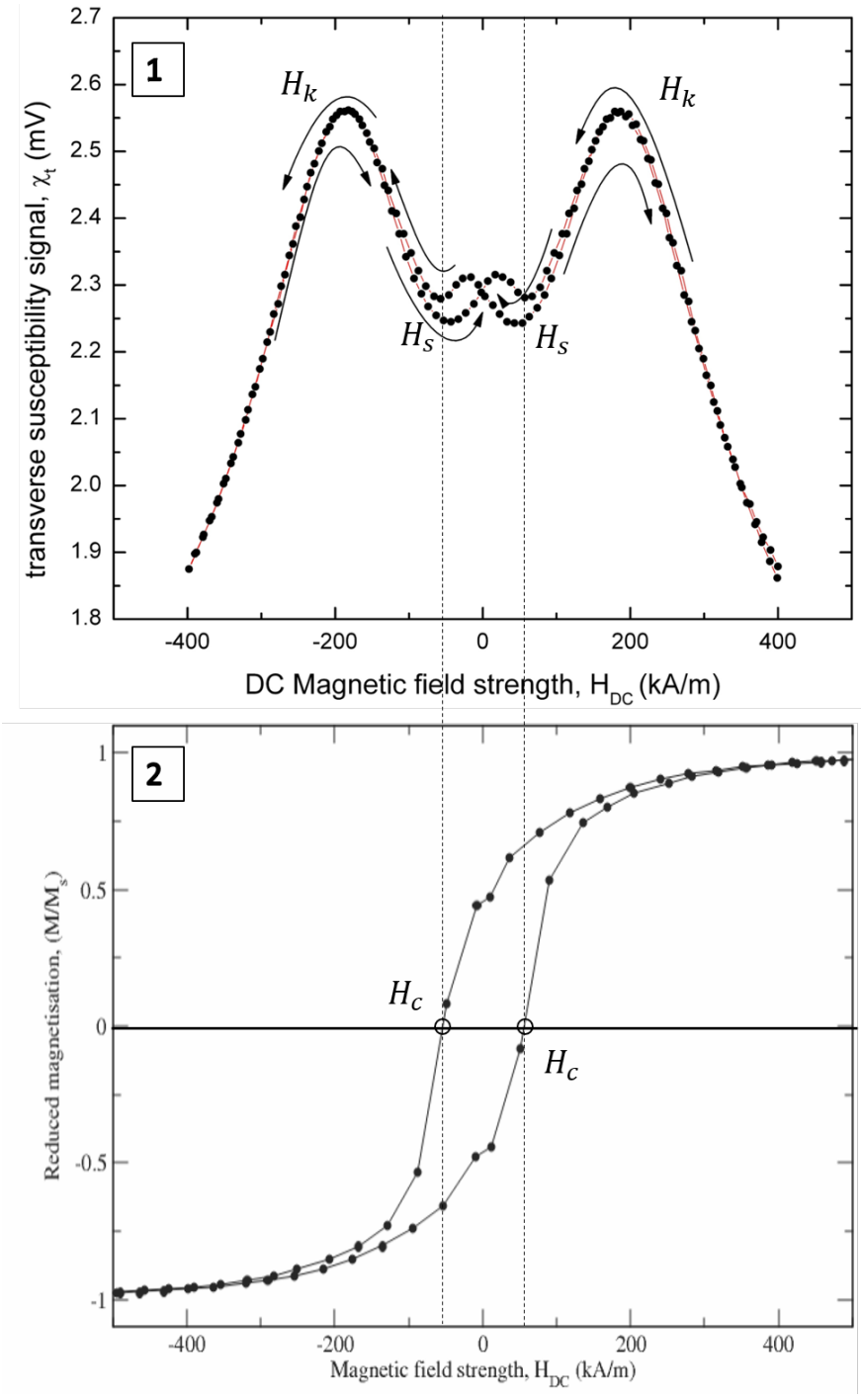

Figure 4.5: Plot 1 contains the linear transverse susceptibility signal against DC Bias field for a random powder sample of CrO_2 set in araldite. Plot 2 is the hysteresis loop for that same sample plotted on the same scale.

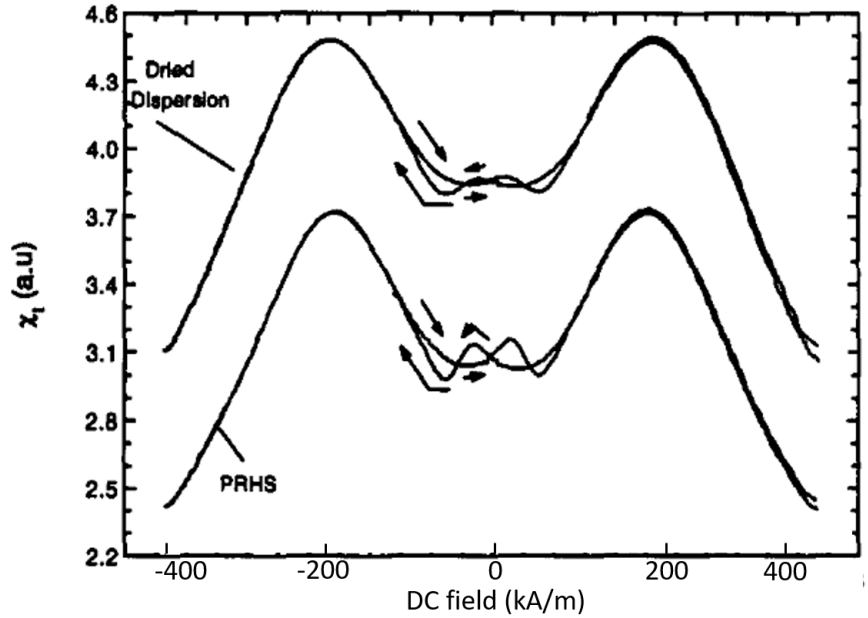

Figure 4.6: Plot of the transverse susceptibility against applied magnetic field H, of a powder sample of CrO_2 by Sollis et al [51].

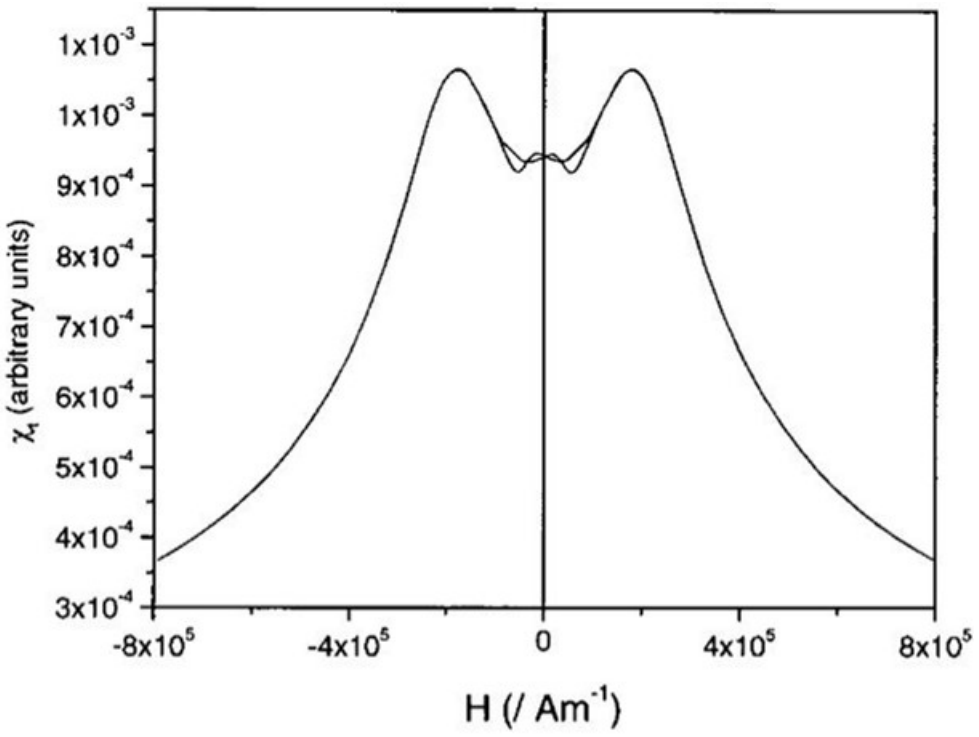

Figure 4.7: Plot of the transverse susceptibility against DC field measured by Cookson [45].

Magnetite - Fe_3O_4

The final sample measured using this method is a magnetite powder sample. The sample is a randomly packed powder of superparamagnetic nanoparticles. The plot produced by the measurements should not produce anisotropy peaks due to its superparamagnetic properties where its effective anisotropy is masked. The results can be seen in figure 4.8. The only distinguishable feature is two sharp peaks, when examined closely it can be seen that the peaks occur on both sweeps of the DC field. This would indicate them being related to anisotropy. This would be possible as the interactions of the particles would induce an anisotropy. This anisotropy is of the same magnitude as the coercivity measured using the VSM which has caused a loss in coercivity information. What is likely to have happened here is that the coercivity and anisotropy information have smeared together, as reported by Lu et al [58–62], due to the interactions of moments causing the anisotropy to shift to lower field values.

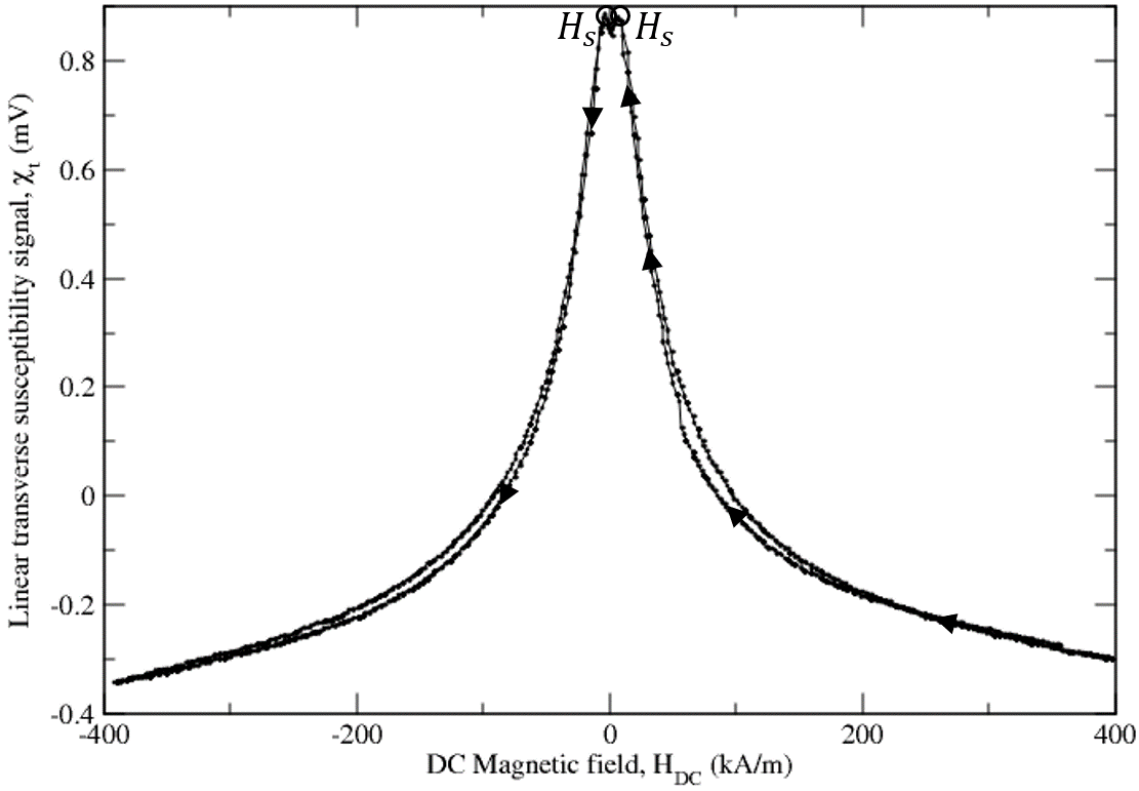

Figure 4.8: Plot of linear transverse susceptibility signal against DC Bias field for a magnetite powder sample.

Figure 4.9 Shows figure 4.8 across a short DC range to highlight the peaks that occur on both sweeps. The measured value is $4\pm2\,kA/m$ averaged across both peaks. When this value is compared to the hysteresis measurement of the same sample, seen in plot 2 of figure 4.9 the coercivity measured was $3\pm1\,kA/m$. Therefore, both values are within error of each other. This brings into question what the switching event in these peaks represent. It could be as was theorised by Lu et al [58–62], where the coercivity and anisotropy had smeared together. Due to the nature of the sample, behaving as a superparamagnet, no coercivity or anisotropy is expected. However, the visible switching maybe due to the slight agglomeration of the particles and may not be directly attributed to coercivity or anisotropy.

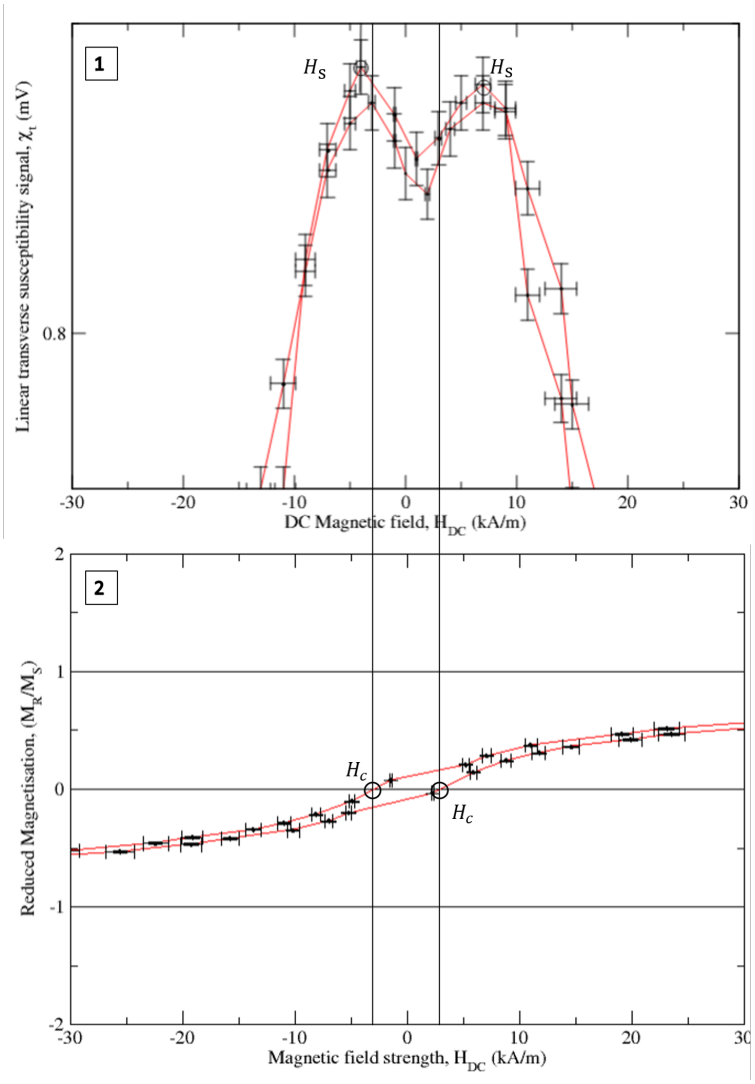

Figure 4.9: Plot 1 is figure 4.8 re-plotted on a smaller scale. Plot 2 is the hysteresis loop of the same magnetite sample on the same scale. The points labelled H_c correspond to the coercivity of the sample. H_s is the switching field which aligns with H_c in this measurement.

4.4 Summary

The method of using linear transverse susceptibility to measure the anisotropy distributions of magnetic materials produces the same features suggested by Aharoni et al [3]. These features a positive and a negative anisotropy field peak and a coercivity peak for each sweep of the DC field. However, the peaks were curved rather pointed. This is due to the texture effects in the material which cause a spreading of the peaks as texture was not taken into account in Aharoni's model. The other point of note when looking at Aharoni's theory is that there should be a peak representing the coercivity of the sample. However, experimentally the only switching event that has occurred at the coercive field value is a smooth trough which indicates a range of coercivity values due to the same texture effects the anisotropy experiences.

The tape sample of Cobalt surface modified maghemite produced both anisotropy and coercivity features which were consistent with that proposed by Aharoni [3]. The anisotropy was measured as $123 \pm 10\,kA/m$ this closely matches the value measured by Cookson, who measured a value of $125 \pm 10\,kA/m$. The coercivity was measured as $27 \pm 10\,kA/m$ when compared to the value measured by the VSM it does not agree within error. This has been found to be a repeatable problem in the work by both Cookson and Sollis. It is still unknown why there is a discrepancy in coercivity measurements between the VSM and the linear transverse susceptibility method.

The sample of Chromium Dioxide (CrO_2), was found to produce both anisotropy and coercivity features consistent with the theory presented by Aharoni et al [3]. Two anisotropy features and two coercivity features can be identified in the linear transverse susceptibility curve. The coercivity of the CrO_2 sample was measured as $183 \pm 10\,kA/m$ which when compared with that materials to previous work by Sollis et al [51] can be found to agree. The measurement by Sollis, which measured the anisotropy as $200 \pm 20kA/m$, can be seen in figure 4.6. The susceptibility curve can also be compared with the measurements on a randomly orientated powder sample of CrO_2 by Cookson who found agreeable results. The coercivity measured for the sample of CrO_2 was $57 \pm 10\,kA/m$ this agrees within

error of the value measured by the VSM. There does remain a question as to why the chromium dioxide produces significantly more distinguished features, than the maghemite sample despite both being randomly orientated. It is possibly due to CrO_2 having a much smaller particle size and possessing both a larger shape anisotropy due to development in it's refinement process.

The linear transverse susceptibility measurement of magnetite showed only 2 very sharp peaks with no other features. They have been measured at $4 \pm 2\, kA/m$. When comparing this value to the coercivity measured by the VSM they agree closely within error. Therefore it is possible this feature is a coercivity. The particles in this sample are $10\, nm$ in size and spherical so due to their uniformity should produce no anisotropy and by extension no coercivity. However, the particles are un-coated so are free to interact with neighbouring particles. This can induce an anisotropy in the sample. However, the magnetic moment produced is much weaker than what would be present in a ferromagnetic or ferrimagnetic sample. It is likely behaving as a superparamagnetic material. The features here are similar in magnitude to the coercivity measured using the VSM. However, the peaks appear twice on each sweep which is a feature usually only found with anisotropy not coercivity. The likely cause of this being a merging of the induced anisotropy and coercivity together leaving only the anisotropy features present.

Finally as was previously found, the maghemite ($\gamma - Fe_2O_3$) powder sample, an untextured material, produces no distinguishable anisotropy information. This can be seen in figure 4.2. The anisotropy information has been completely smeared out by the opposing easy axes. This is a useful confirmation of previous research by Cookson [45] who recorded the same shape with the original susceptometer. The coercivity or switching event that occurred peaked at $18 \pm 10\, kA/m$. When compared to the hysteresis measurement of that same samples coercivity it is found to agree within error. Both the shape of the curve and position of the coercivity peak agree with the equivalent measurement by Cookson, who measured coercivity as $20 \pm 10\, kA/m$. What is clear with this measurement is that texture plays a much greater role in the measurement of transverse susceptibility as method for measuring the anisotropy. Therefore, a method independent of magnetic texture is required.

This will be explored in the following chapter as the method of Non-linear transverse susceptibility.

Sample	Susceptometer		*VSM*
	$H_k(kA/m)$	H_s(kA/m)	$H_c(kA/m)$
$Co-\gamma-Fe_2O_3\,tape$	123 ± 10	27 ± 10	57 ± 10
$\gamma-Fe_2O_3\,powder$	/	18 ± 10	32 ± 10
$CrO_2\,powder$	183 ± 10	57 ± 10	55 ± 15
$Magnetite$	/	4 ± 2	3 ± 1

Table 4.1: Comparison table of anisotropy and coercivity values for the tested samples.

Chapter 5 begins on the following page.

Chapter 5

Non-Linear Transverse Susceptibility

5.1 Theory and previous work

A number of randomly orientated powder samples, when characterised by linear transverse susceptibility measurements, do not show any discernible anisotropy features. The reason the anisotropy is indistinguishable from those measurements is the bulk magnetic moment of the sample being greatly reduced by opposing easy axes. This causes a drop in the transverse susceptibility signal which results in the switching features smearing together. A method was proposed by Chantrell et al [36] capable of measuring the magnetic anisotropy of randomly orientated powder samples. This was called non-linear transverse susceptibility due to the relationship between the AC field and transverse susceptibility.

The aim of this chapter was to reconfigure the susceptometer to measure non-linear susceptibility and to test if anisotropy information can be obtained from the previous powder samples. The non-linear transverse susceptibility takes its name from the relationship between the measured susceptibility and the magnitude of the AC field. This will be shown experimentally later in the chapter.

The phenomenon of non-linear transverse susceptibility, χ_t was observed experimentally in soft magnetic materials in 1988 by Lütke-Stetzkamp et al [71]. A theory for measuring anisotropy peaks using the method of non-linear transverse susceptibility was theorised and described by Roy Chantrell et al [36] in 1989 in which the method given would be capable of overcoming the effects of texture due to a much more divergent peak at the anisotropy position. In this paper, they proposed a single point detection technique to determine the distributions of the anisotropy peaks, H_k and the orientational texture of the sample system. However, early work was unable to replicate the theoretical expectations or Lütke-Stetzkamp's measurements [72].

Figure 1.19 shows the non-linear susceptibility responses of an aligned system of Stoner–Wohlfarth particles. Both techniques have a clear feature when the DC bias field is equal to the anisotropy field but with the non–linear technique being divergent. As a degree of misalignment is introduced into the model, the linear susceptibility response becomes less pronounced (as observed experimentally [51]) while the non-linear response remains divergent [36]. This indicates that this method should be less texture dependent than the linear method. However, the change in moment is smaller for this method so there will be a smaller signal measured. This will likely affect how sharp and defined some of the features are when comparing them to the linear method.

Some preliminary work was completed in non-linear transverse susceptibility by Cookson [45] in 2002. Within this work it was shown that for the experimental setup used (Based at UCLan) the transverse susceptibility, χ_{nl}, is proportional to the square of the magnitude of the AC field, H_{AC}. As well as this, tests of both magnetic tape samples and powdered samples were completed. The tape sample showed a positive anisotropy peak in the positive quadrant and a mirror image in the negative quadrant. These results also displayed a peak which could possibly be associated with a switching or coercivity peak [45]. In comparison to the χ_t measurements the powdered samples still displayed anisotropy and possible switching peaks. Where before the anisotropy was suppressed, it can be identified with this technique.

5.2 Experimental setup

As was previously explained in Chapter 2, the non-linear transverse susceptibility measurements have a different configuration to the linear measurements. The susceptometer configuration was shown in figure 2.10. The difference in measurement technique is first that the sensing coil is mounted orthogonal to the previous sensing direction. It is therefore in plane with the DC field and transverse to the AC field when it is at it's peak. This can be visualised through figure 5.1. The method also differs in that the induced transverse susceptibility is measured at twice the frequency of the AC field. The theory that underpins this was described in section 1.6. The sensing coils are mounted on a similar insert to the linear apparatus. However, previous work found that the coils do not behave in the same way as the linear measurements. The outcome of this was that only one sensing coil was needed as the sensing coil did not interfere with the measurement of the susceptibility as was the case with the linear measurement.

Whichever sensing coil is being used is then directly connected to the lock-in amplifier. As only one coil is being used no balance circuit is required. The lock-in amplifier is set up to then only read the induced susceptibility signal at twice the reference frequency of 20 kHz. The orientation of the sample in this set up can be seen in figure 5.1 where the DC field goes along the axis of the sample and the AC field is orthogonal to the sample length. The feature common in all measurements using this method is that during the reverse sweep of the DC field the signal is inverted. This is because the moments are reversed with respect to the direction of measurement of the susceptibility.

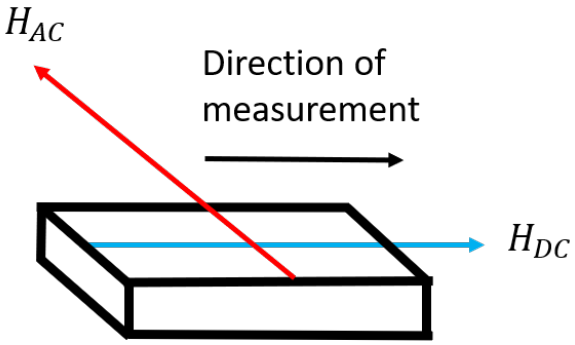

Figure 5.1: Orientation of the magnetic fields for non-linear transverse susceptibility measurements on a cuboid sample of a magnetic material.

5.3 Results

5.3.1 Tape samples

The non-linear transverse susceptibility method was first tested on a textured sample of cobalt surface modified gamma ferric oxide VHS tape. This was the same sample that had been measured using the linear method in chapter 4. The results of this measurement can be seen in figure 5.2. This figure is split into 3 plots, the hysteresis loop (1), the linear susceptibility measurements (2) and the non-linear transverse susceptibility measurement (3). Looking at plot 3 it can be seen that there are 4 distinct features. Two points related to the magnetic anisotropy and two points which are labelled H_s. Here, H_s is the switching field it behaves like a coercivity point in the linear measurements however does not match up with the coercivity values. For this sample the anisotropy was measured as $115 \pm 5\, kA/m$ which matches within error of the anisotropy measured using the linear method which was measured as $123 \pm 5\, kA/m$. What is questionable however is when a VHS tape sample of $Co-\gamma-Fe_2O_3$ was measured by Cookson, he recorded a value of 171kA/m without an uncertainty. The figure he included does have a broad range of anisotropy values so it greatly depends where he measured that value on the peak.

The value measured from the features labelled H_s in this plot is $31 \pm 5\, kA/m$. When compared to the linear transverse susceptibility coercivity measurement it is found to match within uncertainty. However, as with the linear measurement neither agrees with the value measured by the VSM. This leads to the same issue of if the feature being measured is a coercivity. For this reason it has been labelled as a switching feature and will continue to be labelled as such for all non-linear measurements.

Comparing the measurement to the theoretical expectations by Chantrell et al [36], it can be seen that there is both an anisotropy peak and another switching feature in each sweep. Theory predicted a strongly divergent response resulting in a singularity at the anisotropy point. This was predicted for all distributions of easy axes. What can be seen here however is not divergent the reason for this is likely due to several factors omitted from the model. These were thermal activation, inter-

particle interactions and anisotropy distributions [45]. The tape sample measured here is not perfectly aligned therefore within the sample there will be a distribution of easy axes causing the broad feature we observe. In the model, only a single anisotropy value is used for every particle assuming uniformity which is never the case in this sample.

The next page shows Figure 5.2.

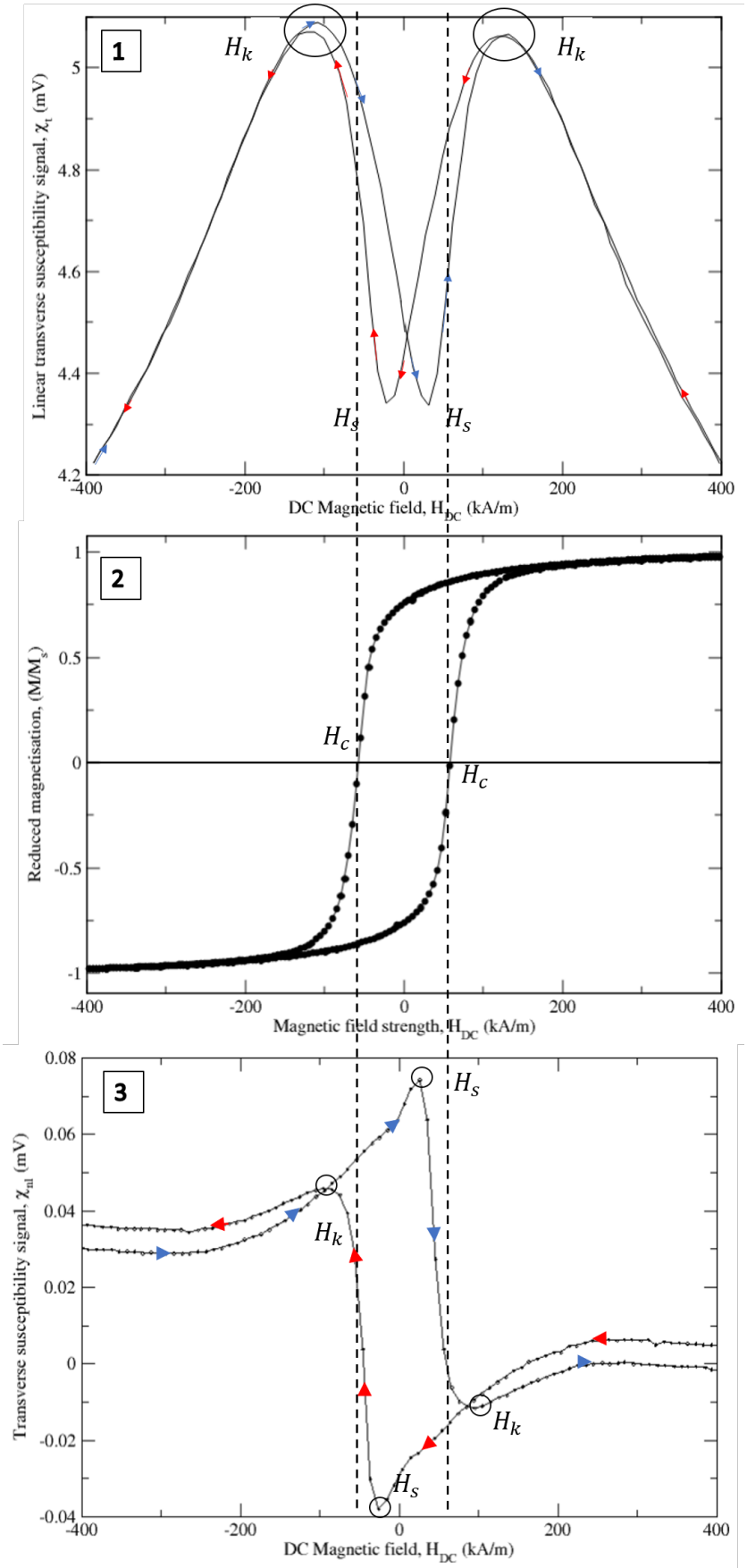

Figure 5.2: Plot 1 consists of the linear transverse susceptibility plot previously seen in figure 4.1. Plot 2 is the hysteresis loop for the tape sample. Plot 3 is the measured non-linear transverse susceptibility against DC field. Here, H_k is the anisotropy field and H_s is being used to identify switching field values. H_c is the coercivity field value.

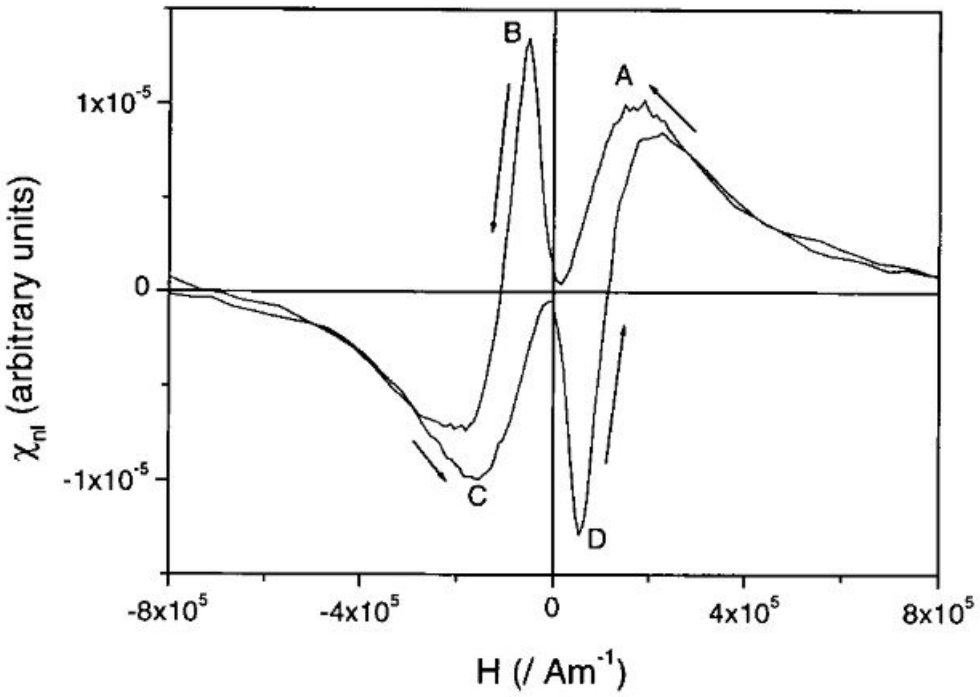

Figure 5.3: Non-linear susceptibility response against DC field measured by Cookson [45] for a $Co-\gamma-Fe_2O_3$ tape sample.

5.3.2 Powder samples

Measurements of randomly orientated powder samples were completed using the linear transverse susceptibility measurement. Of the samples tested only the chromium dioxide produced distinguishable anisotropy features. The method proposed by Chantrell et al [36] theorised that the χ_{nl} anisotropy peak would be strongly divergent for both textured samples and those with a random distribution of easy axes.

Maghemite ($\gamma - Fe_2O_3$)

As was seen with the linear transverse susceptibility measurements in figure 4.2 for the powder sample of $\gamma - Fe_2O_3$ there were no anisotropy features just heavily suppressed coercivity peaks. Figure 5.4 is divided into 3 plots: the non-linear transverse susceptibility measurement for the randomly orientated maghemite powder sample; the linear transverse susceptibility measurement and the hysteresis loop of that same sample. The magnetic anisotropy was measured to be $105 \pm 5\,kA/m$. This can be compared to previous work by Cookson [45] who

measured a value of $97 \pm 5\,kA/m$ which agrees within error to the results measured in figure 5.4. Cookson's measurements can be seen in figure 5.5.

What is clear is that the method was successful in distinguishing the anisotropy data from other signals. However, it did not display a divergence as was predicted. Instead, as with the tape sample, a distribution of anisotropy values was measured. In this case, it mostly due to the model excluding the distribution of anisotropy values. Previous work by Hoare et al, [50] has shown that when applying a distribution of anisotropy values to the theoretical expectation of linear transverse susceptibility measurements, a much more rounded peak is produced. In the case of non-linear measurements the peak already displays a broad anisotropy peak and it is likely that it instead a measurement of the distribution of anisotropy values.

The switching field value was measured to be $17 \pm 5\,kA/m$. This value agrees within error with the value measured using the linear method which was measured to be $18 \pm 5\,kA/m$. When compared to the value measured by the VSM it does agree within error as can be seen in figure 5.4.

Magnetite

The second sample measured using the non-linear transverse susceptibility method was a magnetite sample made of $10\,nm$ spherical particles. When measured using the linear transverse susceptibility method, seen in figure 4.8, no anisotropy measurements were possible from the distinguishable features. The only visible switching behaviour was a reversible switching which is likely related to coercivity. In an isolated scenario, the magnetite sample should produce no coercivity or anisotropy values. The spherical shape of the particle means there is no shape anisotropy and so each axis of the particle can be easily magnetised. In reality a small amount of coercivity was measured due to the particles agglomerating to form irregular clumps inducing a small shape anisotropy. This was not distinguishable from other switching events in the linear measurements. The measurement of this sample can be seen in figure 5.6.

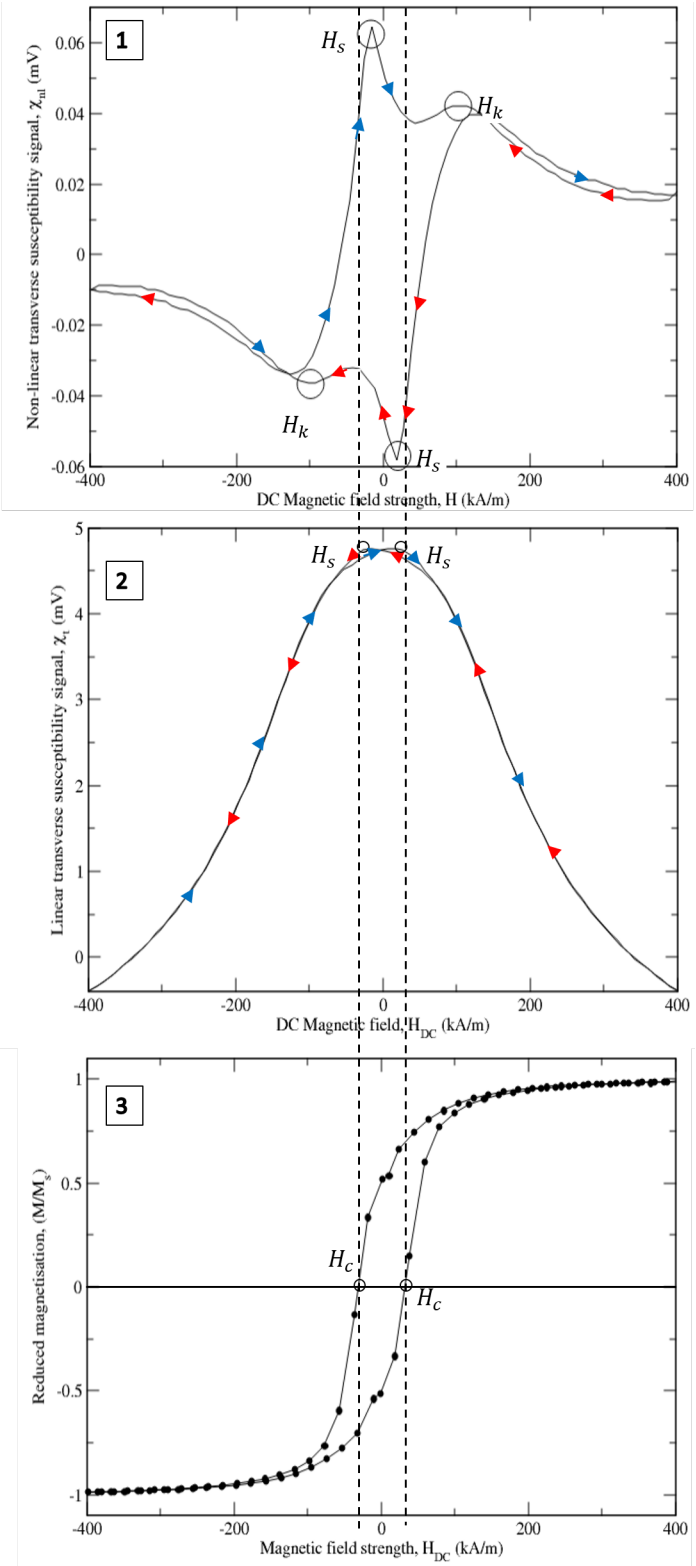

Figure 5.4: Plot 1 contains the non-linear transverse susceptibility measurement for the randomly orientated maghemite powder sample. Plot 2 contains the linear transverse susceptibility measurement of that same sample. Plot 3 contains the hysteresis measurement of that same sample. Here, H_s is a field value where switching occurs, H_k is the anisotropy and H_c is the coercivity.

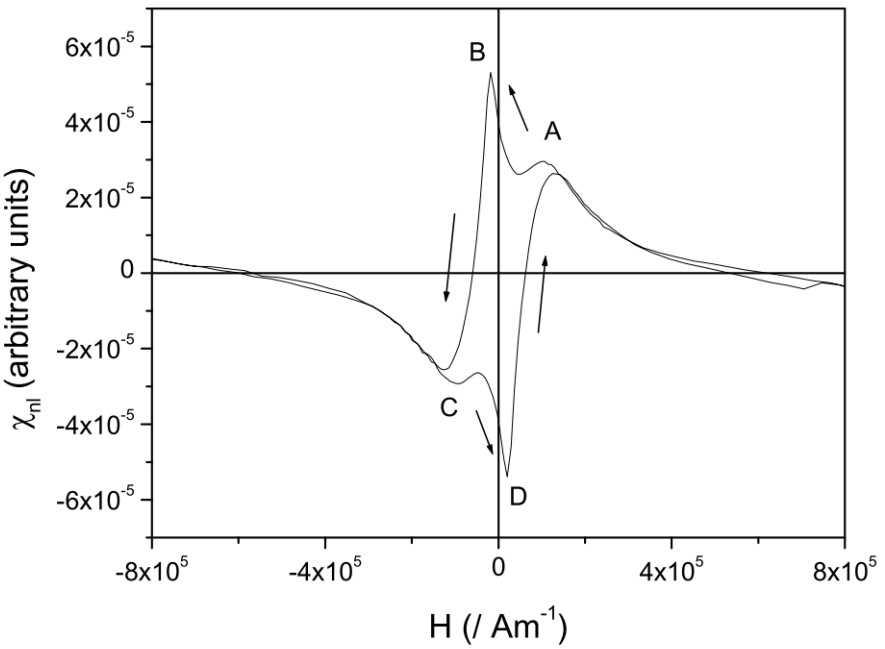

Figure 5.5: A plot of non-linear transverse susceptibility against DC magnetic field for a randomly orientated powder sample of maghemite measured by Cookson [45].

The figure is split into 3 plots: the non-linear transverse susceptibility measurement for the randomly orientated magnetite powder sample; the linear transverse susceptibility measurement and the hysteresis loop of that same sample. The switching field from the non-linear method was measured to be $7 \pm 5\,kA/m$. The value measured using the linear method was $4 \pm 2\,kA/m$ it can be seen that the value agrees within error. However, when comparing the switching points to the values measured from the hysteresis loop, which was $2.9 \pm 1\,kA/m$, it can be seen that there is a discrepancy between the measurements. Although they agree within error, the uncertainty in the non-linear measurement is quite large. There is reason to believe in both the linear and non-linear measurements that this feature is in fact a measurement of the induced anisotropy. This is because the feature occurs twice on both the positive and negative sweep. This is a behaviour only common in the anisotropy. For example, figure 5.4 shows only one coercivity or switching peak on the positive sweep and one on the negative. Whereas the anisotropy peak occurs twice on each sweep. Therefore, it is likely that this double peak observed in both the linear and non-linear measurement is in fact an anisotropy or some smeared form of it. The smearing of the anisotropy and coercivity fields was proposed as a theory for this observation [58–62], who

proposed that due to interactions of the particles magnetic moments the bulk anisotropy would be reduced and so would peak at lower field values.

Figure 5.6 is shown on the next page.

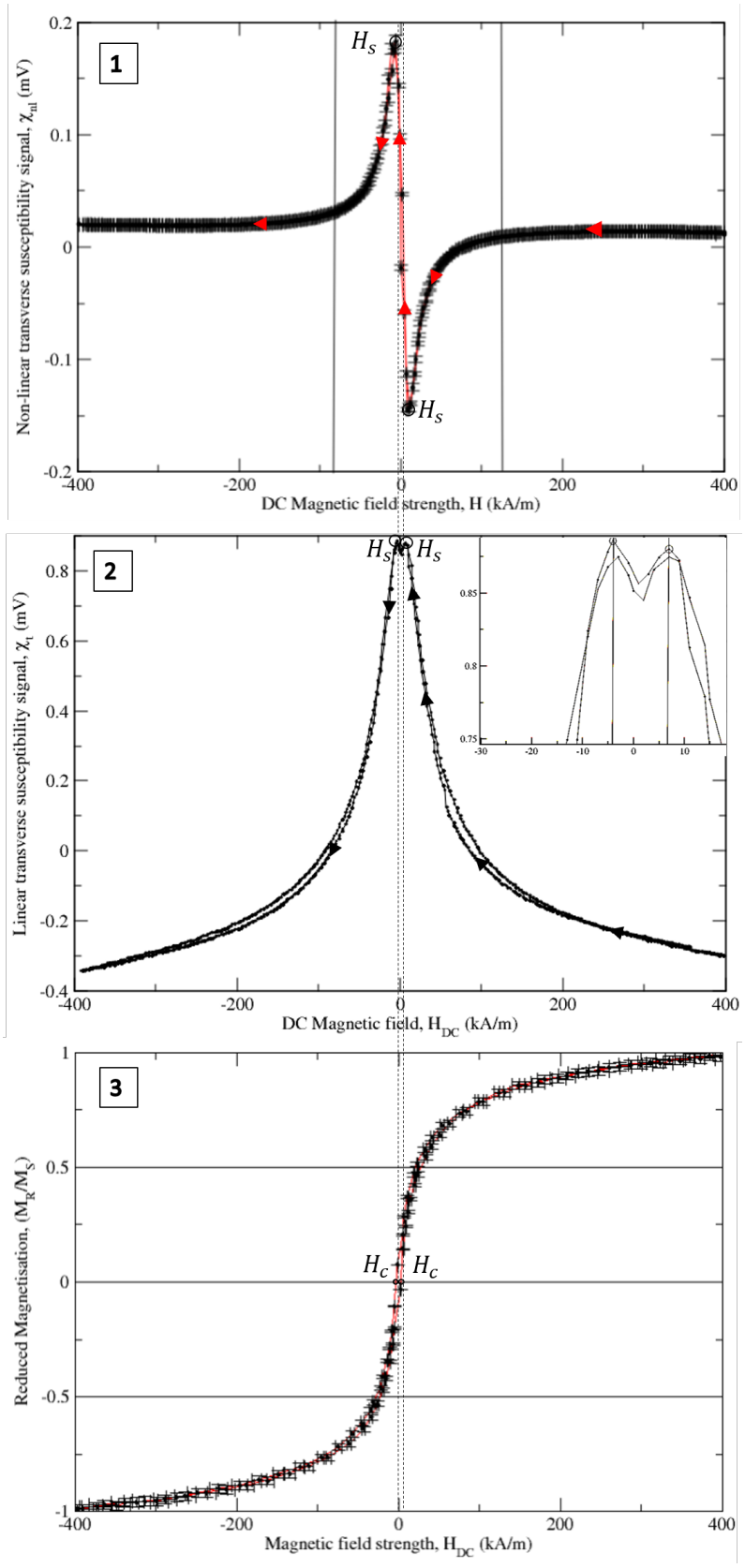

Figure 5.6: Plot 1 contains the non-linear transverse susceptibility measurement for the randomly orientated magnetite powder sample. Plot 2 contains the linear transverse susceptibility measurement of that same sample. Plot 3 contains the hysteresis measurement of that same sample. Here, H_s is a field value where switching occurs, H_k is the anisotropy and H_c is the coercivity.

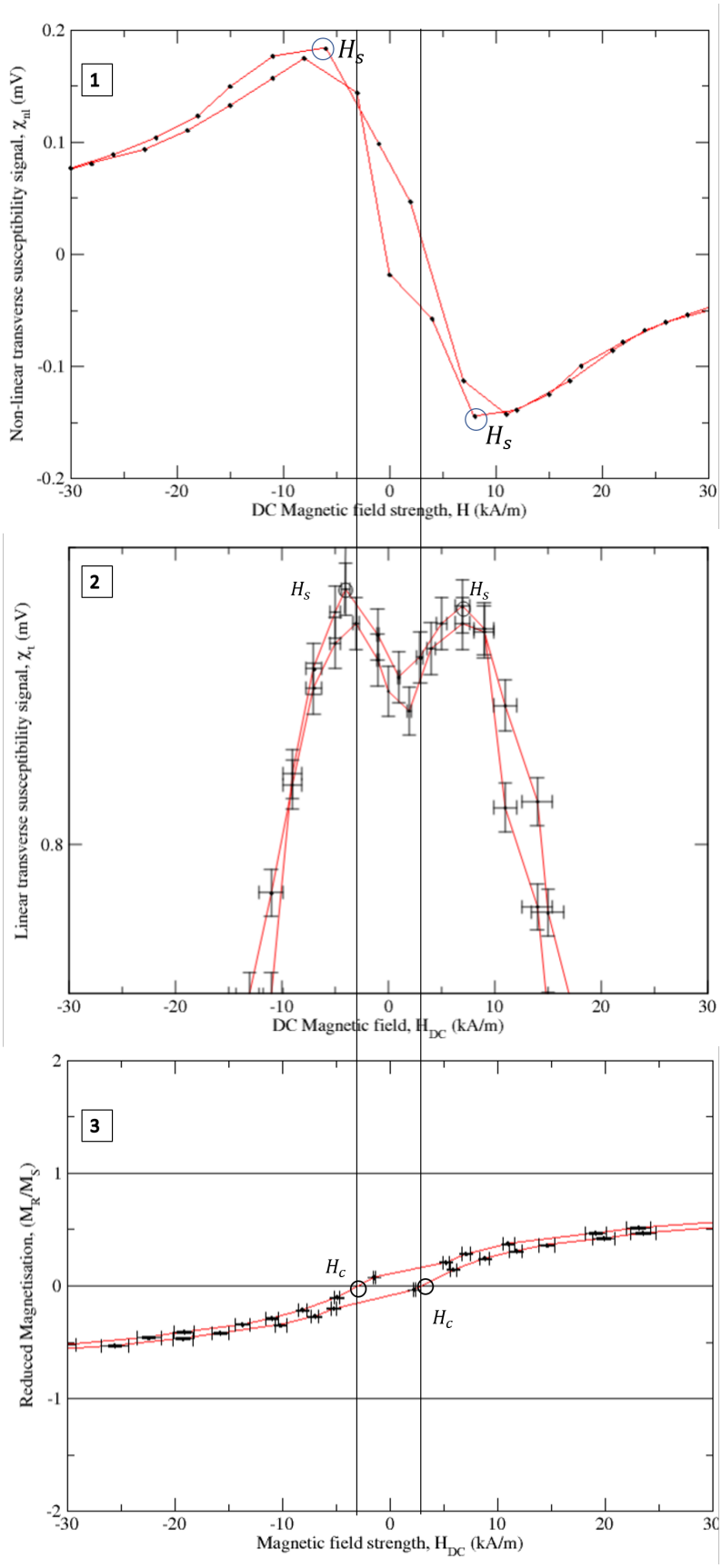

Figure 5.7: Figure 5.6 with each plot focused around the coercivity peak.

Chromium dioxide

The measurement of the chromium dioxide sample using the linear transverse susceptibility method produced both distinguishable coercivity and anisotropy features in the resulting plot. Therefore, in the non-linear transverse susceptibility measurement those same features should be presented with comparable values. Figure 5.8 is divided into 3 plots: the non-linear transverse susceptibility measurement for the randomly orientated CrO_2 pseudo-tape; the linear transverse susceptibility measurement and the hysteresis loop of that same sample. The magnetic anisotropy for the non-linear method was measured to be $205 \pm 5\, kA/m$. This value can first be compared with the measurement using the linear method which was $183 \pm 5\, kA/m$. These values do not agree within error. When compared to the previous work of Cookson the χ_{nl} measurement for the anisotropy was $208\, kA/m$ which is very close although no uncertainty was supplied. the results of Cookson's measurement on the chrome dioxide sample can be seen in figure 5.9. The shape of the figures is comparable however, the switching points occur on opposing halves of the x axis. This is due to the direction the measurements were started in.

As was stated in chapter 3, the anisotropy measured using the linear method matched closely with that measured by Cookson. Therefore, in both the measurements carried out here, and that measured by Cookson, there was a disagreement of $20kA/m$ between the linear and non-linear measurements of anisotropy. This is likely due to the non-linear method being less receptive to texture effects. It has been observed that the anisotropy value measured in using chi_t occurs at lower field values as the samples easy axes become more randomly distributed [73, 74]. This fits with the theoretical expectation from Chantrell, where the anisotropy response is less influenced by texture [36].

The measured switching point was at $20 \pm 5\, kA/m$. When compared to the linear measurement of $54 \pm 15\, kA/m$, it can be observed that they are not within error of each other. This is consistent with the measurements by Cookson who measured the non-linear switching as $22.5kA/m$ with no uncertainty. There is some contention as

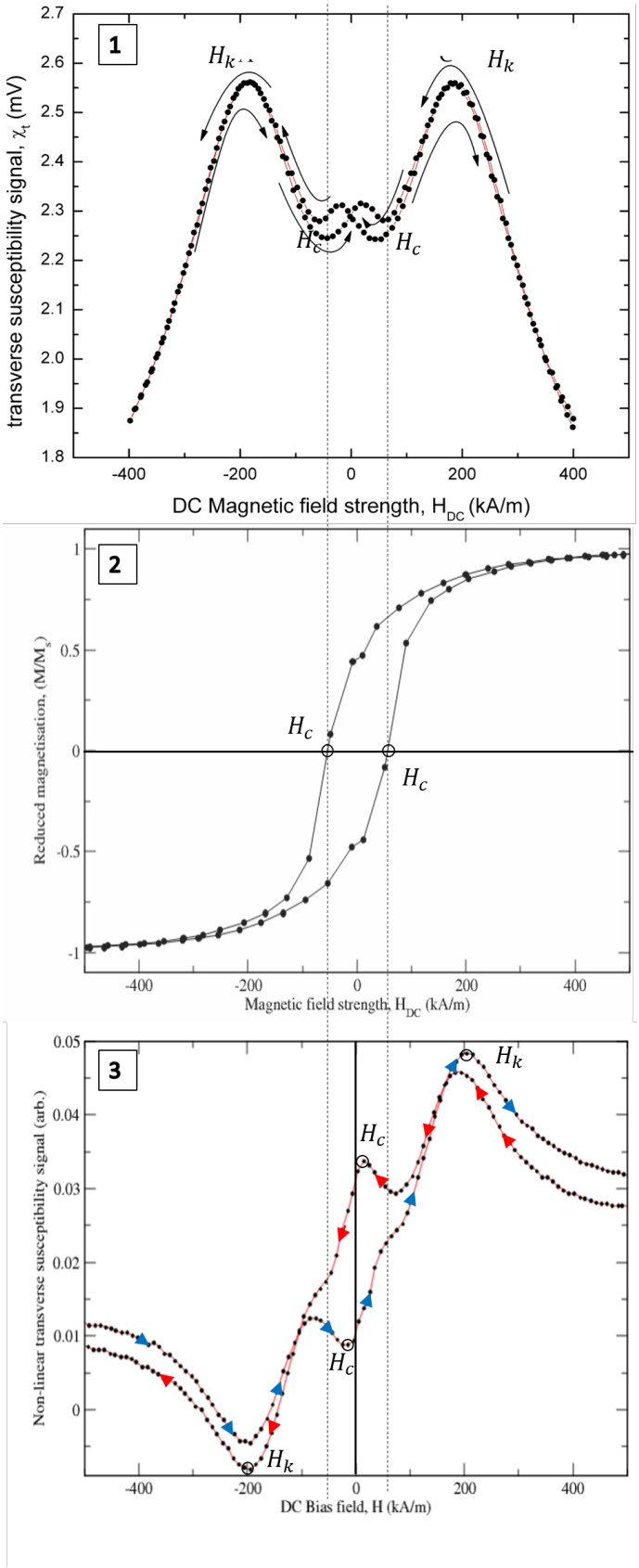

Figure 5.8: Plot 1 contains the non-linear transverse susceptibility measurement for the randomly orientated CrO_2 pseudo-tape sample. Plot 2 contains the linear transverse susceptibility measurement of that same sample. Plot 3 contains the hysteresis measurement of that same sample. Here, H_s is a field value where switching occurs, H_k is the anisotropy and H_c is the coercivity

to whether there is another switching event in the non-linear measurement. This feature is a third circled trough which is close to aligning with both the coercivity measurements through the VSM and linear method seen in figure 5.8. This trough occurs at $74 \pm 5\,kA/m$ which is within error of both measurements of coercivity. This feature does occur in Cookson's measurement although he only identifies the points labelled B & D as switching points.

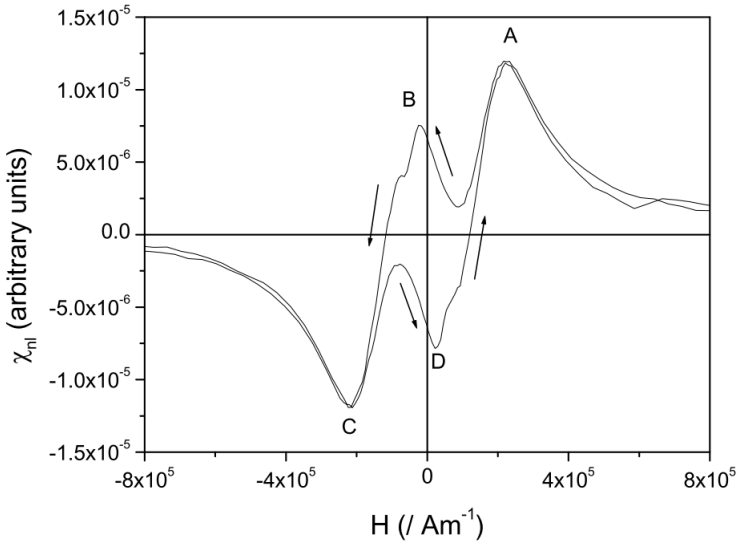

Figure 5.9: A plot of non-linear transverse susceptibility against DC magnetic field for a randomly orientated powder sample of chromium dioxide measured by Cookson [45].

Section 5.4 starts on the next page.

5.4 Summary

The method of non-linear transverse susceptibility adapted from work by Chantrell et al [36] has produced distinguishable anisotropy features for randomly packed magnetic powders. The method has produced results for both tape samples and randomly orientated powder samples of three different magnetic powders with differing particulate sizes and packing fractions. The measurement did behave as theory proposed with features being much less susceptible to texture affects although not divergent. Another aspect that occurred for each measurement was that the susceptibility response was negative on the reverse field sweep. This was found to be due to the easy axes of the particles being anti-parallel to the measurement direction and so the recorded susceptibility was 180° out of phase with the initial lock-in amplifier signal. This resulted in a negative value recorded by the lock-in.

The measurement of the highly textured, cobalt surface modified gamma ferric oxide VHS tape sample, produced both anisotropy measurements and a switching point which differed from the coercivity. The anisotropy was measured to be $95 \pm 5\,kA/m$. This value is smaller than that measured using the linear method by a significant margin which was measured as $123 \pm 5\,kA/m$. When compared to the measurement by Cookson on a comparable sample he found the anisotropy to be $171\,kA/m$ which follows the expected trend of the non-linear measured anisotropy being higher than the linear due to it being resistant to texture effects. The reason for this discrepancy is likely due to the nature of textured samples. All of the particles are aligned along one axis. Therefore, when the measurement is performed at a different angle to the particle alignment, a weaker single will be induced. This has likely caused the rift between the two measurements. Further testing More so when the shape is compared to that measured by Cookson seen in figure 5.3. It is likely that the susceptometer was not correctly configured for this measurement with a textured sample. The AC field may have been too low to sufficiently induce switching in the particles resulting in very broad peaks with little definition. This would need further testing to try and replicate the measurement by Cookson.

The switching peak seen here is measured to be $31 \pm 5\,kA/m$ this agrees with the linearly measured value of coercivity. However, neither of these methods measure the same value as is found in the VSM. Therefore, the discrepancy reported in chapter 3 for the difference in coercivity measured values for this sample are still present in the non-linear method.

The randomly orientated powder sample of $\gamma - Fe_2O_3$ did not produce any distinguishable anisotropy features when using the linear method. Using the non-linear method has produced clearly defined anisotropy peaks and a two switching peaks. The anisotropy was measured as $105 \pm 5\,kA/m$. This can be compared to the value measured by Cookson who measured an equivalent anisotropy peak to be $97\,kA/m$. The measurement therefore agrees within error. The sharper peaks are certainly switching events of the samples magnetic moment. This switching field value, H_s was measured to be $17 \pm 5\,kA/m$. This value agrees, within error, with the coercivity measured using both the linear method and VSM. However, due to the size of the uncertainty it is possible the true coercivity is much closer to the value measured by the VSM. When the result is compared with previous work by Cookson [45] it can be seen that the shape and peak positions of the magnetic anisotropy are almost identical. With Cookson measuring a value of $97\,kA/m$ which is very close to the value measured here. Cookson measured the switching point to be $20\,kA/m$ which also agrees within error of the measured value.

The main conclusion to draw from this method is that it is successful in measuring the magnetic anisotropy for a randomly orientated powder sample. It is clear that the method is not as strongly influenced by the magnetic texture and so it becomes possible to identify anisotropy peaks for samples where the information would usually be smeared out. However, it can be seen that the anisotropy peak is not divergent but is instead a broader distribution of values. This lack of divergent behaviour is due to the model taking a single anisotropy field point for all particles rather than accounting for a distribution of anisotropy values for each particle. Work by Hoare et al [50] has shown that applying a distribution of anisotropy values to the theoretical χ_t measurement, at the anisotropy field, produces a much

broader peak which matches the experimental measurements for the linear method. As the χ_{nl} response for anisotropy field is already producing a distribution of anisotropy values it is possible that this is a direct measure of the anisotropy distribution for the range of particles and thus the deconvolution used to find the anisotropy distribution from the χ_t measurements are not needed.

The magnetite sample was measured using the non-linear transverse susceptibility method, seen in figure 5.6. What can be seen from the resulting plot is that the susceptibility response is strongly divergent around the visible switching event. This is visible in both the linear and non-linear measurement. The value measured at this switching point was $7 \pm 5\,kA/m$, which is within error of both the linearly measured value and the coercivity measured by the VSM. Which can be seen in table 5.1. This divergent switching event, occurs twice in both halves of the plot. This indicative of anisotropy behaviour as coercivity features only occur once on each sweep. The magnetite sample is composed of spherical nanoparticles which display superparamagnetic behaviour. It is then expected that this measurement along with the VSM measurement would return neither coercivity nor anisotropy field values. This is due to them having no shape anisotropy due to their uniform shape. The reason these switching events occur in both is due to induced anisotropy caused by particles agglomerating into clumps that possess a small induced shape anisotropy. It has been shown that the anisotropy can be shifted to smaller field values which can cause a merging of the coercivity and anisotropy features[58]. This is what has possibly happened here. The feature measured from the χ_{nl} method could be the anisotropy with the coercivity being a fraction of that value. The best way to examine this behaviour would be to take new measurements of much higher resolution with steps of $\sim 0.5\,kA/m$.

Finally, the Chromium dioxide pseudo-tape sample was tested. This material was the only powder to produce distinguishable anisotropy peaks using the linear transverse susceptibility method which was measured to be $183 \pm 5\,kA/m$. The measurements obtained from the non-linear method also produce distinguishable anisotropy peaks as well as switching peaks. The anisotropy measured using the non-linear method was measured to be $205 \pm 5\,kA/m$. Although these values do not

agree withing error, the result is consistent with measurements by Cookson who also found the non-linear measurement to be higher than the linear. It is understood this behaviour is due to the susceptibility response being less influenced by texture which reduces any broadening of peaks. What can also be identified here is that the anisotropy features do not contain a single point value for all particles causing a singularity. They instead display a distribution of anisotropy values dependent on the easy axis distribution. This behaviour however could mean that the non-linear method is a direct measurement of the particles anisotropy distributions and so complex methods for finding that distribution when using the linear method can be avoided.

The measured switching peak value for CrO_2 was $20 \pm 5\,kA/m$. This value is surprisingly small when compared to the measurement of the coercivity in both the linear transverse susceptibility and VSM results. There is another switching event though that occurs slightly before this switching peak. A point of inflection occurs directly before that peak. When that point is compared visually to the coercivity measurement in the linear and VSM measurement it is found to agree within error where the peak occurs at $74 \pm 5\,kA/m$. However, it is unknown if either or none of these features on the χ_{nl} plot are coercivity.

Sample	Susceptometer χ_t		Susceptometer χ_{nl}		*VSM*
	$H_k(kA/m)$	H_s(kA/m)	$H_k(kA/m)$	H_s(kA/m)	$H_c(kA/m)$
$Co-\gamma-Fe_2O_3\,tape$	123 ± 5	27 ± 5	95 ± 5	31 ± 5	57 ± 5
$\gamma - Fe_2O_3\,powder$	/	18 ± 5	105 ± 5	17 ± 5	32 ± 5
$CrO_2\,powder$	183 ± 5	57 ± 5	205 ± 5	20 ± 5	55 ± 15
$Magnetite$	/	4 ± 2	/	7 ± 5	3 ± 1

Table 5.1: Comparison table of anisotropy and coercivity values for the tested samples.

Chapter 6

Conclusions and further work

There were two main aims to this research project. The first was to improve the sensitivity and stability of the linear transverse susceptibility measurements and then compare measurements of magnetic materials with previous work. The second aim was to modify the susceptometer to be capable of measuring the non-linear transverse susceptibility.

The susceptometer was characterised so that its properties were understood and preliminary linear transverse susceptibility measurements were carried out. The main issue found with the original susceptometer that needed improving was the AC field generation. The alternating current was generated by the internal oscillator of a lock-in amplifier where the output current was amplified via an audio amplifier. The output current was producing a large amount of noise as seen in figure 2.5. This was causing inconsistency in the AC field which affected the measurement of the samples susceptibility. Changing this equipment corrected for a lot of the stability measurements, as the old lock-in amplifier was frequently dropping signal and had degraded with age. The new lock-in amplifier was more sensitive and could pick-up signals of a smaller voltage and to a higher precision than previously possible. This resulted in the susceptibility curves being much smoother with better defined features.

Once the stability issue had been addressed several measurements on commonly used magnetic samples were completed. The first was on a sample of cobalt surface modified gamma ferric oxide ($Co-\gamma-Fe_2O_3$) VHS tape. This was done for historical reasons as many previous measurements of materials transverse susceptibility was done on magnetic tape. The linear transverse susceptibility measurement was identical in shape to previous measurements of the same material. The anisotropy from the χ_t response was found to be $123 \pm 5\,kA/m$. This value matched closely with the previous work of Cookson [45] who measured a value of $125 \pm 5\,kA/m$ which matches closely with the measurement here. The coercivity was measured to be $27 \pm 5\,kA/m$. When comparing this value to the VSM measurement, which was found to be $57 \pm 5\,kA/m$, it does not agree within error. This is a consistent feature with Cookson's measurement as he also recorded a much lower coercivity response for the tape sample. This measurement did conform with the theoretical expectation of Aharoni et al [3], where two anisotropy field values were observed and one coercivity field value per sweep of the DC field. This was a good confirmation of the susceptometer working as expected.

The next sample was a randomly orientated powder sample of maghemite. This sample was used as previous research indicated this material could not produce distinguishable anisotropy data when being measured with a linear susceptometer. This was shown in figure 4.2. There were no features other than very shallow peaks which could coincide with the coercive field position. The peaks were measured to be $18 \pm 5\,kA/m$. The shape produced by this sample is almost identical to that measured by Cookson [45] who measured the coercivity to be $20 \pm 5\,kA/m$. These values can be seen to agree within error. When compared to the VSM measurement, which was $32 \pm 5\,kA/m$, which agrees within error with both the measurement of this samples coercivity and Cookson's measurement. The results of this measurement can be seen in table 6.1. It was clear that a different method was needed for measuring the anisotropy of this powder.

A sample of magnetite nanoparticles was also tested. This sample consists of spherical nanoparticles, both this material and this particle size are regularly used in modern applications making it a useful sample to test. The results for the linear

measurement consisted of only 2 peaks. The peak was measured to be $4 \pm 2\,kA/m$. This agrees within error of the coercivity value measured using the VSM, which was $3 \pm 1\,kA/m$. These peaks occur on the sweep of the DC field which is indicative of an anisotropy not a coercivity. Due to being spherical there should be no shape anisotropy. However, there could still be an induced anisotropy from particle interactions causing a small induced shape anisotropy. The issue with being able to measure that anisotropy is that the anisotropy energy is dependent on the size of the particle so for a small particle there would be low anisotropy energy. This can then be overcome by thermal energy which can cause random switching and rotation not due to an applied magnetic field. This could be the case with this measurement. What is most likely however, is that the anisotropy and coercivity features have merged together causing the single peak due to particle interactions [58–62]. The values measured here is listed in table 6.1. Further work is required to properly understand the behaviour of this material when using the susceptometer. The best way to approach this would be to take further measurement at much higher resolutions of at least $0.5\,kA/m$.

The final sample tested using the linear susceptometer was Chromium dioxide. This was a pseudo-tape sample with a random orientation of easy axis but its particles were fixed in place with an adhesive. This measurement produced both anisotropy and coercivity measurements. The anisotropy was measured to be $183 \pm 5\,kA/m$ which agreed within error of Sollis' measurement which was $200 \pm 20\,kA/m$. The coercivity was measured to be $57 \pm 5\,kA/m$. This value when compared to the coercivity measured from the hysteresis loop, which was $55 \pm 15\,kA/m$, agrees within error. The results of this measurement were consistent with the theoretical prediction of Aharoni et al, [3]. A comparison of the measurements can be clearly seen in table 6.1. When comparing the shape of this sample's plot with previous work, it can be seen that it matches closely to work by Sollis et al [51]. What remains unclear is why CrO_2 behaves as expected by Aharoni compared to maghemite when both have randomly orientated easy axes. The possible cause for this is that the CrO_2 particles are much smaller in size and can be elongated further inducing a larger shape anisotropy. This would allow for more particles to fit into a sample of equal volume which would give a much

stronger susceptibility response.

Sample	Susceptometer		*VSM*
	$H_k(kA/m)$	H_s(kA/m)	$H_c(kA/m)$
$Co-\gamma-Fe_2O_3\,tape$	123 ± 5	27 ± 5	57 ± 5
$\gamma - Fe_2O_3\,powder$	/	18 ± 5	32 ± 5
$CrO_2\,powder$	183 ± 5	57 ± 5	55 ± 15
$Magnetite$	/	4 ± 2	3 ± 1

Table 6.1: Comparison table of anisotropy and coercivity values for different test materials.

The modification of the susceptometer to measure non-linear susceptibility was discussed in chapter 2. This modification was required as the theoretical expectation was that it should produce anisotropy features with less dependence on magnetic texture. The only hardware change needed for this method was re-orientating the sensing coils as seen in figure 2.10.

The maghemite powder sample produced distinguishable anisotropy features which were not present when using the linear method. This anisotropy was measured to be $105 \pm 5\,kA/m$. This value can be compared to the equivalent measurement by Cookson who found the anisotropy to be $97\,kA/m$. The measurement also displayed a switching field response on both the forward and reverse sweep of the DC field. The switching field was measured as $17 \pm 5\,kA/m$, which agrees within error of the coercivity measured by the χ_t method and the VSM. This leads to the belief it may be a coercivity feature however further testing would be required to confirm this. This comparison can clearly be seen in table 6.2. The switching point measured by Cookson was $20\,kA/m$ which agrees with the value measured on the non-linear susceptometer. The outcome of this measurement remains that the magnetic anisotropy field was measured using the non-linear method for a randomly orientated powder sample of maghemite. It is evident that the issue of texture dependence on the linear method is not as prevalent with non-linear measurements. The resulting anisotropy measurements are observed as a distribution of anisotropy measurements and could be a direct measure of that distribution. This successful result helps confirm that the theoretical expectation of the non-linear method works as a means to measure the anisotropy.

The magnetite sample when measured using the non-linear configuration produced 2 large switching features which occurred on both the forward and reverse field sweeps. This was consistent with the behaviour of the linear measurement of the same sample. This switching value was measured to be $7 \pm 5\, kA/m$. As was discussed in the previous chapter, it is indicative behaviour of an anisotropy feature as it occurs twice on both sweeps. It is understood that the anisotropy and coercivity features can merge together at sufficiently small fields. So, although it agrees within error of the coercivity measured using the VSM it is possible that this is an anisotropy field measurement. The only way to test with this is further measurements of the sample at a much higher field resolution.

The chromium dioxide produced the same four features as it did linearly. The anisotropy field value was measured to be $205 \pm 5\, kA/m$ this value is not within error of the linearly measured anisotropy field, which was $183 \pm 5\, kA/m$. However, they are consistent with measurements by Cookson who also saw a difference in linear and non-linear anisotropy measurements. The reason for this difference is likely due to the χ_{nl} method being less texture dependent and so the anisotropy is not shifted or smeared as much which leads to a higher measured anisotropy. The non-linear results can be seen clearly in table 6.2.

Sample	Susceptometer χ_t		Susceptometer χ_{nl}		*VSM*
	$H_k(kA/m)$	H_s(kA/m)	$H_k(kA/m)$	H_s(kA/m)	$H_c(kA/m)$
$Co-\gamma-Fe_2O_3\, tape$	123 ± 5	27 ± 5	95 ± 5	31 ± 5	57 ± 5
$\gamma - Fe_2O_3\, powder$	/	18 ± 5	105 ± 5	17 ± 5	32 ± 5
$CrO_2\, powder$	183 ± 5	57 ± 5	205 ± 5	20 ± 5	55 ± 15
Magnetite	/	4 ± 2	/	7 ± 5	3 ± 1

Table 6.2: Comparison table of anisotropy and coercivity values for different test materials.

The results observed from the non-linear transverse susceptibility measurement have shown varied success when compared to the linear method. For random powder samples, the non-linear measurement has shown more defined switching field points which align with the coercivity and the switching of the linear measurement. The anisotropy was successfully measured for the maghemite, cobalt doped tape sample and CrO_2 powder. However, the anisotropy measured for the tape sample and the CrO_2 sample do not agree within error of the linearly measured anisotropy. The

reason for this is currently unknown. What is clear is that the linear method remains ideal for use with textured samples and samples with high particle concentration such as CrO_2. The powder samples such as $\gamma - Fe_2O_3$ can be measured using the non-linear method. The resulting peaks are much clearer for these samples. Further testing of samples with similar properties as the maghemite is required. However, the non-linear method is viable for measuring the anisotropy.

The questions that remain from this project are first, are the values measured for the magnetite indeed a merged anisotropy or coercivity or some other feature? The Second is, why CrO_2 follows the model of Aharoni despite being randomly orientated when the maghemite does not?

The further work to this will be completing a process called deconvolution on the susceptibility measurements made using both the linear and non-linear susceptometer. This process proposed by Chantrell et al [63] states that measured anisotropy is not a direct measure and the features are instead a distribution of anisotropy field values that need to be extracted. Research by Hoare et al [50] assumes a log normal distribution of anisotropy fields. The deconvolution would need to be theoretically explored with all past work confirmed. Then these new measurements can be evaluated to assess if they do directly measure the materials anisotropy.

Other areas that should be explored include complex transverse susceptibility. This is an area of research that has had some theoretical background published suggesting that there is evidence for thermal effects altering the measured magnetic anisotropy [75]. It is also a useful avenue of study due to the reliance of the phase of the AC field causing a change in the susceptibility signal so it would be useful to measure the imaginary signal. There is not a large amount of experimental work in this area and it would likely require a susceptometer with a temperature control system which we do not currently have access to.

References

[1] R. Gans. Zur Theorie des Ferromagnetismus. 3. Mitteilung: Die reversible longitudinale und transversale Permeabilität. *Annalen der Physik*, 334(7):301–315, 1909. doi: 10.1002/andp.19093340705. URL `https://onlinelibrary.wiley.com/doi/abs/10.1002/andp.19093340705`.

[2] E. C. Stoner and E. P. Wohlfarth. A Mechanism of Magnetic Hysteresis in Heterogeneous alloys. *Philosophical Transactions of the Royal Society of London. Series A, Mathematical and Physical Sciences*, 826(May), 1948.

[3] A. Aharoni, E.H. Frei, S. Shtrikman, and D. Trevers. The reversible susceptibility tensor of the Stoner-Wohlfarth model. *Bulletin of the research council of Israel*, 6A:215–238, 1957.

[4] L. Pareti and G. Turilli. Detection of singularities in the reversible transverse susceptibility of an uniaxial ferromagnet. *Journal of Applied Physics*, 61(11): 5098–5101, 1987. ISSN 00218979. doi: 10.1063/1.338335.

[5] S. R. Hoon and D. M. Paige. The use of torque magnetometry in determining particle anisotropy and orientation distributions in magnetic tape materials. *IEEE Transactions on Magnetics*, 23(1):183–185, 1987. ISSN 19410069. doi: 10.1109/TMAG.1987.1064787.

[6] B.D. Cullity and C.D. Graham. *Introduction to Magnetic Materials*. Wiley, second edition, 2009. ISBN 9780471477419.

[7] J. Hurt, A. Amendola, and R. E. Smith. Morphologies of acicular γ-Fe2O3particles. *Journal of Applied Physics*, 37(3):1170–1171, 1966. ISSN 00218979. doi: 10.1063/1.1708383.

[8] Christian Lang Andreas Tschöpe Rainer Birringer, Helmut Wolf and Andreas Michels. Magnetic Nanorods: Genesis, Self-Organization and Applications. *Z. Phys. chem*, 222:319–354, 2008. doi: 10.1524/zpch.2008.222.2.

[9] K. Nielsch, R. B. Wehrspohn, J. Barthel, J. Kirschner, S. F. Fischer, H. Kronmüller, T. Schweinböck, D. Weiss, and U. Gösele. High density hexagonal nickel nanowire array. *Journal of Magnetism and Magnetic Materials*, 249(1-2):234–240, 2002. ISSN 03048853. doi: 10.1016/S0304-8853(02)00536-X.

[10] Li Cheng-Zhang and J. C. Lodder. The influence of the packing density on the magnetic behaviour of alumite media. *Journal of Magnetism and Magnetic Materials*, 88(1-2):236–246, 1990. ISSN 03048853. doi: 10.1016/S0304-8853(97)90033-0.

[11] J. Henderson, S. Shi, S. Cakmaktepe, and T. M. Crawford. Pattern transfer nanomanufacturing using magnetic recording for programmed nanoparticle assembly. *Nanotechnology*, 23(18), 2012. ISSN 09574484. doi: 10.1088/0957-4484/23/18/185304.

[12] Maneesh K. Gupta, Dhaval D. Kulkarni, Ren Geryak, Swati Naik, and Vladimir V. Tsukruk. A robust and facile approach to assembling mobile and highly-open unfrustrated triangular lattices from ferromagnetic nanorods. *Nano Letters*, 13(1):36–42, 2013. ISSN 15306984. doi: 10.1021/nl303268s.

[13] Ahmed Alfadhel and Jürgen Kosel. Magnetic Nanocomposite Cilia Tactile Sensor. *Advanced Materials*, 27(47):7888–7892, 2015. ISSN 15214095. doi: 10.1002/adma.201504015.

[14] Joung Man Park, Sung Ju Kim, Jung Hoon Jang, Zuojia Wang, Pyung Gee Kim, Dong Jin Yoon, Jaehwan Kim, George Hansen, and K. Lawrence DeVries. Actuation of electrochemical, electro-magnetic, and electro-active actuators for carbon nanofiber and Ni nanowire reinforced polymer composites. *Composites Part B: Engineering*, 39(7-8):1161–1169, 2008. ISSN 13598368. doi: 10.1016/j.compositesb.2008.03.009.

[15] Mingsheng Wang and Yadong Yin. Magnetically Responsive Nanostructures with Tunable Optical Properties. *Journal of the American Chemical Society*, 138(20):6315–6323, 2016. ISSN 15205126. doi: 10.1021/jacs.6b02346.

[16] Konstantin G. Kornev, Derek Halverson, Guzeliya Korneva, Yury Gogotsi, and Gary Friedman. Magnetostatic interactions between carbon nanotubes filled with magnetic nanoparticles. *Applied Physics Letters*, 92(23):2006–2009, 2008. ISSN 00036951. doi: 10.1063/1.2940303.

[17] Gregor Ferk, Peter Krajnc, Anton Hamler, Alenka Mertelj, Federico Cebollada, Miha Drofenik, and Darja Lisjak. Monolithic magneto-optical nanocomposites of barium hexaferrite platelets in PMMA. *Scientific Reports*, 5:1–8, 2015. ISSN 20452322. doi: 10.1038/srep11395. URL `http://dx.doi.org/10.1038/srep11395`.

[18] M. Shuai, A. Klittnick, Y. Shen, G. P. Smith, M. R. Tuchband, C. Zhu, R. G. Petschek, A. Mertelj, D. Lisjak, M. Čopič, J. E. Maclennan, M. A. Glaser, and N. A. Clark. Spontaneous liquid crystal and ferromagnetic ordering of colloidal magnetic nanoplates. *Nature Communications*, 7, 2016. ISSN 20411723. doi: 10.1038/ncomms10394.

[19] R. Geryak, J. Geldmeier, K. Wallace, and V. V. Tsukruk. Remote Giant Multispectral Plasmonic Shifts of Labile Hinged Nanorod Array via Magnetic Field. *Nano Letters*, 15(4):2679–2684, 2015. ISSN 15306992. doi: 10.1021/acs.nanolett.5b00342.

[20] E. Ferain and R. Legras. Templates for engineered nano-objects for use in microwave, electronic devices and biomedical sensing application. *Nuclear Instruments and Methods in Physics Research, Section B: Beam Interactions with Materials and Atoms*, 267(6):1028–1031, 2009. ISSN 0168583X. doi: 10.1016/j.nimb.2009.02.013. URL `http://dx.doi.org/10.1016/j.nimb.2009.02.013`.

[21] Maruša Mur, Junaid Ahmad Sofi, Ivan Kvasić, Alenka Mertelj, Darja Lisjak, Vidur Niranjan, Igor Muševič, and Surajit Dhara. Magnetic-field tuning of whispering gallery mode lasing from ferromagnetic nematic liquid crystal microdroplets. *Optics Express*, 25(2):1073, 2017. ISSN 1094-4087. doi: 10.1364/oe.25.001073.

[22] Jianping Ge, Howon Lee, Le He, Junhoi Kim, Zhenda Lu, Hyoki Kim, James Goebl, Sunghoon Kwon, and Yadong Yin. Magnetochromatic microspheres:

Rotating photonic crystals. *Journal of the American Chemical Society*, 131 (43):15687–15694, 2009. ISSN 00027863. doi: 10.1021/ja903626h.

[23] Alenka Mertelj, Darja Lisjak, Miha Drofenik, and Martin Čopič. Ferromagnetism in suspensions of magnetic platelets in liquid crystal. *Nature*, 504(7479):237–241, 2013. ISSN 00280836. doi: 10.1038/nature12863.

[24] Mingsheng Wang, Chuanbo Gao, Le He, Qipeng Lu, Jinzhong Zhang, Chi Tang, Serkan Zorba, and Yadong Yin. Magnetic tuning of plasmonic excitation of gold nanorods. *Journal of the American Chemical Society*, 135(41):15302–15305, 2013. ISSN 00027863. doi: 10.1021/ja408289b.

[25] Joseph M. Kinsella and Albena Ivanisevic. Magnetotransport of one-dimensional chains of CoFe2O4 nanoparticles ordered along DNA. *Journal of Physical Chemistry C*, 112(9):3191–3193, 2008. ISSN 19327447. doi: 10.1021/jp712002a.

[26] Shaozhou Li and Chee Lip Gan. Ultrathin β-FeOOH and ϵ-Fe2O3 nanowires. *Chemical Physics Letters*, 616-617:40–43, 2014. ISSN 00092614. doi: 10.1016/j.cplett.2014.10.014. URL `http://dx.doi.org/10.1016/j.cplett.2014.10.014`.

[27] Hui Min Zhang, Yu Guo Guo, Li Jun Wan, and Chun Li Bai. Novel electrocatalytic activity in layered Ni-Cu nanowire arrays. *Chemical Communications*, 3(24):3022–3023, 2003. ISSN 1364548X. doi: 10.1039/b309624f.

[28] Fang Liu, Jim Yang Lee, and Weijiang Zhou. Template preparation of multisegment PtNi nanorods as methanol electro-oxidation catalysts with adjustable bimetallic pair sites. *Journal of Physical Chemistry B*, 108(46): 17959–17963, 2004. ISSN 15206106. doi: 10.1021/jp0472360.

[29] Jo V. Rushworth, Asif Ahmed, Heledd H. Griffiths, Niall M. Pollock, Nigel M. Hooper, and Paul A. Millner. A label-free electrical impedimetric biosensor for the specific detection of Alzheimer's amyloid-beta oligomers. *Biosensors and Bioelectronics*, 56:83–90, 2014. ISSN 09565663. doi: 10.1016/j.bios.2013.12.036.

[30] K. Žužek Rožman, D. Pečko, S. Šturm, U. Maver, P. Nadrah, M. Bele, and S. Kobe. Electrochemical synthesis and characterization of Fe 70Pd 30

nanotubes for drug-delivery applications. *Materials Chemistry and Physics*, 133 (1):218–224, 2012. ISSN 02540584. doi: 10.1016/j.matchemphys.2012.01.013.

[31] Lin Guo, Fang Liang, Xiaogang Wen, Shihe Yang, Lin He, Wangzhi Zheng, Chinping Chen, and Qunpeng Zhong. Uniform magnetic chains of hollow cobalt mesospheres from one-pot synthesis and their assembly in solution. *Advanced Functional Materials*, 17(3):425–430, 2007. ISSN 1616301X. doi: 10.1002/adfm.200600415.

[32] Slavko Kralj and Darko Makovec. Magnetic Assembly of Superparamagnetic Iron Oxide Nanoparticle Clusters into Nanochains and Nanobundles. *ACS Nano*, 9(10):9700–9707, 2015. ISSN 1936086X. doi: 10.1021/acsnano.5b02328.

[33] Guangbao Yang, Hua Gong, Teng Liu, Xiaoqi Sun, Liang Cheng, and Zhuang Liu. Two-dimensional magnetic WS2@Fe3O4 nanocomposite with mesoporous silica coating for drug delivery and imaging-guided therapy of cancer. *Biomaterials*, 60:62–71, 2015. ISSN 18785905. doi: 10.1016/j.biomaterials.2015.04.053. URL `http://dx.doi.org/10.1016/j.biomaterials.2015.04.053`.

[34] Akira Ito, Masashige Shinkai, Hiroyuki Honda, and Takeshi Kobayashi. Medical application of functionalized magnetic nanoparticles. *Journal of Bioscience and Bioengineering*, 100(1):1–11, 2005. ISSN 13891723. doi: 10.1263/jbb.100.1.

[35] Sébastien Fournier-Bidoz, André C. Arsenault, Ian Manners, and Geoffrey A. Ozin. Synthetic self-propelled nanorotors. *Chemical Communications*, (4):441–443, 2005. ISSN 13597345. doi: 10.1039/b414896g.

[36] R. W. Chantrell, A. Hoare, D. Melville, H. J. Lutke-Stetzkamp, and S. Methfessel. Transverse Susceptibility of a Fine Particle System. *IEEE Transactions on Magnetics*, 25(5):4216–4218, 1989. ISSN 19410069. doi: 10.1109/20.42573.

[37] D C Jiles. *Introduction to Magnetism and Magnetic materials*. Springer-science, 1991. ISBN 9780412386404.

[38] Ashima Arora. *Optical and electric field control of magnetism*. PhD thesis, Helmholtz-Zentrum Berlin, 2018.

[39] Ralph Skomski, G. C. Hadjipanayis, and D. J. Sellmyer. Effective demagnetizing factors of complicated particle mixtures. *IEEE Transactions on Magnetics*, 43(6):2956–2958, 2007. ISSN 00189464. doi: 10.1109/TMAG.2007.893798.

[40] G. Briet. Calculations of the effective permeability and dielectric constant of a powder. *Communications from the Physical Laboratory at Leiden.*, 1(46), 1922.

[41] R. Bjørk and C. R.H. Bahl. Demagnetization factor for a powder of randomly packed spherical particles. *Applied Physics Letters*, 103(10), 2013. ISSN 00036951. doi: 10.1063/1.4820141.

[42] B Bleaney and R A Hull. The effective susceptibility of a paramagnetic powder. *Proceedings of the Royal Society of London. Series A. Mathematical and Physical Sciences*, 178(972):86–92, 1941. ISSN 2053-9169. doi: 10.1098/rspa.1941.0045.

[43] R. Bjørk and Z. Zhou. The demagnetization factor for randomly packed spheroidal particles. *Journal of Magnetism and Magnetic Materials*, 476 (January):417–422, 2019. ISSN 03048853. doi: 10.1016/j.jmmm.2019.01.005. URL `https://doi.org/10.1016/j.jmmm.2019.01.005`.

[44] M. J. Donahue and D. G. Porter. Analysis of switching in uniformly magnetized bodies. *IEEE Transactions on Magnetics*, 38(5 I):2468–2470, 2002. ISSN 00189464. doi: 10.1109/TMAG.2002.803616.

[45] R.D. Cookson. *Transverse Susceptibility studies of recording media*. PhD thesis, University of Central Lancashire, 2002.

[46] P. Langevin. Une formule fondamentale de theorie cinetique. *annales de Chimie et de Physique*, 5(70):245–288, 1905.

[47] C. P. Bean and J. D. Livingston. Superparamagnetism. *Journal of Applied Physics*, 30(4):S120–S129, 1959. ISSN 10897550. doi: 10.1063/1.2185850.

[48] P . M. Sollis, A. Hoare, A. Peters, T. Orth, P. R. Bissell, R. W. Chantrell, and J. Pelzl. Experimental and theoretical-studies of transverse susceptibility in recording media. *IEEE Transactions on Magnetics*, 28(5, 2):2695–2697, 9 1992. ISSN 0018-9464. doi: 10.1109/20.179600.

[49] P. M. Sollis, P. R. Bissell, P. I. Mayo, R. W. Chantrell, R. G. Gilson, and K. O'Grady. Characterisation of the dispersion process using transverse susceptibility measurements. *Journal of Magnetism and Magnetic Materials*, 120(1-3):94–96, 1993. ISSN 03048853. doi: 10.1016/0304-8853(93)91294-H.

[50] A. Hoare, R. W. Chantrell, W. Schmitt, and A. Eiling. Reversible transverse susceptibility of particulate recording media. *Journal of Physics D: Applied Physics*, 26(3):461–468, 1993. ISSN 00223727. doi: 10.1088/0022-3727/26/3/019.

[51] P. M. Sollis, P. R. Bissell, and R. W. Chantrell. Effects of texture and interactions on transverse susceptibility measurements of particulate media. *Journal of Magnetism and Magnetic Materials*, 155(1-3):123–125, 1996. ISSN 03048853. doi: 10.1016/0304-8853(95)00674-5.

[52] Carlos Pecharromán, T. González-Carreño, and Juan E. Iglesias. The infrared dielectric properties of maghemite, γ-Fe2O3, from reflectance measurement on pressed powders. *Physics and Chemistry of Minerals*, 22(1):21–29, 1995. ISSN 03421791. doi: 10.1007/BF00202677. URL `https://doi.org/10.1007/BF00202677`.

[53] Khong Nee Koo, Ahmad Fauzi Ismail, Mohd Hafiz Dzarfan Othman, Mukhlis A Rahman, and Tai Zhong. Preparation and characterisation of superparamagnetic magnetite nanoparticles: A short review. *Malaysian Journal of fundamental and applied sciences*, 15(1):23–31, 2019. ISSN 10002413. doi: 10.1007/s11595-017-1555-4.

[54] G Gatta, Innokenty Kantor, T Ballaran, Leonid Dubrovinsky, and Catherine Mccammon. Effect of non-hydrostatic conditions on the elastic behaviour of magnetite: An in situ single-crystal X-ray diffraction study. *Physics and Chemistry of Minerals*, 34:627–635, 11 2007. doi: 10.1007/s00269-007-0177-3.

[55] Oskar Glemser, Ulrich Hauschild, and Franz Trüpel. Über Chromoxyde zwischen Cr2O3 und CrO3. *Zeitschrift für anorganische und allgemeine Chemie*, 277(3-4):113–126, 11

1954. ISSN 0044-2313. doi: 10.1002/zaac.19542770302. URL https://doi.org/10.1002/zaac.19542770302.

[56] K. Le Dang, P. Veillet, G. Suran, and K. Ounadjela. Study of induced uniaxial anisotropy in magnetic thin films by transverse susceptibility. *Journal of Applied Physics*, 62(8):3328–3330, 1987. ISSN 00218979. doi: 10.1063/1.339318.

[57] H. J. Richter. Determination of magnetic anisotropy of magnetically hard materials. *Journal of Applied Physics*, 67(6):3081–3087, 3 1990. ISSN 00218979. doi: 10.1063/1.345408.

[58] Jing Ju Lu, Huei Li Huang, Ching Ray Chang, and Ivo Klik. Reversible transverse susceptibility of particulate recording media. *Journal of Applied Physics*, 75(10):5499–5501, 1994. ISSN 00223727. doi: 10.1088/0022-3727/26/3/019.

[59] Huei Li Huang and Jing Ju Lu. Thermal relaxation, textural and sweep rate effects on reversible transverse susceptibility of magnetic particles. *Journal of Applied Physics*, 77(7):3323–3330, 1995. ISSN 00218979. doi: 10.1063/1.358618.

[60] Huei Li Huang and Jing Ju Lu. Thermal relaxation, textural and sweep rate effects on reversible transverse susceptibility of magnetic particles. *Journal of Applied Physics*, 77(7):3323–3330, 1995. ISSN 00218979. doi: 10.1063/1.358618.

[61] Jye Lee, Ivo Klik, and Ching Ray Chang. The reversible transverse susceptibility of coupled uniaxial systems. *Journal of Magnetism and Magnetic Materials*, 129(2-3), 1994. ISSN 03048853. doi: 10.1016/0304-8853(94)90104-X.

[62] Ching Ray Chang and Jyh Shinn Yang. Detection of anisotropy in the reversible transverse susceptibility. *Applied Physics Letters*, 65(4):496–498, 1994. ISSN 00036951. doi: 10.1063/1.112305.

[63] R. W. Chantrell, P. R. Bissell, P. Sollis, A. Hoare, and Th Orth. Deconvolution of anisotropy field distributions from transverse susceptibility measurements. *Journal of Magnetism and Magnetic Materials*, 177-181(PART 2):894–895, 1998. ISSN 03048853. doi: 10.1016/S0304-8853(97)00740-3.

[64] L. Spinu, H. Srikanth, E E Carpenter, and C. J. O'Connor. Dynamic radio-frequency transverse susceptibility in magnetic nanoparticle systems.

Journal of Applied Physics, 87(9):5490–5492, 2000. ISSN 00189464. doi: 10.1109/20.908668.

[65] L. Spinu, H. Srikanth, J. A. Wiemann, S. Li, J. Tang, and C. J. O'Connor. Superparamagnetism and transverse susceptibility in magnetic nanoparticle systems. *IEEE Transactions on Magnetics*, 36(5 I):3032–3034, 2000. ISSN 00189464. doi: 10.1109/20.908668.

[66] P. Görnert, W. Schüppel, E. Sinn, F. Schumacher, K. A. Hempel, G. Turilli, A. Paoluzi, and M. Rösler. Comparative measurements of the effective anisotropy field H a for barium ferrites. *Journal of Magnetism and Magnetic Materials*, 114(1-2):193–201, 1992. ISSN 03048853. doi: 10.1016/0304-8853(92)90344-N.

[67] Dorin Cimpoesu, Leonard Spinu, and Alexandru Stancu. Transverse susceptibility method in nanoparticulate magnetic media. *Journal of Nanoscience and Nanotechnology*, 8(6):2731–2744, 6 2008. ISSN 1533-4880. doi: 10.1166/jnn.2008.006.

[68] Ioan Dumitru, Dorin Cimpoesu, and Alexandru Stancu. Measurements on real and imaginary parts of transverse susceptibility of particulate system. *IEEE Transactions on Magnetics*, 50(11), 2014. ISSN 00189464. doi: 10.1109/TMAG.2014.2331176.

[69] Darja Lisjak and Alenka Mertelj. Anisotropic magnetic nanoparticles: A review of their properties, syntheses and potential applications. *Progress in Materials Science*, 95:286–328, 2018. ISSN 00796425. doi: 10.1016/j.pmatsci.2018.03.003. URL `https://doi.org/10.1016/j.pmatsci.2018.03.003`.

[70] P. Fournier M.M. Gospodinov. M. Balli, S. Jandl. Anisotropy-enhanced giant reversible rotating magnetocaloric effect in HoMn2O5 single crystals. *Applied Physics Letters*, 104 (6868)(232402–):1 to 5, 2014.

[71] H. J. Lütke-Stetzkamp, S. Methfessel, and R. W. Chantrell. Relation between the transverse ac susceptibility and anisotropy distribution in fesi. *Le Journal de Physique Colloques*, 49(C8):8–1313, 1988. ISSN 0449-1947. doi: 10.1051/jphyscol:19888599.

[72] P. M. Sollis. *Transverse susceptibility measurements on particulate recording media.* PhD thesis, University of Central Lancashire, Preston, UK, 1995.

[73] G R Jones, L S Prichard, J A Hutchings, H Laidler, and K O'Grady. Determination of anisotropy fields in recording media. *Journal of Applied Physics*, 87(9):5711–5713, 4 2000. ISSN 0021-8979. doi: 10.1063/1.372498. URL `https://doi.org/10.1063/1.372498`.

[74] P Sollis, P R Bissell, and Roy Chantrell. The effects of texture and interactions on transverse susceptibility measurements of particulate media. *Journal of Magnetism and Magnetic Materials - J MAGN MAGN MATER*, 155:123–125, 3 1996. doi: 10.1016/0304-8853(95)00674-5.

[75] C Papusoi. The complex transverse susceptibility. *Physics Letters a*, 265(5-6): 391–402, 2 2000. ISSN 0375-9601.

Appendix

Susceptometer control software - LabVIEW VI

This section contains the block diagram of the LabVIEW VI used to control the susceptometer. The VI was originally designed by Dr Steve McCann.

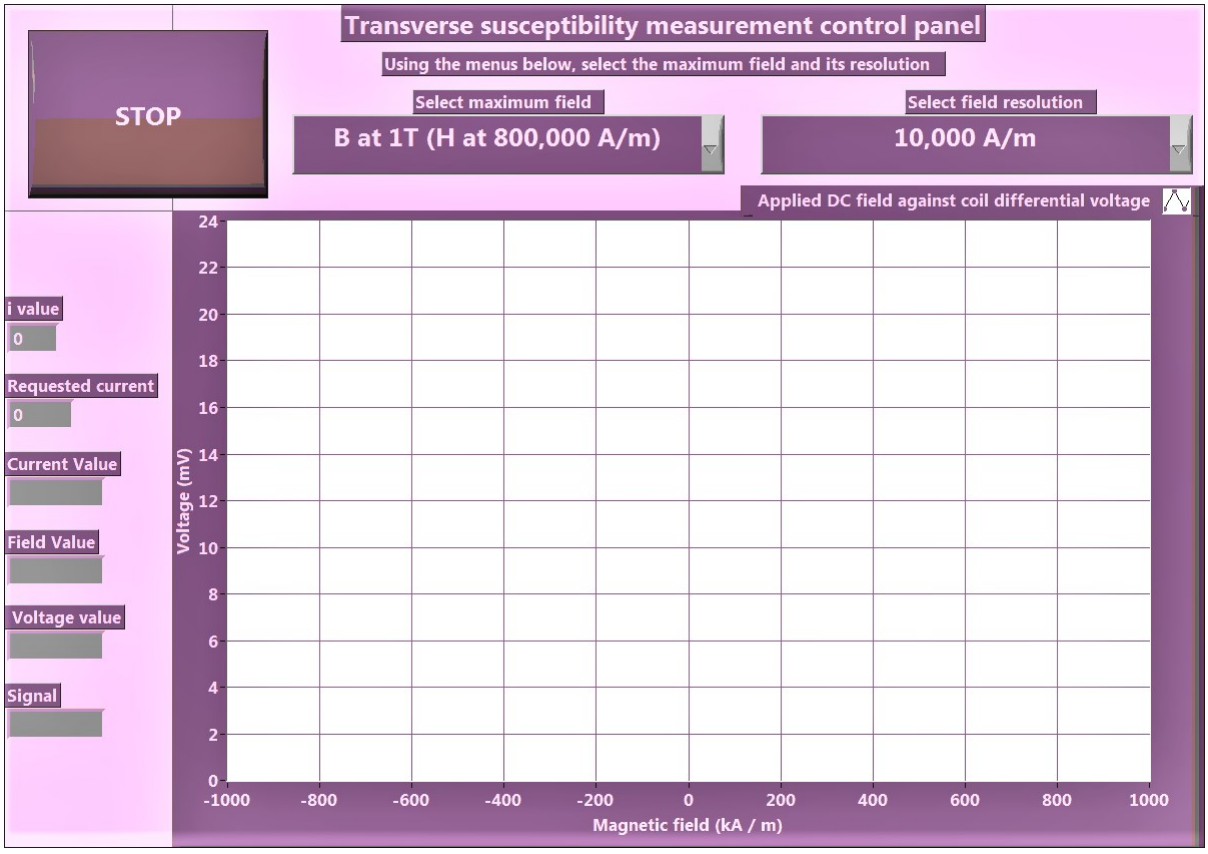

Figure 6.1: Front panel of the LabVIEW VI used to control the susceptometer

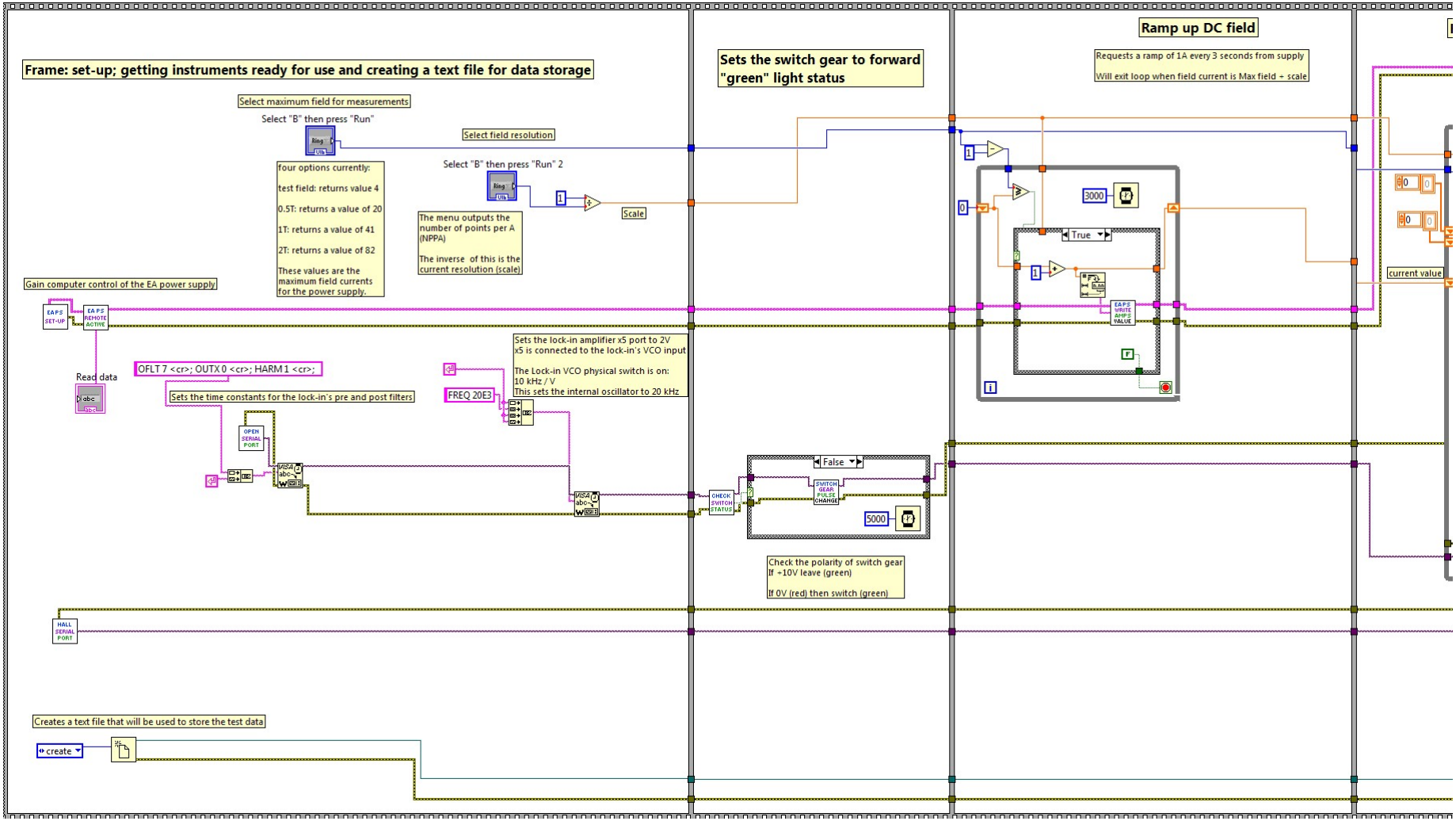

Figure 6.2: Page one of the block diagram for the LabVIEW VI controlling the susceptometer.

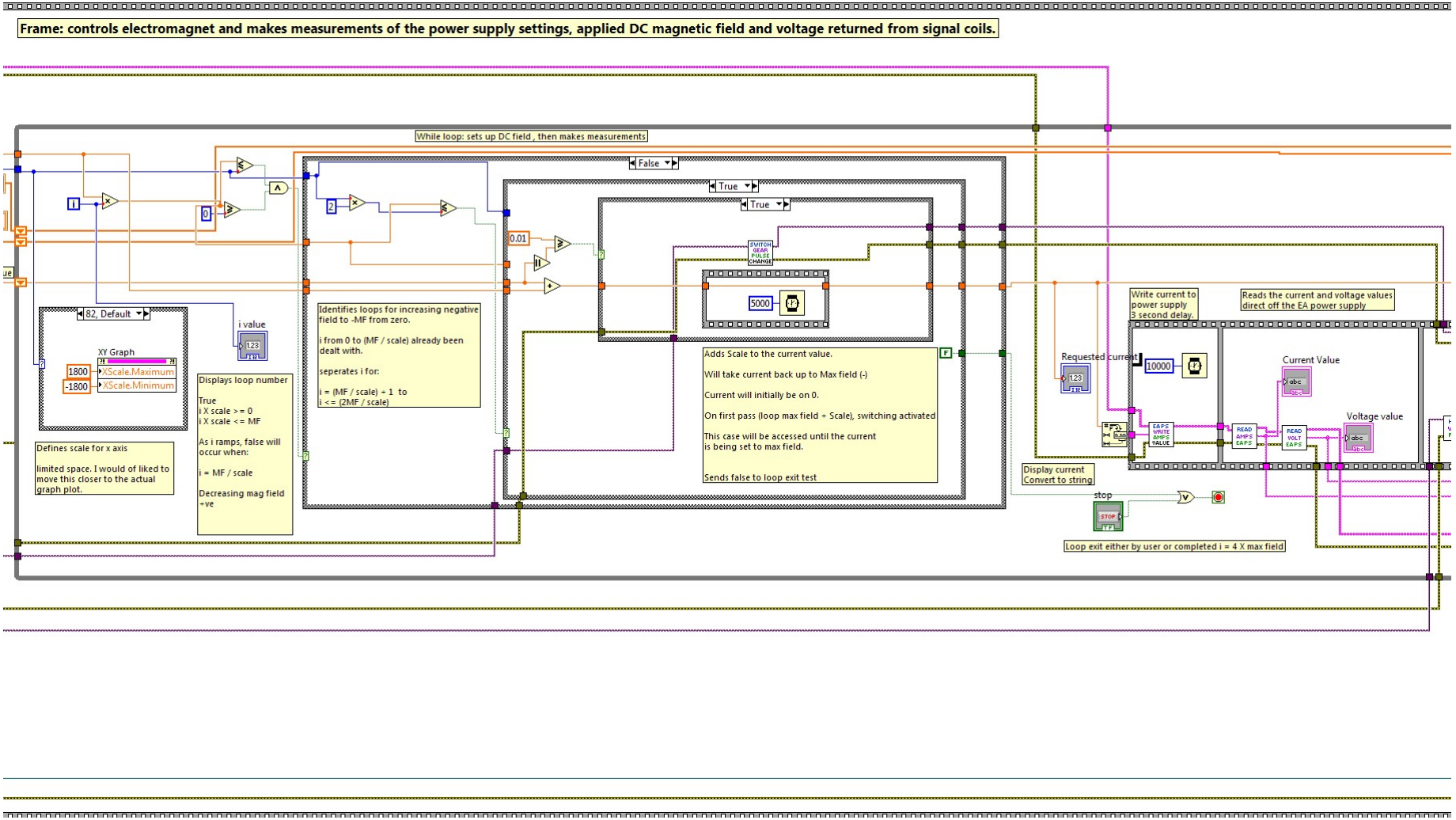

Figure 6.3: Page two of the block diagram for the LabVIEW VI controlling the susceptometer

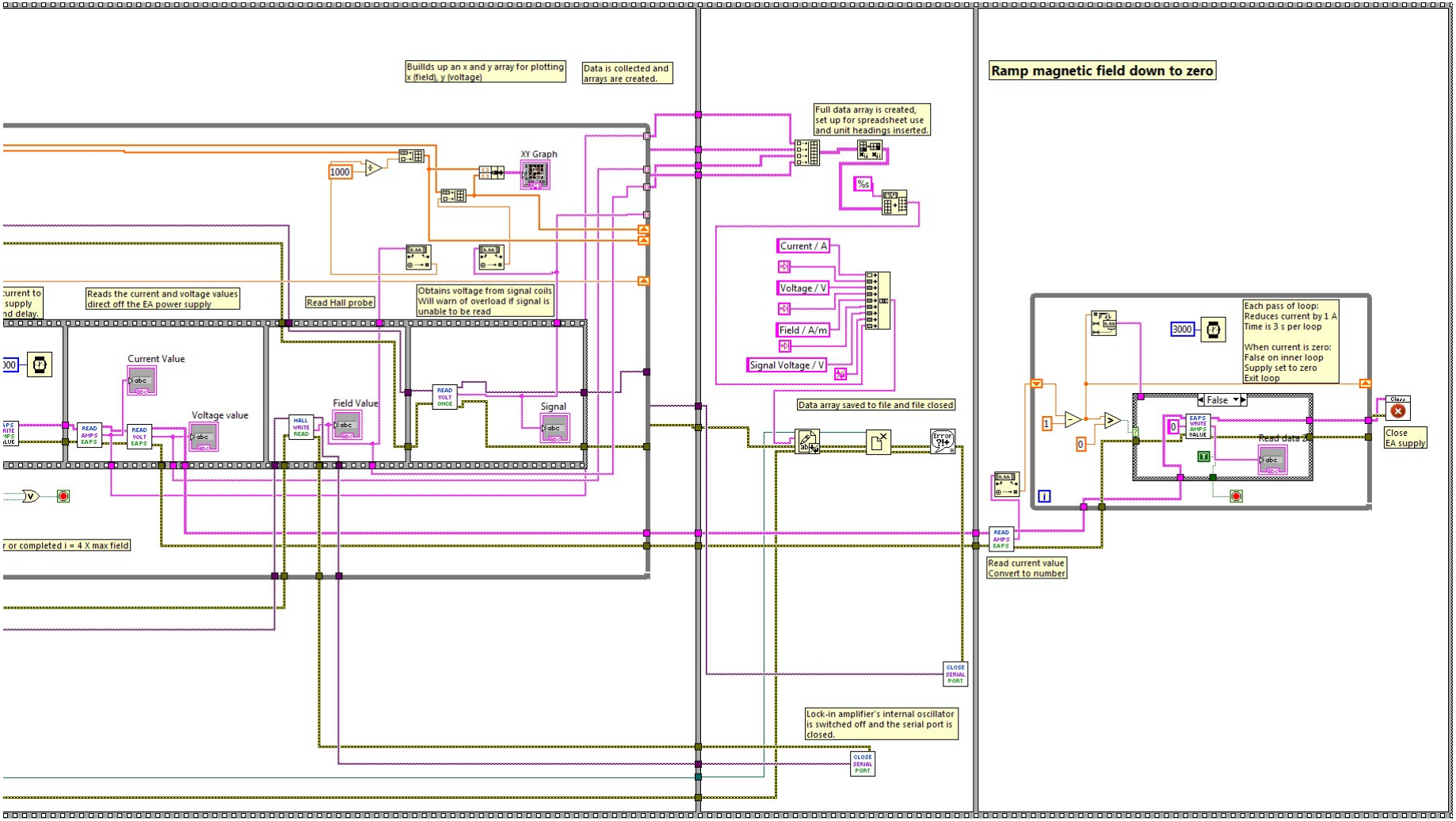

Figure 6.4: Page three of the block diagram for the LabVIEW VI controlling the susceptometer